

ACTIN REGULATORY DYNAMICS REQUIRED FOR T CELL ACTIVATION:
A QUANTITATIVE AND SYSTEMS-LEVEL PERSPECTIVE

APPROVED BY SUPERVISORY COMMITTEE

Christoph Wülfing, Ph.D.

Michael K. Rosen, Ph.D.

Elizabeth Sally Ward, Ph.D.

Chandrashekhar Pasare, Ph.D.

ACKNOWLEDGEMENTS

I would first like to thank my thesis advisor Christoph Wülfing for constant support and intellectual push, which has provided a solid foundation to proceed in academic science. I would also like to thank my Graduate Committee, especially Michael Rosen, for critical advice to further my research and help me to develop as a scientist. Furthermore, I would like to thank Nicolai van Oers for in many regards being a second mentor to me. My successes as a graduate student would not have been possible without all of the aforementioned guidance. I would also like to thank my loving and supportive girlfriend Elma, my parents Kerry and Paula Roybal, my sister Kade, and my dog Buster Brown. Without their love and support life would be unbalanced and largely unfilled.

ACTIN REGULATORY DYNAMICS REQUIRED FOR T CELL ACTIVATION:
A QUANTITATIVE AND SYSTEMS-LEVEL PERSPECTIVE

by

KOLE THOMAS ROYBAL

DISSERTATION

Presented to the Faculty of the Graduate School of Biomedical Sciences

The University of Texas Southwestern Medical Center at Dallas

In Partial Fulfillment of the Requirements

For the Degree of

DOCTOR OF PHILOSOPHY

The University of Texas Southwestern Medical Center at Dallas

Dallas, Texas

May, 2013

Copyright

By

KOLE THOMAS ROYBAL, 2013

All Rights Reserved

ACTIN REGULATORY DYNAMICS REQUIRED FOR T CELL ACTIVATION:
A QUANTITATIVE AND SYSTEMS-LEVEL PERSPECTIVE

KOLE THOMAS ROYBAL, Ph.D.

The University of Texas Southwestern Medical Center at Dallas, 2013

Supervising Professor: Christoph Wülfing, Ph.D.

T cell activation occurs through interaction with an antigen-presenting cell (APC). Upon activation, signaling ensues with the coordination of dozens of diverse signaling molecules in space and time, a feature of cell signaling we call ‘spatiotemporal patterning’. We performed a systems-scale analysis of the spatiotemporal patterning of T cell signaling and have found that it is highly diverse. Over 50 signaling sensors were imaged in live primary T cells activated with APCs under various physiological stimulation conditions, and no two signaling intermediates showed the same dynamic localization. The activation environment controlled spatiotemporal features of T cell signaling and specific spatiotemporal features correlated with efficient T cell activation.

To identify underlying cell biological mechanisms controlling spatiotemporal organization of signaling, we complimented our live cell imaging with microscopy across multiple scales and identified a dense transient F-actin network that extends from a highly interdigitated T cell:APC interface several micrometers deep into the T cell lamellum. Systems-scale imaging revealed a large network of proximal T cell signaling intermediates that localized to the lamellar actin network and shared the spatial, temporal, and mobility features of F-actin. Interference with lamellar actin dynamics modulated the activity of the associated proteins and impaired IL-2 production. These data strongly suggest that the transient deep F-actin network by controlling lamellar localization modulates the activity of a substantial part of the T cell signal transduction system.

As a next step in understanding how spatiotemporal dynamics of signaling controls T cell activation, we have developed a quantitative 4D analysis approach for signaling networks and coupled it with traditional cell biological techniques to uncover higher order mechanisms of the control of actin dynamics by CD28 co-stimulation during T cell activation. A group of nine actin regulatory proteins that mediate actin polymerization, capping, and severing were assessed and CD28 co-stimulation was required for their sustained activity at the T cell:APC interface. WAVE2 and Cofilin were especially sensitive to blockade of CD28 signaling. Functional relevance of the loss of WAVE2 and Cofilin enrichment was shown by the treatment of T cells with constitutively active Rac1 and Cofilin, which bypassed the requirement of co-stimulation for normal actin dynamics and AKT activation. This study highlights how a systems analysis of actin regulation could identify mechanisms that are inaccessible to more traditional single protein/gene approaches.

TABLE OF CONTENTS

ABSTRACT	v
TABLE OF CONTENTS	vii
PRIOR PUBLICATIONS	x
LIST OF FIGURES	xi
LIST OF TABLES	xvi
LIST OF ABBREVIATIONS	xvii

CHAPTER ONE: INTRODUCTION

<i>T cell activation and coordinated signaling at the T cell:APC interface</i>	<i>1</i>
<i>Actin cytoskeleton regulation in T cells</i>	<i>4</i>
<i>The importance of actin regulation for T cell function.....</i>	<i>6</i>
<i>Regulation of signaling at the T cell:APC interface by co-stimulation</i>	<i>10</i>
<i>Conclusions</i>	<i>11</i>

CHAPTER TWO: MATERIALS AND METHODS

<i>Antibodies, purified Proteins, and reagents</i>	<i>12</i>
<i>Mice and cells</i>	<i>13</i>
<i>Retroviral transduction</i>	<i>14</i>
<i>Antibody stimulation and APC stimulation of T cells</i>	<i>15</i>
<i>Quantitative immunoblotting, immunoblots, and Phos-tag immunoblots</i>	<i>16</i>
<i>Time-lapsed imaging of T cell:APC interactions.....</i>	<i>18</i>
<i>Long-term time-lapsed fluorescence microscopy of T cell:APC conjugates</i>	<i>19</i>

<i>Image analysis</i>	20
<i>T cell volumetric measurement</i>	22
<i>Fluorescence recovery after photobleaching (FRAP)</i>	23
<i>Fixed T cell:APC conjugate preparation and fluorescence imaging</i>	24
<i>Expression and purification of cell permeable tat-tagged proteins</i>	25
<i>IL-2 intracellular stains</i>	26

CHAPTER THREE: RESULTS

Spatiotemporal Patterning of T cell Activation is Highly Diverse

<i>A Systems-level perspective of the spatiotemporal patterning of T cell signaling</i>	31
---	----

A Deep and Transient Actin Network Controls T cell Activation

<i>Signal transduction in the T cell lamellum</i>	36
<i>F-actin and lamellar signaling intermediates share deep lamellar localization</i>	37
<i>Lamellar localized signaling intermediates and actin diffuse at similar rates</i>	39
<i>Diminished interface actin recruitment prevents lamellar localization</i>	40
<i>Diminished interface actin impairs proximal signaling and cytokine production</i>	41
<i>The T cell:APC interface has an actin-dependent undulating and interdigitated architecture that reaches deep into the T cell lamellum</i>	43

Systems-scale Integration of T cell Receptor and Co-stimulatory Signals Regulate

Actin Dynamics Required for T cell Activation

<i>Systems-scale assessment of actin regulation at the T cell:APC interface reveals the requirement of CD28 co-stimulation for sustained actin regulation</i>	63
---	----

<i>CD28 sustains recruitment and activation of regulators of the WAVE2 complex</i>	<i>67</i>
<i>System-scale assessment reveals a loss in coordinated spatiotemporal regulation of the actin regulatory network</i>	<i>69</i>
<i>Constitutively active Rac1 and Cofilin restore actin enrichment at the T cell:APC interface and AKT activation despite inhibition of CD28 co-stimulation</i>	<i>70</i>
<i>Quantification of the spatiotemporal organization of the actin regulatory machinery in live T cells</i>	<i>72</i>
<i>Concentrations of the actin regulatory network in primary T cells</i>	<i>73</i>
<i>Actin regulation at the T cell:APC interface is highly dynamic</i>	<i>75</i>
<i>High-throughput assessment of dynamic local concentrations of fluorescently labeled molecules in live T cells</i>	<i>76</i>

CHAPTER FOUR: DISCUSSION

Spatiotemporal Patterning of T cell Activation is Highly Diverse	103
A Deep and Transient Actin Network Controls T cell Activation	104
Systems-scale Integration of T cell Receptor and Co-stimulatory Signals Regulate Actin Dynamics Required for T cell Activation	107

REFERENCES	112
-------------------------	------------

PRIOR PUBLICATIONS

- Roybal, K.T.**, B.K. Cho., R.F. Murphy, M. Meier-Schellersheim, C. Wülfing. Systems-scale Integration of T cell Receptor and Co-stimulatory Signals Regulate Actin Dynamics Required for T cell Activation. In preparation.
- Roybal, K.T.**, E.M. Mace, J.S. Orange, C. Wülfing. A Deep and Transient Actin Network Controls T cell Activation. Submitted.
- Roybal, K.T.**, and C. Wülfing. 2012. New TACTICS for finding Numb. *Immunol Cell Biol.* doi:10.1038/icb.2012.63
- Eitson J., J. Medeiros, A. Hoover, S. Srivastava, **K. T. Roybal**, J. Ainsa, E. Hansen, T. Gumbo. N. S. van Oers. 2012. Mycobacterial Shuttle Vectors Designed for High Level Protein Expression in Infected Macrophages. *Appl. Environ. Microbiol.* 78:6829-6937
- Deford-Watts, L.M., D.S. Dougall, S. Belkaya, B.A. Johnson, J.L. Eitson, **K.T. Roybal**, B. Barylko, J.P. Albanesi, C. Wülfing, and N.S. van Oers. 2011. The CD3 {zeta} Subunit Contains a Phosphoinositide-Binding Motif That Is Required for the Stable Accumulation of TCR-CD3 Complex at the Immunological Synapse. *J Immunol.* 186:6839-6847.
- Roybal, K.T.**, and C. Wülfing. 2010. Inhibiting the inhibitor of the inhibitor: blocking PKC-theta to enhance regulatory T cell function. *Sci Signal.* 3:pe24.
- Sinai, P., **K.T. Roybal.**, and C. Wülfing. 2010. Tentative and transient natural killer cell polarization balances the requirements for discriminatory recognition and cytolytic efficacy. *Commun Integr Biol.* 3:545-548
- Singleton, K.L.*., **Roybal K.T.***, Y. Sun, G. Fu, N.R. Gascoigne, N.S. van Oers, and C. Wülfing. 2009. Spatiotemporal patterning during T cell activation is highly diverse. *Sci Signal.* 2:ra15. (* equal contribution)
- Roybal, K.T.**, D. Theobald, A. Graham, J.A. DiNieri, S.J. Russo, V. Krishnan, S. Chakravarty, J. Peevey, N. Oehrlein, S. Birnbaum, M.H. Vitaterna, P. Orsulak, J.S. Takahashi, E.J. Nestler, W.A. Carlezon, Jr., and C.A. McClung. 2007. Mania-like behavior induced by disruption of CLOCK. *Proc Natl Acad Sci U S A.* 104:6406-6411.

LIST OF FIGURES

Materials and Methods

Figure 1: Classification criteria for spatiotemporal patterns of signaling intermediate accumulation at the T cell:APC interface	29
Figure 2: <i>Interface diameter to length ratio and F-actin structure analysis</i>	30
 A Deep and Transient Actin Network Controls T cell Activation	
Figure 3: <i>T cells recruit molecules critical for signal transduction to the T cell:APC interface in distinct patterns</i>	34
Figure 4: <i>T cells recruit molecules critical for signal transduction to the T cell:APC interface in distinct patterns</i>	35
Figure 5: <i>Spatiotemporal patterning of the T cell signaling system</i>	45
Figure 6: <i>Cluster analysis of the spatiotemporal patterning of the T cell signaling system identifies a lamellar network of T cell signaling</i>	46
Figure 7: <i>Actin and lamellar localized signaling intermediates distribute across the entire T cell:APC interface and extend several micrometers into the T cell</i> ...	47
Figure 8: <i>Activated SLP-76 localizes to the T cell lamellum</i>	48
Figure 9: <i>Activated LAT localizes to the T cell:APC interface center</i>	49
Figure 10: <i>Activated SLP-76 localizes to lamellar F-actin structures</i>	50
Figure 11: <i>Lamellar signaling intermediates diffuse at similar rates as actin</i>	51
Figure 12: <i>Diminished actin at the T cell:APC interface disrupts lamellar localization of SLP-76</i>	52

Figure 13: <i>Diminished actin at the T cell:APC interface disrupts lamellal localization and activation of SLP-76</i>	53
Figure 14: <i>Activated SLP-76 associates with F-actin despite disruption of actin at the T cell:APC interface</i>	54
Figure 15: <i>Diminished actin at the T cell:APC interface disrupts lamellal localization of PLCδPH and enhances lamellal localization of Vav1</i>	55
Figure 16: <i>Disruption of actin dynamics diminishes sustained central localization of LAT and PKCθ</i>	56
Figure 17: <i>Disruption of actin dynamics with Jasplakinolide selectively modulates the activation of lamellal signaling intermediates.....</i>	57
Figure 18: <i>Disruption of actin with Latrunculin A severely diminishes T cell signaling.....</i>	58
Figure 19: <i>Selective disruption of actin dynamics during the first hour of T cell activation diminishes IL-2 production.</i>	59
Figure 20: <i>Deconvolution microscopy shows the early T cell:APC interface has an undulating and interdigitated architecture that is supported by actin</i>	60
Figure 21: <i>Electron microscopy shows the early T cell:APC interface has an undulating and interdigitated architecture that is supported by actin.....</i>	61
Figure 22: <i>The early F-actin structures at the T cell:APC interface are discreet, limited in size, and oriented perpendicular to the interface plane</i>	62

Systems-scale Integration of T cell Receptor and Co-stimulatory Signals Regulate Actin Dynamics Required for T cell Activation

Figure 23: <i>A systems-level view of actin regulation during early T cell activation</i>	77
Figure 24: <i>Spatiotemporal patterning of actin-GFP is retained without CD28 co- stimulation but the amount actin at the T cell:APC interface is reduced</i>	78
Figure 25: <i>Spatiotemporal patterning of ARP3-GFP at the T cell:APC interface is more transient without CD28 co-stimulation.....</i>	79
Figure 26: <i>Lamellar localization of CPa1-GFP is more transient without CD28 co stimulation.....</i>	80
Figure 27: <i>Peripheral localization of Cofilin-GFP at the T cell:APC interface is lost and overall enrichment is more transient without CD28 co-stimulation</i>	81
Figure 28: <i>Spatiotemporal organization of Coronin1A-GFP at the T cell:APC interface is more transient without CD28 co-stimulation.....</i>	82
Figure 29: <i>Spatiotemporal organization of HSI-GFP at the T cell:APC interface is more transient without CD28 co-stimulation and diffuse localization is reduced at early time points.....</i>	83
Figure 30: <i>Myosin regulatory light chain-GFP is more rapidly recruited to the T cell:APC interface but more transient without CD28 co-stimulation</i>	84
Figure 31: <i>Spatiotemporal organization of WASp-GFP at the T cell:APC interface is more transient without CD28 co-stimulation.....</i>	85
Figure 32: <i>Spatiotemporal features of WAVE2-GFP at the T cell:APC interface are lost and are more transient without CD28 co-stimulation</i>	86

Figure 33: <i>Most actin regulators show reduced enrichment at the T cell:APC interface without CD28 co-stimulation</i>	87
Figure 34: <i>Spatiotemporal features of Vav1-GFP at the T cell:APC are diminished and more transient without CD28 co-stimulation</i>	88
Figure 35: <i>Activated Rac1 sensor recruitment to the T cell:APC interface is more transient without CD28 co-stimulation</i>	89
Figure 36: <i>Enrichment of Vav1 and the active Rac1 sensor at the T cell:APC interface is reduced and less sustained without CD28 co-stimulation</i>	90
Figure 37: <i>Systems-scale changes in spatiotemporal organization of the actin regulatory machinery without CD28 co-stimulation</i>	91
Figure 38: <i>Constitutively active Rac1 and Cofilin restore actin and WAVE2 enrichment at the T cell:APC interface when CD28 co-stimulation is blocked</i>	92
Figure 39: <i>Constitutively active Rac1 and Cofilin restore AKT phosphorylation when CD28 co-stimulation is blocked</i>	93
Figure 40: <i>Constitutively active Rac1 and Cofilin dose not restore IL-2 production when CD28 co-stimulation is blocked</i>	94
Figure 41: <i>Outline of parameters required for generation of 4D models to quantify contribution of CD28 costimulation to actin dynamics during early T cell activation</i>	95
Figure 42: <i>Volume measurements of 5C.C7 T cells</i>	96
Figure 43: <i>Quantitative immunoblots of actin regulators</i>	97
Figure 44: <i>Cell-to-cell variability in actin regulator expression</i>	98

Figure 45: <i>Cell-to-cell variability in expression of actin regulatory proteins plotted against the mean expression level in transduced T cells.....</i>	99
Figure 46: <i>Protein expression scales with T cell size</i>	100
Figure 47: <i>Actin regulation is highly dynamic during early T cell activation.....</i>	101
Figure 48: <i>High-throughput determination of dynamic local molar concentrations of molecules in live cells for modeling of spatial regulation of cellular signal transduction</i>	102

LIST OF TABLES

Table 1: Fluorescent sensors for the assessment of the spatiotemporal organization of early T cell activation	28
---	----

LIST OF DEFINITIONS

APC – Antigen-presenting cell

ARP2/3 – Actin related protein 2/3

BSA – Bovine serum albumin

CofilinCA – Constitutively active Cofilin

CCD – Charge coupled device

CCF – Cross-correlation coefficient

CD – Cluster of differentiation (e.g. CD4)

CD2AP – Cluster of differentiation 2 associated protein

Cdc42 – Cell division control protein 42 homolog

Cin85 – Cbl-interacting protein of 85 kDa

CP α 1 – Capping protein α 1

CRAC – Calcium release activated channel

cSMAC – Central supramolecular activation cluster

CXCR4 – CXC chemokine receptor 4

DIC – Definition goes here

DMEM – Dulbecco's modified Eagle's medium

ELISA – Enzyme-linked immunosorbent assay

F-actin – Filamentous actin

FBS – Fetal bovine serum

GEF – Guanine nucleotide-exchange factor

GFP – Green fluorescent protein

Grb2 – Growth factor receptor-bound protein 2

HS1 – Hematopoietic lineage cell-specific protein 1

ICAM1 – Intercellular adhesion molecule 1

IL – Interleukin (e.g. IL-2)

IPTG – Isopropyl-beta-D-thiogalactopyranoside

ITAM – Immunoreceptor tyrosine-based activation motif

Itk – Interleukin 2 inducible T cell kinase

JASP – Jasplakinolide

kDa – kilo Dalton

LatA – Latrunculin A

LAT – Linker of activated T cells

Lck – Leukocyte-specific protein tyrosine kinase

LFA – Lymphocyte function-associated antigen

MAPK – Mitogen-activated protein kinase

MHC – Major histocompatibility complex

MLCK – Myosin light chain kinase

MTOC – Microtubule-organizing center

MRLC – Myosin regulatory light chain

mRNA – Messenger ribonucleic acid

NF κ B – Nuclear factor kappa-light-enhancer of activated B cells

NFAT – Nuclear factor of activated T cells

NPF – Nucleation-promoting factor

PBS – Phosphate buffered saline

PH – Plekstrin homology

PIP₃ – Phosphatidylinositol (3,4,5) triphosphate

PIP₂ – Phosphatidylinositol (4,5) bisphosphate

PI3K – Phosphoinositide 3-kinase

PKC – Protein kinase C

PLC – Phospholipase C

PP – Protein phosphatase

pSMAC – Peripheral supramolecular activation cluster

Rac1 – Ras homolog gene family member 1

Rac1CA – Constitutively active Rac1

RhoA – Ras homolog gene family member A

RPMI – Roswell Park Memorial Institute medium

SDS-PAGE – Sodium dodecyl sulfate polyacrylamide gel electrophoresis

SH2 – Src homology 2

SH3 – Src homology 3

SKAP55 – Src kinase-associated phosphoprotein of 55 kDa

SLP-76 – SH2 domain containing leukocyte protein of 76 kDa

STIM – Stromal interaction molecule

TCR – T cell receptor

TIRF – Total internal reflection fluorescence

WASp – Wiskott-Aldrich syndrome protein

WAVE2 – WASp-family-verprolin homologous protein 2

Y – Tyrosine

ZAP-70 – ζ-associated protein of 70 kDa

CHAPTER ONE

INTRODUCTION

T cell activation and coordinated signaling at the T cell:APC interface

T cell activation occurs through cellular interaction with an antigen-presenting cell (APC). T cells utilize their major antigen receptor, the T cell receptor (TCR), to sense often low numbers of major histocompatibility complexes (MHC) loaded with antigenic peptides derived from pathogens or altered host proteins (e.g. from cancer cells) on the surface of APCs. This initial recognition event along with co-stimulatory receptor engagement results in T cell activation [1], which culminates in a variety of T cell responses including cytokine production, T cell help for induction of humoral immunity, and direct killing of cancer or infected cells [2]. T cells also undergo clonal expansion in response to antigen and subsequently differentiate into multiple T cell subsets that provide varied functionality for eradication of the host insult [3]. In order for T cells to perform such functions, the T cell must first coordinate a large-scale T cell signaling network at the cellular junction with the APC for activation [4,5,6,7].

The activating interface between the T cell and APC has been studied for over two decades, most rigorously from the T cell perspective. Upon TCR engagement, the T cell instantly coordinates a host of signaling molecules in space and time at the interface [7]. The first studies revealing higher order organization of molecules at the T cell:APC interface were performed by Abraham Kupfer's group. Critical molecules required for T cell activation such as the TCR, protein kinase C θ (PKC θ), lymphocyte function-

associated antigen 1 (LFA1), and talin not only polarize to the interface but also further segregate into specific interface regions. The TCR and PKC θ localize to the interface center while LFA1 and talin are in a ring structure around the centrally localized molecules. A static *en face* view of the T cell:APC interface is thus segregated into a bulls-eye like structure with the center termed the central supramolecular activation cluster (cSMAC) and the surrounding ring the peripheral SMAC (pSMAC) . These observations elicited numerous questions that apply both to mechanisms governing T cell activation, and more general cell biological questions involving the control of cell signaling by a parameter of signal transduction referred to as spatiotemporal organization [4]. First, can we provide a comprehensive view of T cell signaling in space and time under physiologically relevant conditions? Second, what are the critical mechanisms that organize the T cell signaling machinery? Finally, does spatiotemporal organization matter and how does it contribute to T cell activation and function?

Soon after the seminal findings by the Kupfer group, Dustin and colleagues further characterized and provided mechanistic insight into formation of what would become known as the immunological synapse (IS) [5]. Unlike the previous work performed with T cell:APC conjugates, T cells were stimulated on supported lipid bilayers embedded with peptide MHC (pMHC) and intracellular adhesion molecule 1 (ICAM-1). While the overall structure of the T cell:APC interface was recapitulated by bilayer-mediated activation, the kinetics of molecule segregation were significantly slowed compared to activation on an APC. Notably, the clustering of MHC at the interface center took nearly 5 minutes [5] whereas similar central enrichment is essentially instantaneous with primary *ex vivo* mouse T cells stimulated with antigenic

peptide-loaded MHC [7]. Presumably, such discrepancies are due to lack of signal integration from co-stimulatory receptors such as cluster of differentiation 28 (CD28), which is critical for maintenance of signaling at the T cell:APC interface [8,9,10]. Functional importance of the cSMAC was shown as its formation correlated with the T cell proliferative response. Subsequent research on the importance of formation of the cSMAC has proven controversial as there is evidence that signaling complexes turn over rapidly in the region (negative regulation) [11,12,13,14] and there is also evidence that it is a region of intense and active signaling (positive regulation) [7,15]. These two functions of the cSMAC, signal dampening and amplification, are not mutually exclusive and likely occur in parallel.

High resolution imaging of the IS with T cells activated on coated antibody coverslips or supported lipid bilayers led to the discovery of signaling microclusters (MC) composed of the TCR and proximal signaling intermediates such as leukocyte-specific protein tyrosine kinase (Lck), ζ -associated protein of 70 kDa (ZAP-70), linker of activated T cells (LAT), Src-homology 2 (SH2) domain-containing leukocyte protein of 76 kDa (SLP-76), and growth factor receptor-bound protein 2 (Grb2). Microclusters were shown to form in an actin-dependent manner in the IS periphery and then moved via centripetal actin retrograde flow to the cSMAC [11,12,13,16]. The requirement of actin dynamics for the recruitment and segregation of molecules into large scale patterns of accumulation at the T cell:APC interface as well as formation and directed movement of microcluster in T cells activated on APC substitutes elicited intensive research on the regulation of actin dynamics required for T cell activation.

Actin cytoskeleton regulation in T cells

Actin is a globular ATP binding protein that polymerizes into filamentous actin (F-actin). Nucleation of actin filaments is energetically unfavorable; therefore, cells have a host of actin regulatory proteins to regulate the formation of F-actin and its turn over. Actin filaments have intrinsic polarity where the barbed end (growing end) favors actin monomer addition and disassociation rates are slow, and the pointed end favors actin monomer release. This disparate behavior at the opposing ends of actin filaments causes the characteristic actin tread milling that provides force generation in cells [17]. The ATP status of the actin monomers changes along the filament length with ATP-actin at the barbed end and ADP-P_i-actin and ADP-actin monomers closer to the pointed end. The status of the ATP provides a marker of filament age and regulates turn over [18]. The overall regulation of the assembly and turn over of actin filaments as well as entire interconnected actin networks allows cells to coordinate a wide variety of cell processes such as polarized signaling, vesicle trafficking, and phagocytosis.

TCR and co-stimulatory receptors induce rapid polymerization of actin at the T cell:APC interface [19,20]. Pharmacological interference and genetic alteration of the actin regulatory network has established that actin dynamics are critical for T cell activation and function, e.g. in the regulation of cell conjugate formation, receptor clustering, lytic granule release, directed cytokine release, and activation of transcription factors. T cell actin dynamics are regulated by coordinated nucleation, polymerization, stabilization, capping, and severing of actin filaments [19,20]. Currently, the actin network at the T cell:APC interface is thought to be largely generated by actin related

protein 2/3 (ARP2/3)-dependent branched actin polymerization [20,21]. For branched actin nucleation to proceed in T cells, a variety of upstream signaling events must ensue generally as a result of TCR and CD28 engagement. The most prominent pathways that result in actin regulation involve the activation of the Rho-family guanine nucleotide exchange factor (GEF), Vav1 [22], and subsequent activation of the Rho-family GTPases ras homolog gene family member 1 (Rac1) and cell division control protein 42 homolog (Cdc42) [23]. Rac1 and Cdc42 once in a guanosine triphosphate (GTP) bound active state contribute to activation of the nucleation-promoting factors (NPF) WASP-family-verprolin homologous protein 2 (WAVE2) and Wiskott Aldrich Syndrome protein (WASp), respectively [24,25,26]. Activated WAVE2 and WASp then bind ARP2/3 on the sides of filamentous actin (F-actin) and facilitate the energetically unfavorable nucleation of a new actin filament branch [27]. Once filaments begin to polymerize a host of actin regulatory molecules control their maintenance and turn over. Hematopoietic lineage cell-specific protein 1 (HS1) contributes to filament stabilization [28], capping protein binds to the barbed end of actin filaments preventing further polymerization [29], and Cofilin severs actin filaments releasing actin monomers and generating new barbed ends for further polymerization and branching by ARP2/3 [30,31]. Actin based motor proteins such as Myosins also regulate actin networks by generating contractile forces on adjacent actin filaments [32]. Recent studies have also implicated Myosins in depolymerization of F-actin and thus turn over of actin networks [33]. Other proteins such as the negative regulator of the ARP2/3 complex, Coronin1A, further contribute to the maintenance of actin levels at the T cell:APC interface [34,35]. The balance of activation of the NPFs, stabilization factors, and severing factors controls the longevity of

actin networks as their relative activities can rapidly generate or collapse actin meshworks.

The importance of actin regulation for T cell function

It is clear that nearly all aspects of actin regulation are required for optimal signaling at the T cell:APC interface and subsequent T cell activation. The loss or altered activity of any one of the components of the actin regulatory machinery described above has severe consequences usually for multiple aspects of T cell biology. Vav1 is essential for actin dynamics at the T cell:APC interface, T cell activation, cytokine production, and polarized cell adhesion [36,37,38,39]. These effects are due to the role of Vav1 in a wide range of actin regulatory processes from activation of the Rac1 and Cdc42 to its recruitment of HS1 [28] to the T cell:APC interface.

WASp deficiency has severe effects on T cell function, which results in a primary immune deficiency called Wiskott Aldrich Syndrome (WAS) in humans [40]. Early work on the control of actin dynamics in T cells was focused on WASp due to its relevance to human disease. Initial studies showed that WASp was required for polarized F-actin production, T cell:APC conjugate formation, regulation of TCR internalization, and overall T cell activation [24,41,42]. Later work contradicted these initial studies providing evidence that T cell:APC conjugate formation occurs without WASp and WASp is dispensable for polarized actin dynamics at the T cell:APC interface [43,44]. However, importance of WASp for T cell function is not in dispute. It is currently not clear whether immunodeficiency caused by mutations in WASp is a result of inability of

WASp to regulate actin dynamics or an inability to perform an unrelated function [45]. WASp must remain bound to WASp interacting protein (WIP) for maintained stability. Many of the WAS causing mutations are in the WASP-homology domain (WH1) domain of WASp, which is the domain required for WIP interaction [46,47]. Therefore, altered WIP levels or activity may also contribute to the immunodeficiency. In fact, WIP deficiency causes a more drastic impairment of actin dynamics in T cells [48].

The WAVE2 complex has recently gained more attention given the finding that knockdown of WAVE2 prevents polarized actin dynamics at the T cell:APC interface [43]. Thus, WAVE2 is now thought to be the major activator of the ARP2/3 complex in T cells rather than WASp. WAVE2 requires multiple signals for its activation including acidic phospholipids such as phosphatidylinositol (3,4,5) triphosphate (PIP₃), phosphorylation, and Rac1 activity [26,49]. Given the requirement for coincident signals for WAVE2 activation, its activity at the T cell:APC interface is likely highly regulated. Loss of WAVE2 impairs T cell cytokine production, Ca²⁺ entry via calcium release activated channel (CRAC) channels, and inside-out signaling required for integrin activation [43,50].

HS1 is a leukocyte-specific homolog of the actin regulatory molecule Cortactin. HS1 is recruited to the T cell:APC interface in a phosphorylation-dependent manner and has the ability to catalyze ARP2/3-mediated actin polymerization and aid in the stabilization of actin filaments [28,51]. At least in T cells, the later function of HS1 seems to dominate, as HS1 is not efficient at activating the ARP2/3 complex when compared to WASp and WAVE2. HS1 also acts to sustain Vav1 activity at the T cell:APC interface. Deficiency in HS1 causes multiple T cell defects including disorganized actin

polymerization at the T cell:APC interface, decreased Ca^{2+} signaling, impaired T cell activation, and reduced cytokine secretion [28].

Coronins are actin regulatory proteins that bind F-actin and associate and inhibit the ARP2/3 complex [35]. Coronin1A is a member of the Coronin family that is mainly expressed in hematopoietic cells and when mutated causes a decrease in peripheral T cells via increased apoptosis [52,53]. There has been conflicting evidence on whether Coronin1A is required for T cell migration and whether increased apoptosis is due to altered T cell signaling rather than increased actin levels [54]. A more recent study on mice with a Coronin1A mutation that increases its inhibition of ARP2/3 showed impaired T cell migration and egress from the thymus. Coronin1A knockout T cells showed even more severely compromised migration [55]. Coronin1A deficiency also increases enrichment of the actin regulators at the T cell:APC interface and causes defects in extracellular Ca^{2+} entry and nuclear factor kappa-light-enhancer of activated B cells (NF κ B) activation [56]. Therefore, enhancing or decreasing Coronin1A activity impairs actin-dependent functions in T cells.

While regulators of ARP2/3 are important for T cell function, other more general regulators of actin are also required. Cofilin binds to actin preferentially at the ageing (ADP-Pi or ADP-bound actin monomers) pointed end and severs the filament releasing actin monomers. This activity allows for the maintenance of a free pool of G-actin that is recharged with ATP and added to growing actin filaments [30]. Cofilin activity can also mediate the cessation of F-actin enrichment when cellular processes dependent on actin have run their course. Cofilin is important for polarized actin dynamics at the T cell:APC interface, T cell proliferation in response to antigen, and cytokine secretion [57,58].

Capping protein is a heterodimer consisting of an alpha and beta subunit that caps the barbed ends of growing actin filaments. While the importance of capping protein has been assessed in non-mammalian systems and is important for actin mediated processes such as cell migration [29]. *In vitro* reconstitution of actin polymerization with purified actin regulatory molecules revealed capping protein not only binds and prevents further polymerization, but also regulates nucleation of branched actin filaments by ARP2/3 [59]. While CP is a principle regulator of F-actin network assembly, there are no studies that have addressed its importance in T cells.

Myosins are actin-based motor proteins that use ATPase activity for directed delivery of cellular cargo in cells and in addition apply contractile forces to actin networks [32]. More recent studies have even implicated myosins in the depolymerization of F-actin. Non-muscle myosin IIA has been studied in T cells and there is conflicting evidence for its role in regulation of signaling at the T cell:APC interface [33]. An initial study performed in T cell:APC conjugates showed T cell migration was defective, but polarization of the TCR, LFA-1, actin, and the microtubule organizing center (MTOC) was intact when myosin activity was inhibited [60]. Therefore, myosins were thought to have minimal functional importance in the spatiotemporal organization of T cell signaling. However, a later study using planar bilayers containing α -CD3 and ICAM-1 to activate T cells showed that myosin II was required for microcluster movement, sustained Ca^{2+} signaling, and signaling downstream of Lck [61]. The drastic signaling differences observed in T cells activated on bilayers may be more pronounced due to the lack co-stimulatory receptor engagement that may provide compensatory signals that attenuate the effects of loss of myosin activity. The

importance of myosin II in the turn over of actin networks at the T cell:APC interface has not been assessed.

Research on the actin regulatory network in T cells as described above usually involves the inhibition of one or two actin network components and determination of the effects on T cell conjugate formation, polarized actin dynamics, T cell signaling organization and activity, and cytokine production [19,20]. Actin dynamics are not mediated through the activity of individual actin regulators but the concerted activity of the proteins described above. A major challenge in the field is to provide systems-level understanding of actin regulation in live T cells and delineate the contribution of specific signaling events such as CD28 signaling to coordinated activity of the entire actin regulatory network.

Regulation of signaling at the T cell:APC interface by co-stimulation

T cells have a range of co-stimulatory receptors that provide either positive or negative regulatory signals that control T cell activation. The co-stimulatory receptor CD28 has historically been the most heavily studied as CD28 signaling is critical for T cell activation (especially for naïve T cells) [62,63]. CD28 binds both B7-1 and B7-2 on the APC, which initiates recruitment of molecules such as phosphoinositide 3-kinase (PI3K), Grb2, and IL-2 inducible T cell kinase (Itk) to its cytoplasmic tail [64,65]. These molecules are in turn activated and stimulate signaling cascades that result in T cell survival, proliferation, cytokine production, and regulation of actin dynamics. Because the TCR and CD28 activate many of the same pathways, it has been a challenge to

determine whether CD28 simply amplifies TCR signaling to reach a threshold for T activation or also provides unique signals. Much of the evidence supports the former view of CD28 signaling as a quantitative support for TCR signaling [65,66]. The importance of CD28 can be demonstrated in a simple scenario where T cell must react to a limited number of pMHC complexes and CD28 and its ligands with their higher expression provide support for TCR signaling thus bringing the threshold of pMHC molecules down for T cell activation [67]. In support of this, we have shown that concomitant blockade of CD28 signaling with a 100-fold reduction in antigen dose causes the most severe effects to the spatiotemporal organization of signaling at the T cell:APC interface. CD28 signaling also promotes actin cytoskeleton dependent recruitment of molecules to the T cell:APC interface and sustained actin dynamics for maintenance of proximal T cell signaling intermediates [8,9,10].

Conclusions

A large-scale network of actin regulatory molecules controls T cell actin dynamics and the efficiency of T cell activation. Work in this thesis demonstrates the importance of actin in the organization and activation of a large-scale network of proximal T cell signaling molecules and the contribution of actin dynamics to the architecture of the T cell:APC interface. Furthermore, we provide a quantitative and systems-level overview of actin regulation in T cells and assess the contribution of CD28 co-stimulation to actin dynamics.

CHAPTER TWO

MATERIALS AND METHODS

Antibodies, purified Proteins, and reagents

Antibodies used for quantitative immunoblotting were rabbit α - β actin (Cell Signaling #4967), mouse α -ARP3 Clone FM5338 (Sigma-Aldrich #A5979), chicken α -Capping Protein α 1 (Genway Biotech #15-288-21950F), mouse α -Cofilin (Cell Signaling #3312), mouse α -Coronin1A (Santa Cruz Biotechnology #SC-100925), rabbit α -HS1 (Cell Signaling #4557), rabbit α -WASP (Cell Signaling #4860), rabbit α -WAVE2 (D2C8) XP (Cell Signaling #3659), and mouse α -GFP living colors JL-8 (Clontech #632380).

Antibodies used for immunoblots for monitoring proximal T cell receptor signaling were rabbit α -LAT pY191 (Cell Signaling #3584), rabbit α -LAT (Cell Signaling #9166), rabbit α -PKC θ pT538 (Cell Signaling #9377), rabbit α -PKC θ (Cell Signaling #2059), rabbit α -VAV1 pY174 (Sigma-Aldrich #SAB4300117), and mouse α -SLP76 pY128 (BD Pharmingen #558367). Secondary antibodies for mouse (CS# 7076) and rabbit antibodies (CS# 7074) were purchased from Cell Signaling. The α -chicken IgY secondary was purchased from Millipore.

Antibodies for fixed cell microscopy were Alexa 488 conjugated mouse α -SLP76 pY128 (BD Pharmingen #558439) and rabbit α -LAT pY191 (Cell Signaling #3584). For pY191 LAT stains an Alexa 488 conjugated goat α -rabbit IgG (Invitrogen #A-11008)

was used. F-actin was stained with Alexa 633 conjugated Phalloidin (Invitrogen #A22284). Cell Trace Violet was used as a whole cell stain for the CH27s (Invitrogen #C34557).

Purified proteins used for quantitative immunoblot standards were β -actin (abcam #40624), ARP2/3 protein complex (Cytoskeleton #RP01), Capping Protein α 1 (Genway Biotech #10-288-21950F), Cofilin (Cytoskeleton #CF01-A), and EGFP (BioVision #4999-100).

Antibodies used for blockade of B7-1/2:CD28 co-stimulation were α -mouse CD80 Clone 16-10-A1 (BD Pharmingen #553736) and α -CD86 Clone GL1 (BD Pharmingen #553689). For IL-2 intracellular stain experiments with actin regulatory drugs α -Ie^k Clone 14-4-4S (BD Pharmingen #558735) and the α -mouse IL-2 PE (BD Pharmingen #554428) were used.

Antibody stimulation of T cells was performed with α -CD3 ϵ Clone 145-2C11 (BD Pharmingen #553057) and α -CD28 Clone 37.51 (BD Pharmingen 553295).

Mice and cells

T cells extracted from lymph nodes of B10.BR 5C.C7 TCR transgenic mice were used for all experiments unless otherwise noted. 5C.C7 mice harbor only CD4⁺ T cells, which express a TCR that recognizes the moth cytochrome c peptide fragment 88-103 (ANERADLIAYLKQATK) in the context of I-e^k [68]. Single cell suspensions were made from the lymph nodes of 6-8 week old mice. The cells were adjusted to 4x10⁶ cells/mL and MCC peptide was added to 3 μ M. The cells were then plated at 1mL/well of a 24 well

tissue culture plate. The T cells were stimulated for 24 hours in a 37°C humidified tissue culture incubator at 6% CO₂ and used for retroviral transduction. All animals were maintained in the pathogen-free animal care facility at the University of Texas Southwestern Medical Center and the care and use of the mice was approved by the University of Texas Southwestern Animal Care and Use Committee.

The CH27 B cell lymphoma cell line was used in all experiments as antigen presenting cells (APC). To load the APCs, the cells were incubated in the presence of 10μM MCC peptide for at least 4 hours.

All cells were maintained in T cell medium composed of RPMI with L-Glutamine, 10% fetal bovine serum (FBS) (Hyclone), 100 IU/mL penicillin, 100μg/mL streptomycin, and 0.5μM β-mercaptoethanol. IL-2 was added to 0.05 U/mL during parts of the retroviral transduction procedure described below.

Retroviral transduction

All fluorescently tagged signaling sensors (table 1) were cloned into the pGC-IRES Moloney murine leukemia virus-derived retroviral vector. Retrovirus was produced by the Phoenix helper-free retrovirus producer cell line (Nolan Lab, Stanford U.) plated on 60cm Falcon Primaria tissue culture plates. Phoenix cells at near 70% confluency were transfected with 10ug of the appropriate plasmid via calcium phosphate transfection on day 0. Transfection medium was replaced 12 hours later on day 1 with 3mLs of fresh medium containing DMEM high glucose (4.5g/L), 10% FBS, L-Glutamine, 100 IU/mL penicillin, 100μg/mL streptomycin, and non-essential amino acids. Phoenix cells were

not kept under selection with diphtheria toxin (List Biologics) and Hygromycin B (Fisher Scientific) during the procedure. On day 2, T cells were prepared as described above and stimulated overnight. On day 3, viral supernatant was removed from each plate of transfected Phoenix cells, centrifuged briefly and 2mLs of the supernatant was added to 4×10^6 T cells (1 well of T cells on a 24 well plate). To facilitate retroviral transduction, the cells were centrifuged at 2500rpm for 2 hours at 32°C in a 24 well tissue culture plate. After spinfection, the plates were put back in the 37°C incubator overnight. The morning of day 4, the viral supernatant was carefully removed and replaced with T cell medium containing IL-2. The T cells were then allowed to grow until day 7. On day 7, the T cells were sorted based on their fluorescence intensity (usually GFP). All cells were sorted on a Mo Flo high-speed cell sorter (Beckman Coulter). Forward and side scatter was used to delineate live cells and single cells were gated on by pulse-width characteristics. Fluorescent T cells expressing the fluorescently tagged protein of interest 1-1.5 logs from the negative population were then sorted and used in all imaging experiments.

Antibody stimulation and APC stimulation of T cells

For experiments to quantify active Cofilin in response to TCR stimulation, T cells were incubated at 37°C with 10µg/mL α -CD3 ϵ Clone 145-2C11 (BD Pharmingen #553057) and α -CD28 Clone 37.51 (BD Pharmingen 553295) in imaging buffer without FBS (PBS, 1mM CaCl₂, 0.5mM MgCl₂) for the indicated period of time. The cells were

then lysed at a final concentration of 1×10^7 cells/mL as described below and assessed by Phos-tag SDS-PAGE followed by immunoblotting.

For experiments assessing the affect of disruption of the actin cytoskeleton on early TCR signaling events, peptide-loaded APCs were used to stimulate the T cells. Briefly, 1×10^6 5C.C7 T cells and equal numbers of peptide loaded CH27s were resuspended in imaging buffer containing MCC peptide but no FBS at a concentration of 1×10^7 cells/mL. Jasplokinolide or Latrunculin A (both from Calbiochem) was added as indicated (40nM Jasplokinolide, 10nM Latrunculin A) to both the T cells and APCs and the cells were incubated for 10 minutes in a 37°C water bath before mixing. Since the drugs were resuspended in DMSO, and T cells are sensitive to relatively low levels of the reagent, we kept the amount of DMSO to 0.5% of the imaging medium. 1×10^6 5C.C7 T cells were then mixed 1:1 with the CH27s and centrifuged at 2000rpm for 15 seconds. This forces contact between the cells and is considered time 0. Cells were immediately placed back into a 37°C waterbath and allowed to incubate for the indicated time points. The cells were immediately frozen in liquid N₂ and subsequently lysed at a final concentration of 1×10^7 cells/mL as described below.

Quantitative immunoblotting, immunoblots, and Phos-tag immunoblots

5C.C7 T cells expressing each of the actin regulatory proteins were sorted and lysed under standard conditions. Briefly, precise numbers of T cells were sorted into PBS and lysed in 1% Triton X-100 lysis buffer pH 7.6 containing 20 mM Tris-HCl, 150 mM NaCl, 2 mM EDTA and supplemented with protease and phosphatase inhibitors (1mM

PMSF, 50 μ M Leupeptin, 1 μ M Pepstatin A, 10mM NaF, 200 μ M NaOrthovanadate). For quantitative immunoblotting a known number of T cells was loaded onto a 10% SDS-PAGE gel alongside purified protein standards (see *Antibodies, Purified Proteins, and Reagents*). A standard curve was generated from the densitometry measurements for each purified protein standard and the nanogram level of endogenous protein and retrovirally expressed GFP-tagged protein was simultaneously calculated per T cell based on the standard curve. The nanogram level of protein was converted into an average single T cell molar concentration based on the average size of a 5C.C7 T cell (see *T cell Volumetric Analysis*) and the kDa size of the protein. Proteins for which the purified protein was not available, the GFP-tagged protein band was used to calculate the endogenous level. Based on previous work, we have determined that the average single cell molar concentration of GFP-tagged protein in our sort gate (1 to 1.5 logs from the negative population) is 2.6 μ M. Thus, the ratio of the densitometry measurements of the endogenous protein band and the retrovirally expressed GFP-tagged protein band was used to calculate endogenous levels of the protein. All other immunoblots not requiring protein standards were performed according to standard immunoblot procedures. All antibodies used for immunoblots are cataloged in the above section.

Phos-tag immunoblots used to determine the amount of phosphorylated Cofilin (pS3) were performed according to the manufacturer protocol (NARD #AAL-107). Briefly, cells were lysed as described above. For all Phos-tag experiments, 10% SDS-PAGE gels were made with 100 μ M Phos-tag reagent and 200 μ M MnCl₂. Electrophoresis of Phos-tag gels proceeds according to standard procedures. Before transfer to PVDF for

immunoblotting, the Phos-tag gel was washed twice in 100mLs of transfer buffer containing 1mM EDTA to remove MnCl_2 and facilitate efficient protein transfer.

Time-lapsed imaging of T cell:APC interactions

Time-lapsed fluorescent microscopy was performed with retrovirally transduced T cells generated as described above and CH27 APCs loaded with 10 μM MCC unless otherwise noted. T cells and APCs were imaged in imaging buffer (PBS, 10% FBS, 1mM CaCl_2 , 0.5mM MgCl_2) on 384 well glass bottom plates (Matrical MGB101-1-2-HG). All imaging of actin regulatory proteins and actin was performed on a Perkin Elmer spinning disk confocal systems fitted onto a Zeiss Axiovert 200M microscope body equipped with full environmental control, a Hamamatsu C9100-50 EMCCD, and 6 laser lines from 405 to 647nm. A Zeiss PlanFluoro 40x oil objective (NA=1.3) was used for all imaging. Automated control of the microscope was performed with Volocity software (Perkin Elmer). For each time-lapsed imaging experiment, from 3×10^5 to 6×10^5 5C.C7 T cells were added to the imaging plate followed by addition of peptide loaded CH27s. Once the CH27s had settled, cell interactions were imaged for 15 minutes (46 time points spaced 20 seconds). At each time point, a DIC reference image was collected and a fluorescent z-stack consisting of 51 z-planes with a 0.4 μm step-size (total z-volume=20 μm). Time-lapsed images were analyzed with Metamorph (Molecular Devices), Image J (NIH, <http://rsb.info.nih.gov/ij/>), and Imaris (Bitplane).

For experiments where B7-1/2:CH28 co-stimulation was blocked, peptide loaded CH27s were incubated on ice for 30 minutes in the presence of 10 $\mu\text{g/mL}$ $\alpha\text{-CD80}$ Clone

16-10-A1 and α -CD86 Clone GL1 (BD Pharmingen) antibody before adding APCs to imaging plate with the T cells. The antibodies were present in the imaging medium at 10 μ g/mL during the entire acquisition period to ensure full blockade.

For experiments with Jasplakinolide and Latrunculin A (Calbiochem), T cells were incubated for 10 minutes in the imaging well with drug concentrations of 40nM and 10nM, respectively. After the 10 minute incubation, the CH27s were added to the well and imaging was performed as previously described.

Long-term time-lapsed fluorescence microscopy of T cell:APC conjugates

All long-term imaging was performed with the Perkin Elmer spinning disk microscope described above. In addition a Pathological Devices LiveCell chamber was fitted over the 384 well imaging plate. This chamber kept the imaging plate humidified to prevent evaporation, which is a major issue when imaging cells suspended in buffer volumes from 50 to 100 μ l. For further prevention of evaporation, neighboring imaging wells were filled with sterile water. Antibiotics were also added to the imaging buffer to prevent bacterial growth. Because T cells and APCs clump and obscure analysis of single cells during long-term imaging experiments a method to adhere the APCs to the glass was developed. First, biotinylated BSA (Pierce Biotech #29130) was diluted to 1mg/mL in T50 buffer containing 10mM Tris-HCl pH 8.0 and 50mM NaCl. The T50 buffer containing biotinylated BSA was heated to 37°C and added to the imaging well for 5 minutes. A brief wash with T50 buffer was then performed followed by addition of 50 μ l of 0.2mg/mL neutravidin (Pierce Biotech #31000) to the imaging well for 1 minute at

37°C. The imaging well was then washed 1x with T50 buffer and 2x with imaging buffer without FBS. Now the glass is prepared to bind any biotinylated antibody of choice. For experiments with the CH27 B cell lymphoma line, a α -CD19 antibody (BD Pharmingen #553784) was used to adhere the cells. The antibody was diluted in imaging buffer containing FBS, antibiotics, and MCC peptide to 10 μ g/mL and was allowed to bind to the prepared glass of the imaging well for 10 minutes at 37°C. After the glass was prepared with antibody, the APCs were added to the well and allowed to settle and immobilize (~5 minutes). Once the APCs are immobilized, the T cells were added and image acquisition proceeds as previously described. Focus drift is a problem for the long-term imaging experiments but can be monitored and adjusted.

Image analysis

Analysis of the spatiotemporal organization of signaling sensors at the T cell:APC interface during early T cell activation has been previously described in detail[7]. Pattern classification criteria are shown in figure 1.

For the actin regulatory proteins, an enrichment index was calculated by measuring the fluorescence intensity in the area of accumulation (region 1.35x the cellular background) at the interface and dividing it by the average intensity of the cell. The fold-enrichment value at each time point was then multiplied by the fraction of T cells that showed enrichment of the protein at the corresponding time point. An enrichment index value was calculated for each time point analyzed from -20 seconds before cell conjugate formation to 7 minutes after conjugate formation.

To calculate the accumulation index, interface enrichment was calculated by measuring the intensity in the area of accumulation and then dividing it by the average intensity of the cell. This fold-enrichment value was then multiplied by the fraction of T cells that show accumulation at the corresponding time point. Finally, the resulting value was multiplied by the accumulation volume to obtain the ‘accumulation index’. Accumulation volumes were calculated by first measuring the area of accumulation. Then assuming a rough spherical shape for the region of accumulation we calculated the radius of the area of accumulation and converted the 2D area measurement into a spherical volume.

Interface length to diameter ratios measured for electron micrographs of T cell:APC conjugates were calculated as described in figure 2A.

The depth to width ratio of F-actin structures in Phalloidin stained T cell:APC conjugates imaged by STED was determined by first identifying interface F-actin structures 1.35x the cellular background, then measuring their depth perpendicular to the interface plane and width parallel to the interface (analysis methodology in fig 2B). The average intensity to area ratio was also calculated for each F-actin structure.

Actin and lamellal localized signaling intermediate depth measurements were calculated using the box tool in Image J (NIH). Colocalization analysis for pSLP-76 and F-actin was performed with the JACoP plugin [69] for Image J. Briefly, a binary mask for each channel was generated by linear thresholding and colocalization was assessed by calculation of the Pearson’s correlation coefficient, Mander’s overlap coefficient, and colocalization measurements were substantiated by calculation of a Van Steensel’s cross correlation function where one channel was shifted in the x-dimension and the change in

the PCC was plotted. Sharp drop off of the PCC is observed as one channel is shifted providing evidence that colocalization values are valid. Phosphorylated SLP-76 cluster depth was assessed by line scans. First, a line was drawn perpendicular to the T cell:APC interface plane from the interior of the APC through the phosphorylated SLP-76 cluster. The APC boundary was defined as the point at which APC fluorescence dropped to half-maximum along the line. The boundary of the APC was considered 0, and the cluster depth was measured at the center of the fluorescence profile of the phosphorylated SLP-76 cluster. Phosphorylated SLP-76 clusters were evaluated with the Object Counter 3D plugin for Image J. Linear thresholding was first performed to delineate objects above the calculated cellular background and the plugin identified cluster features such as size and intensity in the 3D volume. Interdigitated T cell:APC interfaces were identified by assessing the relation of the APC outline delineated (Cell Trace Violet) to pSLP-76 clusters. If the APC outline extended into the T cell or past interface clusters of pSLP-76 the interface was considered interdigitated.

T cell volumetric measurements

T cells were labeled with SNARF-1 (Invitrogen #S22801) as a whole cell stain and Hoechst 34580 (Invitrogen #H21486) to delineate the nucleus. T cells were imaged with the Perkin Elmer spinning disk confocal described above. Whole T cell volume measurements and nuclear volume measurements were calculated by first measuring the full-width half maximum of the Gaussian profile from line scans across the center plane of each T cell (SNARF, red channel) and nucleus (Hoechst, blue channel). Once the

radius of the cell and nucleus was calculated, the upper and lower intensity values were set for each channel and object surfaces and volumes were measured for the whole T cell and the nucleus in Imaris (Bitplane).

Fluorescence recovery after photobleaching (FRAP)

For all FRAP experiments, T cells were incubated with peptide loaded CH27s in imaging plates as described above. Individual T cell:CH27 conjugates were focused on and bleaching was done within the first 2 minutes of cell conjugate formation. A pDVRT Deltavision deconvolution microscope equipped with an environmental chamber, a Quantitative laser module for FRAP, an Olympus APO 40x oil objective (NA=1.3), and Cool Snap HQ2 camera was used. The microscope was controlled with Deltavision SoftWoRx software. The 488 laser line and appropriate filter set was used for all FRAP experiments given that the proteins imaged were GFP fusions. The bleaching protocol was set to acquire 3 prebleach images and then 10x10ms laser pulses (100% power) bleached a ~1µm Gaussian spot at the T cell:APC interface to near 50% of the prebleach intensity. Cells in which the total fluorescence of the cell was depleted by more than 10% were not analyzed. Post bleach images were acquired every 255ms for a total of 30 seconds to 2 minutes depending on the protein. Analysis of recovery was performed manually in Image J by calculating the intensity in the bleach spot before and after bleaching. Background subtracted data was normalized to the average intensity of the 3 prebleached images and was fitted in Prism software with the equation $Y_{(t)} = (Y_{\max} - Y_{\min})(1 - e^{-kt}) + Y_{\min}$. $Y_{(t)}$ is the intensity of fluorescence at time t, Y_{\max} and Y_{\min} are the

maximum and minimum intensities of fluorescence post-bleaching and k is the rate constant of recovery [70]. In all cases, the half-time of recovery was derived from at least 10 fitted recovery curves together with the s.e.m.

Fixed T cell:APC conjugate preparation and fluorescence imaging

5C.C7 T cells and CH27s were used for all fixed cell imaging. T cells and peptide loaded CH27s were resuspended in imaging buffer without FBS to facilitate binding to poly-L-lysine coated coverslips. The CH27s were first added to the coverslip as a 50 μ l drop and allowed to adhere in the 37°C incubator for 5 minutes. T cells were then added to the drop. The T cells settle within about 5 minutes and were allowed to adhere and interact with APCs for a subsequent 5 or 15 minutes (early and late time point, respectively). T cells were then fixed with 4% EM grade paraformaldehyde in PBS at 4°C for 20 minutes. All washes were performed with PBS. Permeabilization was performed with 0.02% TritonX-100 in PBS. Cells were blocked with 1% BSA in PBS or 1% goat serum depending on the antibody for 30 minutes at room temperature. For most antibody stains, the primary antibody was diluted according to antibody specification sheets in 1% BSA PBS and cells were incubated overnight in the presence of antibody at 4°C. Secondary anti-mouse and anti rabbit IgG antibodies were conjugated to either Alexa-568 or 488 (Invitrogen). See the *Antibodies and Purified Proteins* section for a list of antibodies used in these experiments. After the T cell:APC conjugates were stained, the coverslips were mounted on Superfrost Plus microscope slides (VWR) with ProLong Antifade (Invitrogen).

For stimulated-emission depletion (STED) microscopy, we sent our stained slides to the laboratory of Jordan Orange at the University of Pennsylvania (now moved to Baylor College of Medicine). T cells stained with Alexa-488 conjugated Phalloidin or other direct Alexa-488 conjugated primary antibodies were imaged with a Leica TCS STED CW microscope equipped with a 100x HCX APO objective (NA=1.4) controlled with Leica AS AF software. Alexa-488 was excited with a 488nm Argon Laser and STED depletion was achieved with a 592nm wave fiber laser. The fluorescence signal was detected with Leica HyD detectors [71].

A pDV Deltavision deconvolution microscope equipped with a Olympus APO 40x oil objective (NA=1.3), Cool Snap HQ2 camera, and DAPI/FITC/TRITC/CY5 filter sets was used for the 3 color microscopy. The microscope was controlled with Deltavision SoftWoRx software. A single DIC reference image and fluorescent z-stacks (0.2 μ m z-step) were acquired for each field. All fixed cell fluorescence imaging was analyzed with Image J.

Expression and purification of cell permeable tat-tagged proteins

Constitutively active Cofilin (S3A) and constitutively active Rac1 (Q61L) was cloned into a ptat-nde vector which provides a N-terminal tat-tag for protein transduction and a 6x His tag for purification with Ni-NTA. The proteins were expressed in BL21(DE3) *E. coli* at room temperature overnight after induction of expression with 1mM Isopropyl-beta-D-thiogalactopyranoside (IPTG). The bacteria were lysed under native conditions by sonication in lysis buffer containing 4x PBS, 0.01% IGEPAL, 10%

Glycerol, 10mM Imidazole, 1mM MgCl_2 (only added for Rho family GTPases), 1% Lysoszyme, 0.14% β -mercaptoethanol, and protease inhibitors at pH 7.5. The proteins were purified over Ni-NTA resin. After protein binding, the resin was washed twice with wash buffer containing 4x PBS, 20mM Imidazole, 1mM MgCl_2 , and 0.14% β -mercaptoethanol. The protein was then released from the column with elution buffer containing 4x PBS, 250mM Imidazole, 1mM MgCl_2 , and 0.14% β -mercaptoethanol. After elution, the protein was dialyzed into PBS and quantified by SDS-PAGE.

For experiments with tat-fusion proteins, T cells were incubated for 30 minutes at 37°C in the imaging plate prior to addition of peptide loaded CH27s. The image acquisition proceeded as described above.

IL-2 intracellular stains

For IL-2 assays, 1×10^5 T cells were mixed with peptide loaded CH27s at a ratio of 1:1. T cells were stained with Cell Trace Violet (Invitrogen) to distinguish them from the CH27s by FACs and to monitor any changes in proliferation. For experiments with actin drugs, Jasplokinolide and Latrunculin A, 96 well round bottom plates were used and cells were mixed and centrifuged together to force interaction. This lessens the chance that the observed changes in IL-2 are due to altered cell motility. We wanted to only assay the contribution of actin dynamics to early T cell signaling and effects on subsequent IL-2 production. Jasplokinolide and Latrunculin A were added to the culture at a concentration of 40nM and 10nM respectively. A time course was also done where the medium containing the actin drugs was removed after 1 and 6 hrs and medium

containing an antibody to I-e^k was added to block further T cell:CH27 interactions. This prevents the T cells from recovering from signaling defects caused by drug induced changes in actin dynamics by further stimulation by CH27s in drug deplete medium. After 24 hours of incubation, the cells were harvested and stained for IL-2 with the mouse Intracellular Cytokine Staining kit (BD Pharmingen). Cells were analyzed for IL-2 production and Cell Trace Violet with a Becton Dickinson LSR II.

Signaling Sensors	Design	Signaling Sensors	Design
actin	GFP-actin	Nck	Nck-GFP
ADAP	ADAP-GFP	NFκB p65	NFκB p65-GFP
αPIX	GFP-αPIX	PI3kinase	PI3k.SH2.interSH2.SH2-GFP
ARP3	ARP3-GFP	Pacsin1	Pacsin1-GFP
CD2	CD48-GFP (ligand on APC)	PIP ₂	PLCδPH-GFP
CD28	B7-2-GFP (ligand on APC)	PIP ₃	GFP-CytohesinPH
CD2AP	GFP-CD2AP	PIP5K α	PIP5K α-GFP
CD3ε	CD3ε-GFP	PIP5K γ87	PIP5K γ87-GFP
Active Cdc42	WASP.GBD-GFP-CAAX	PIP5K γ90	PIP5K γ90-GFP
Chronophin	Chronophin-GFP	PKCη	PKCη-GFP
Cin85	GFP-Cin85	PKCθ	PKCθ-GFP
Cofilin	Cofilin-GFP	PLCγ1	PLCγ1.PH.SH2.SH2-GFP
Coronin1A	Coronin1A-GFP	Active Rac1	POSH.GBD-GFP-CAAX
Capping Protein α1	CPα1-GFP	Active RhoA	Rhotekin.GBD-GFP-CAAX
DAG	tandam C1 domain of PKCθ-GFP	R-pre	R-pre-GFP
CXCR4	CXCR4-GFP	SHP1	SHP1-GFP
GRB2	GRB2-GFP	SKAP55	GFP-SKAP55
HS1	HS1-GFP	SLAT	GFP-SLAT
Itk	Itk.PH.TH.SH3.SH2-GFP	SLP-76	SLP-76-GFP
ITSN2	ITSN2-GFP	STIM1	STIM1-YFP-CFP
LAT	LAT-GFP	TCRζ	TCRζ-GFP
Lck	Lck-GFP	Tee	Tee.PH.TH.SH3.SH2-GFP
LFA-1	ICAM1-GFP (ligand of APC)	Themis	Themis-GFP
Ly108.1	Ly108.1-GFP	Vav1	Vav1-GFP
TCR engage	Ie ^h -GFP (ligand on APC)	WASP	GFP-WASP
MLCK	MLCK-YFP	WAVE2	WAVE2-GFP
MRLC (myl9)	MRLC-GFP	Zap70	Zap70.2SH2-GFP
Myosin1c	Myosin1c-GFP		

Table 1. Fluorescent sensors for the assessment of the spatiotemporal organization of early T cell activation. The left columns list the signaling intermediates monitored to provide a systems-level view of the organization of T cell signaling. The right columns list the sensor design to assess localization of the signaling intermediate of interest.

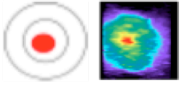
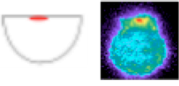
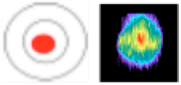
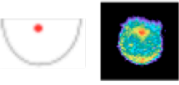
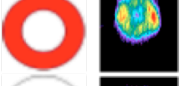
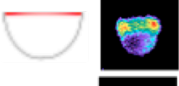
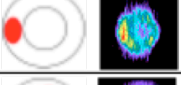
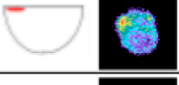
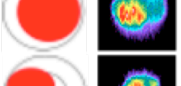
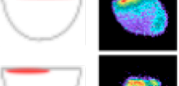


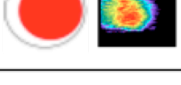

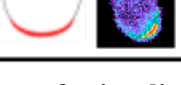
Pattern	Description	En face view	Top down view
Central	Less than .5 x of the interface diameter in all dimensions, more than .2 x of the interface diameter away from the interface edge		
Invagination	as central, but > 1 μ M inside the T cell		
Peripheral	Any pattern excluding the central quarter of the interface		
Asymmetric			
Diffuse	Any pattern containing both central and peripheral elements		
			
Lamellum	Accumulation covering the entire interface more than .2 x the cell diameter deep and coinciding with a visible lamellum		
Distal	Accumulation in a sub region of the posterior half of the T cell		

Figure 1. Classification criteria for spatiotemporal patterns of signaling intermediate accumulation at the T cell:APC interface. Schematic representations of patterns are given along with representative images. The images are maximum projections of 3D fluorescence data shown in false-color intensity scale (increasing in intensity from blue to red). The en face view shows the xz axis and the top down view shows the xy axis.

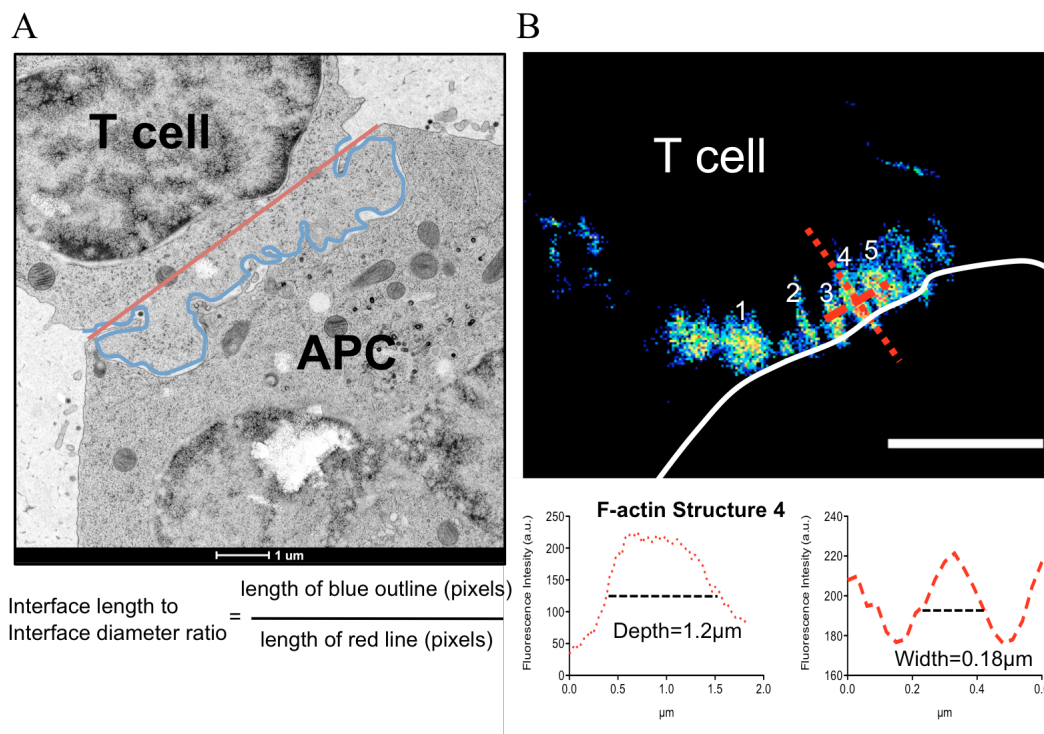


Figure 2. Interface diameter to length ratio and F-actin structure analysis. **A)** A representative electron micrograph of a 5C.C7 T cell:APC conjugate as in fig. 20A. The interface length is outlined (blue) and the interface diameter is drawn (red). The lines were drawn on images in Metamorph and the micrometer lengths were recorded and the ratio was calculated. **B)** Representative 5C.C7 T cell:APC conjugate stained with phalloidin as shown in fig. 21A (APC outline in white, scale bar=2 μ m). The number of F-actin structures (labeled 1-5) were determined by linear scaling and each structure was measured with linescans. One linescan was oriented perpendicular to the interface to measure the depth of the structure (red dotted line) and the other was oriented parallel to the interface to measure the width (purple dashed line). The intensity profile was plotted and the depth and width measurements were made at the full-width half-maximum of the F-actin structure profile (see graphs below image).

CHAPTER THREE

RESULTS

Spatiotemporal Patterning of T cell Activation is Highly Diverse

A systems-level perspective of the spatiotemporal patterning of T cell signaling

Over 50 signaling sensors (table 1) ranging from proximal T cell signaling intermediates, cytoskeletal regulators, signaling lipids, and transcription factors were imaged by live cell time-lapse fluorescent microscopy in *ex vivo* primed 5C.C7 CD4⁺ T cells activated with CH27 B cell lymphoma APCs pulsed with 10 μ M MCC peptide (fig. 3 and 4). Spatiotemporal organization of the signaling sensors was assessed during the first 7 minutes of T cell activation according to previously established criteria (fig. 1). This time window coincides with the peak of biochemical activity of proximal T cell signaling and translocation of transcription factors such as nuclear factor of activated T cells (NFAT) and nuclear factor κ B (NF κ B) into the nucleus [7]. Spatiotemporal patterning of T cell signaling was highly diverse as no two molecules showed identical dynamic localization, suggesting that interaction probabilities and signaling relations vary across time and space thus regulating the efficiency of T cell activation (fig. 3-4).

To provide a systems-scale overview of signaling relations at the T cell:APC interface, we hierarchically clustered signaling intermediates based on their dynamic pattern classification data (fig. 3 and 4). Cluster analysis revealed groups of molecules that predominantly localize to the T cell:APC interface center, periphery, lamellum and

molecules with little preference for a particular region of the interface (diffuse) (fig. 4). The interface center was composed of the TCR and proximal signaling intermediates such as ZAP-70, Lck, Itk, PLC γ 1, PKC θ , LAT, and Rac1. Actin and the actin regulators such as the ARP2/3 complex, capping protein, Cofilin, Coronin1A, HS1, WASp, and WAVE2 were located in the periphery. A novel region of signaling we call the 'lamellal pattern' (detailed extensively below) consisted of actin regulatory molecules such as Myosin IIC and Vav1 and critical T cell signaling adaptors such as SLP-76 that integrate signals controlling integrin activation, calcium signaling, cytoskeletal regulation, and transcription factor activation (fig. 4).

To establish generality of the spatiotemporal control of signaling during T cell activation, DO11.10 and OT-II TCR transgenic CD4⁺ T cells were also imaged and the spatiotemporal features were largely conserved [7]. However, formation and maintenance of the central cluster varied among the transgenes. DO11.10 and 5C.C7 T cells formed the interface center more readily, whereas the OT-II T cells had diminished central localization of proximal T cell signaling molecules. The formation of the central region correlated with higher phosphorylation levels of critical proximal signaling molecules such as PKC θ , LAT, and PLC γ 1 [7]. Thus, specific spatiotemporal features such as the central pattern were reliable indicators of T cell signaling amplitude. Given that the DO11.10, 5C.C7, and OTII TCRs have similar affinity for their cognate pMHC [72], the differences in signal strength may be due to different levels of accessory receptors on the APCs.

T cell activation environments vary depending on the type of pathogen and local tissue in which antigen is detected. Therefore, it is of interest to determine how

spatiotemporal patterning and T cell activation changes under different conditions, e.g. when CD28 co-stimulation or LFA-1 engagement is blocked or when peptide concentration are reduced 100-fold. Blockade of CD28 co-stimulation resulted in more transient enrichment of signaling intermediates at the T cell:APC interface. Enrichment was reduced significantly for most molecules after 1 to 2 minutes of interaction with the APC. Blockade of LFA-1 engagement with ICAM-1 resulted in more complex changes with overall reduction in interface enrichment (with the exception of Cdc42) and impairment of central localization (with the exception of Rac1). Reduction of antigenic peptide levels both impaired rapid segregation of molecules into the distinct central and peripheral patterns and enrichment was more transient as molecules were less enriched after 2 minutes of interaction with the APC [7]. The specific effects elicited by these perturbations yields insight into the control of T cell signaling by important environmental cues and makes clear that T cells are exquisitely sensitive to their activation environment. These varied and graded activation conditions are likely critical regulators of T cell responses *in vivo*.

Overall, these data provide both a global view of signaling relations in time and space under physiological activation conditions in live primary T cells and establish spatiotemporal patterning of signaling as a critical regulator of the efficiency of T cell activation.

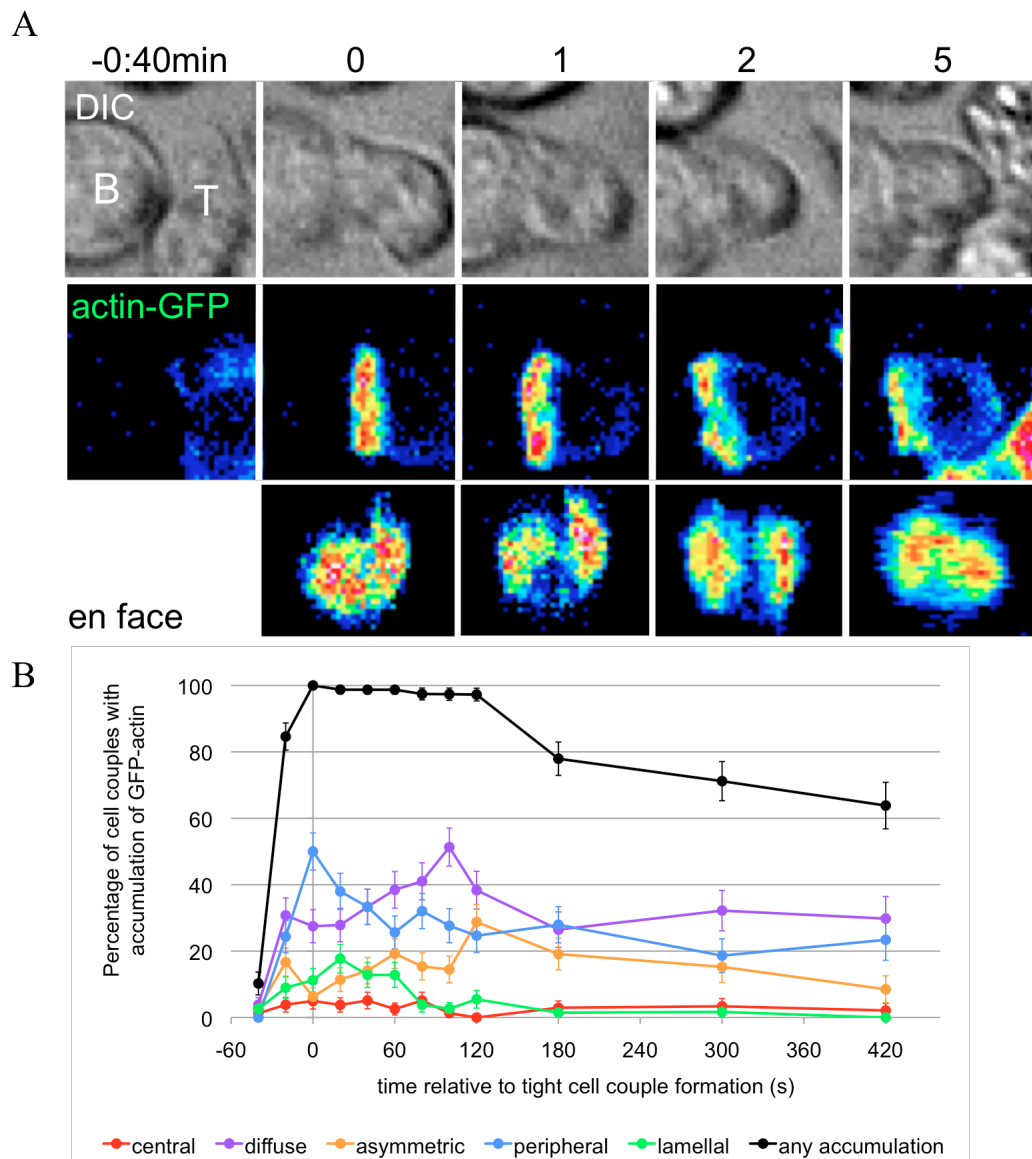


Figure 3. T cells recruit molecules critical for signal transduction to the T cell:APC interface in distinct patterns. A) Representative interaction of a transduced 5C.C7 T cell expressing GFP-actin with an APC in the presence of 10 μ M MCC peptide over the indicated time points relative to tight cell couple formation. DIC images are shown in the top panel, maximum projections of 3D GFP-actin fluorescence data and en face (xz axis) images are shown below in a false-color intensity scale (increasing in intensity from blue to red). **B)** The percentage of T cells showing each spatiotemporal pattern is reported as a separate curve. Error bars represent s.e.m. (n>100 cell couples)

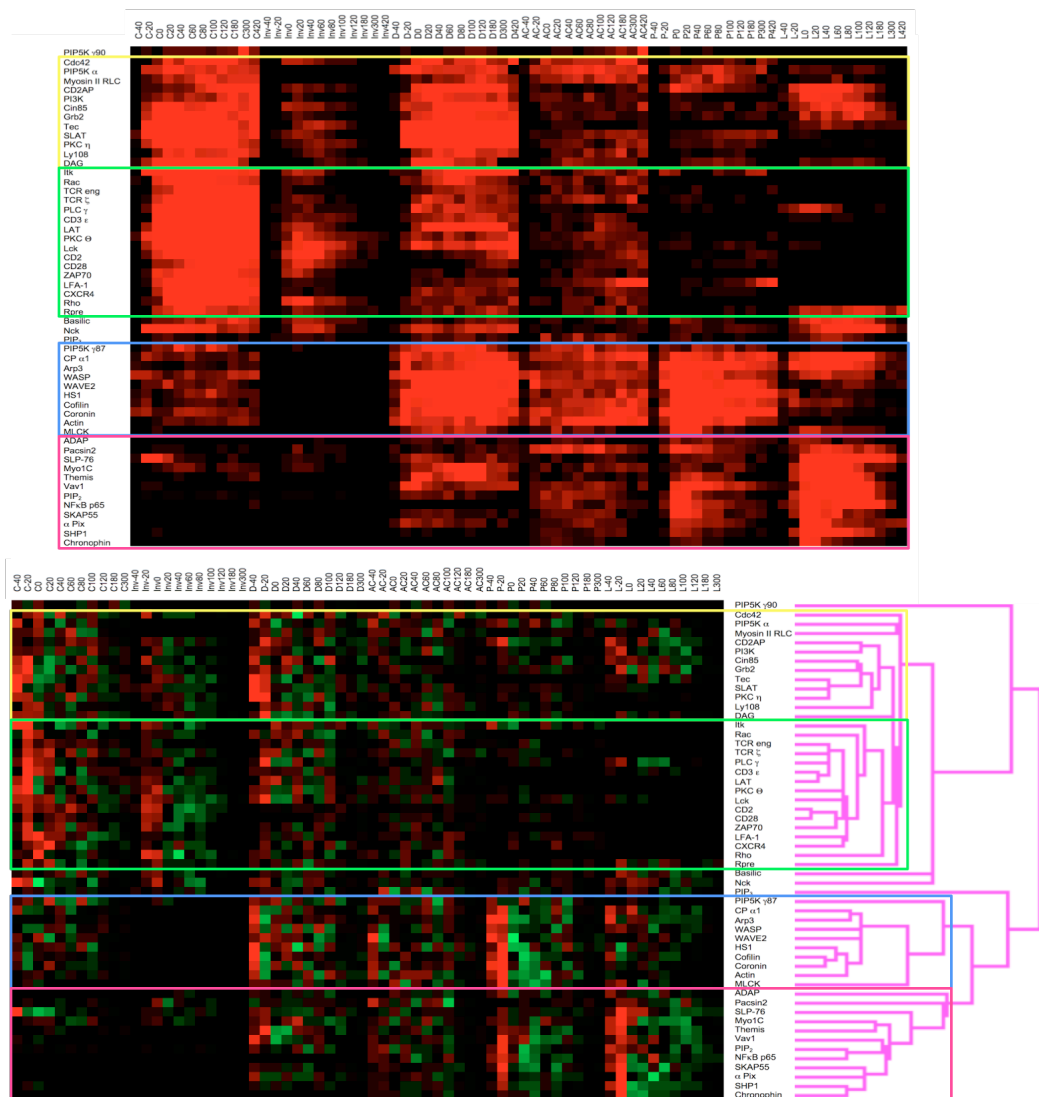


Figure 4. Spatiotemporal patterning of the T cell signaling system. A) 5C.C7 T cells expressing the indicated sensors were activated on peptide loaded CH27s (10 μ M MCC) and patterns of interface enrichment were scored as previously described. Cluster analysis of the data presented is based on the six mutually exclusive interface patterns [central (C), invagination (Inv), diffuse (D), asymmetric (AC), peripheral (P), and lamellum (L)] is given as described previously. The percentage occurrence of each pattern is given in shades of red from C-40 to L420 in the top part of the figure. In addition, to address the rate of pattern change, the percentage change per 20-s interval was tabulated (C-40 to L300 in the bottom part of the figure). Red indicates an increase and green a decrease in the percentage occurrence of a pattern relative to the previous time point. The diffuse (yellow), central (green), peripheral (blue), and lamellum (pink) clusters are delineated by rectangles.

A Deep and Transient Actin Network Controls T cell Activation

Signal transduction in the T cell lamellum

To gain insight into the cellular structures underlying the complex T cell signal transduction system, T cell signaling was imaged at the systems scale. *In vitro* primed primary 5C.C7 TCR transgenic CD4⁺ T cells were retrovirally transduced to express fluorescently tagged signaling sensors (>50 signaling sensors). Time-lapsed fluorescence microscopy was performed with sensor expressing T cells activated by CH27 B cell lymphoma APCs pulsed with 10 μ M MCC antigenic peptide. 3D accumulation patterns at the T cell:APC interface were determined as previously established [7]. This analysis revealed a novel region of signaling, characterized by transient sensor accumulation originating across the entire T cell:APC interface and extending several micrometers into the T cell, henceforth referred to as the ‘lamellal pattern’ (fig. 5-6). Molecules with dominant lamellal accumulation are involved in actin regulation and proximal T cell signaling, including the Rho family guanine nucleotide exchange factor (GEF) Vav1, the adaptor SH2 domain containing leukocyte phosphoprotein of 76 kDa (SLP-76), the regulators of integrin activation adhesion and degranulation promoting factor (ADAP) and Src-kinase associated phosphoprotein of 55 kDa (SKAP55), the actin-based molecular motor Myosin 1C, the T cell thymic positive selection regulator Themis, the phosphatases Chronophin and Src homology domain-containing phosphatase-1 (SHP1), the PIP₂ sensor PLC δ PH, and the transcription factor nuclear factor κ B (NF κ B) (fig. 5-6). The lamellal pattern was a conserved feature of early T cell signal transduction as in an

investigation of a subset of signaling intermediates in DO11.10 T cell:A20 B cell lymphoma cell conjugates similar lamellar patterning occurred (data not shown). Often other patterns occur in parallel, supporting a connective role for the lamellar pattern. For example, Vav1 also localized to the periphery of the T cell:APC interface, with $27\pm6\%$ of T cells showing peripheral and $39\pm5\%$ showing lamellar Vav1 at 1 minute after tight cell conjugate formation (fig. 6C and F). SLP-76 first accumulated at the center ($34\pm6\%$ at 0 minutes) and transitioned rapidly to the lamellum ($60\pm7\%$ of T cells showing lamellar SLP-76 by 1 minute). The transience of the lamellar pattern was a defining feature. For example, $60\pm7\%$ of T cells displayed lamellar accumulation of SLP-76 at 1 minute, but by 3 minutes the percentage was reduced to $32\pm6\%$ ($p=0.007$) (fig. 6A and D). Interestingly, these dynamics of the lamellar pattern match that of much of the biochemically detectable signaling activity in T cell:APC conjugates. The transient co-recruitment of actin regulators, proximal signaling intermediates, lipids, and transcription factors into a wide lamellum suggests that this pattern may constitute a micrometer scale actin-dependent signaling structure.

F-actin and lamellar signaling intermediates share deep lamellar localization

While accumulation of F-actin at the periphery of the T cell:APC interface is established[19], we determined whether F-actin also localizes throughout the lamellum. Using stimulated emission depletion (STED) microscopy, 5C.C7 T cell conjugates with antigen pulsed ($10\mu\text{M}$ MCC) CH27 APCs were fixed and stained with phalloidin at an early (1-2 minutes) and late (>5 minutes) time point. (fig. 7A). The deep F-actin network

was also observed in live 5C.C7 T cells expressing the F-actin sensor, F-tractin-GFP (fig. 7B-C). In the first 2 minutes of T cell activation, the periphery and center of the T cell:APC interface displayed deep F-actin with the phalloidin fluorescent intensity at $57\pm2\%/40\pm3\%$ (periphery/center) above cellular background at $1\mu\text{m}$ and $19\pm1\%/11\pm1\%$ at $2\mu\text{m}$ away from the interface (fig. 7D). By the late time point, peripheral and central F-actin was moderately reduced in depth consistent with the diminished occurrence of the lamellal pattern (fig. 7D). To corroborate the actin depth in live cells, we measured the depth of actin after 1 minute of activation by both GFP-actin and F-tractin. Both showed a deep actin network that covers the entire interface (fig. 7D). Importantly, the localization of SLP-76, Vav1, and PLC δ PH coincided with the actin network in depth and dynamics (fig. 7E). To corroborate our live cell sensor data, we imaged fixed cells stained for phosphorylated SLP-76 Y128 (pSLP-76) (fig. 8) and for comparison a centrally localized molecule, phosphorylated linker of activated T cells Y121 (pLAT) (fig. 9) by STED and deconvolution microscopy. Distributions of pSLP-76 and pLAT in fixed cells were comparable to localization of the SLP-76-GFP and LAT-GFP live cell sensors. Interestingly, however, fixed T cells showed distinct pSLP-76 clusters located both APC proximal and deep into the lamellum, as discussed below (fig. 10A and B).

To corroborate the association of pSLP-76 with lamellal F-actin at the single cell level, fixed 5C.C7 T cell:CH27 conjugates were stained for pSLP-76 and phalloidin. pSLP-76 clusters colocalized with F-actin (average Pearson's correlation coefficient= 0.6 ± 0.1). $34\pm2\%$ of pSLP-76 was imbedded in F-actin. Additionally, pSLP-76 localized along the perimeter of F-actin structures (fig. 10B, top panel). pSLP-76 cluster and F-actin depth correlated strongly (Pearson's correlation coefficient= 0.73 ,

$p=0.002$) (fig 10C-E). These single cell data confirm matched localization of lamellal F-actin with an active proximal signaling intermediate, pSLP-76. To determine whether defined molecular interactions also contribute to lamellal localization of signaling intermediates, we imaged a SKAP55 plextrin homology domain mutant, a Themis proline rich region mutant, and a CD2-associated protein (CD2AP) coil-coil domain mutant, a protein with substantial but not exclusive lamellal patterning. Although, the molecular features of these interactions differed, interface recruitment was consistently diminished (data not shown). The spatiotemporal co-enrichment of a large-scale network of critical signaling intermediates and actin in the lamellal pattern with added support by defined molecular interactions substantiates the view of the lamellal pattern as an actin-based active signaling structure.

Lamellal localized signaling intermediates and actin diffuse at similar rates

Tight association of lamellal localized signaling intermediates with F-actin should constrain their diffusion. Fluorescence recovery after photobleaching (FRAP) experiments with Themis-GFP or PLC δ PH-GFP expressing 5C.C7 T cells activated with peptide-loaded CH27s showed that diffusion of lamellal localized signaling intermediates was comparable to actin. The average half-times of recovery ranged from 1.3 ± 0.2 s for PLC δ PH to 2.1 ± 0.3 s for actin ($p > 0.05$) (fig. 11). GFP recovered more rapidly ($t_{1/2} = 0.32 \pm 0.04$, $p < 0.0001$), suggesting that diffusion in the lamellum is not simply constrained by the geometry of the spreading T cell (fig. 11C-D). Addressing a different localization for comparison, signaling intermediates that accumulate at the center of the T

cell:APC interface (PKC Θ , LAT, and activated Rac1) showed substantially less recovery ($30\pm 2\%$ to $44\pm 1\%$) than lamellal proteins ($63\pm 2\%$ to $76\pm 2\%$) (fig. 11C-D). The comparable rate of diffusion of actin and lamellal signaling intermediates supports the view of the lamellum as an actin-based signaling structure.

Diminished interface actin recruitment prevents lamellal localization

To causally link actin dynamics to lamellal localization, low dose 40nM Jasplakinolide [73] was utilized to disrupt early actin polymerization while retaining the ability of the T cells to conjugate to APCs. While actin spatiotemporal patterning remained similar to control conditions, interface actin amounts were effectively reduced in T cells with JASP treatment at time 0 (accumulation index decreased from 16.7 ± 0.8 to 10.3 ± 0.7 , $p=0.002$) and actin enrichment reached negligible levels by 3 minutes (fig. 12A-C). Reduced actin levels diminished lamellal localization of SLP-76 from $60\pm 7\%$ to $18\pm 5\%$ at 1 minute ($p<0.0001$). Overall recruitment of SLP-76 to the interface was more transient (fig 12D-E). Fixed cell deconvolution microscopy (fig. 13A) revealed a 40% reduction ($p=0.02$) in pSLP-76 intensity at the T cell:APC interface (fig. 13B). Also, the percentage of pSLP-76 clusters localized deep into the lamellum was reduced from $38\pm 4\%$ to $7\pm 2\%$ ($p<0.0001$) with a decrease in depth range from $0.65\text{-}3.0\mu\text{m}$ to $0.5\text{-}1.4\mu\text{m}$ (fig. 13C-D). Interestingly, positive correlation and colocalization between residual pSLP-76 cluster and F-actin depth (Pearson's correlation coefficient=0.83, $p=0.0001$) were retained with the disruption of actin dynamics (fig. 13E and 14A-C). The

concomitant loss of SLP-76/pSLP-76 and actin depth suggests that actin controls lamellal SLP-76 localization at the T cell:APC interface.

Low dose JASP treatment also diminished lamellal localization of PLC δ PH at the 1 minute time point from $38\pm 5\%$ to $13\pm 5\%$ ($p=0.006$), corroborating the SLP-76 data (fig. 15A and C). Surprisingly, JASP enhanced the lamellal localization of Vav1 from $39\pm 6\%$ to $70\pm 6\%$ ($p=0.0005$) but at the expense of peripheral Vav1 recruitment (reduced from $27\pm 6\%$ to $8\pm 4\%$, $p=0.02$) (fig. 15B-D). The peripheral to lamellal shift in Vav1 patterning shows that the effect of F-actin loss on the spatiotemporal organization of signaling intermediates that are distributed across two F-actin-based patterns is more complex. For comparison, we further determined if altered lamellal actin dynamics affected spatiotemporal control of molecules with prominent central accumulation. Central accumulation of LAT and PKC θ during the peak of lamellal patterning was at best moderately impaired, suggesting that actin selectively controls the lamellal signaling network during initial T cell:APC contact. However, sustained central localization was significantly reduced as discussed below (fig. 16).

Diminished interface actin impairs proximal signaling and cytokine production

To establish whether altered lamellal localization of signaling intermediates affected their activation, we assessed their phosphorylation biochemically in T cell:APC conjugates. pSLP-76 levels were reduced $35\pm 2\%$ after 1 minute ($p<0.05$) and $34\pm 9\%$ after 2 minutes ($p<0.005$) with JASP treatment (fig. 17A). These results match the 40% reduction in pSLP-76 intensity at the interface observed by microscopy (fig. 13B).

Consistent with enhanced lamellal recruitment, Vav1 showed a $30\pm 4\%$ increase in phosphorylation after 2 minutes of T cell activation with JASP (fig. 17B). Also, consistent with intact early central localization, LAT and PKC θ phosphorylation was maintained (fig 17C-D). Taken together, these data establish that the F-actin network underlying the wide transient T cell lamellum facilitates activation of the lamellal signaling intermediates. In contrast to JASP treatment, more potent disruption of actin dynamics with 10nM Latrunculin A (LatA) reduced the activation of all proximal TCR signaling intermediates tested (Fig. 18).

We next determined whether functional outcomes of T cell signaling such as IL-2 production were affected by JASP. To focus on earlier T cell signaling, we treated T cell:APC cultures for 1 or 6 hours with JASP, removed the drug and prevented further T cell stimulation with a MHC blocking antibody and assayed IL-2 after 24 hours. JASP treatment during the 1 hour stimulation resulted in a $20\pm 6\%$ reduction ($p=0.02$) in IL-2 positive T cells (fig. 19). T cells stimulated 6 hours in the presence of JASP recovered production of IL-2, supporting a more important role for actin-dependent signaling in early T cell activation (fig. 19). LatA consistently reduced IL-2 production irrespective of T cell stimulation time (at 6hr, $p=0.0002$) in agreement with overall signaling defects observed biochemically (fig. 19).

The T cell:APC interface has an actin-dependent undulating and interdigitated architecture that reaches deep into the T cell lamellum

To determine cell biological structures that may support the formation of the lamellar pattern, we visualized APC outlines at the T cell:APC interface by deconvolution microscopy and membrane topology with electron microscopy. The interfaces were characterized by undulating and interdigitated membrane topology especially less than 2 minutes after cell conjugate formation (fig. 20A and 21A). 5C.C7 T cell:CH27 APC conjugates stained with a whole cell APC stain to delineate the APC outline revealed that $76\pm 7\%$ of T cells had interdigitated T cell:APC interfaces compared to $50\pm 8\%$ when conjugates were treated with JASP ($p=0.03$), supporting a role for actin in formation of the undulating interface architecture (fig. 20). Electron microscopy reinforced the existence of an undulating interface (fig. 21A). The T cell interface length was 2.1 ± 0.2 fold longer than the interface diameter at the early ($<2\text{min.}$) time point and only 1.5 ± 0.1 fold longer at late ($>2\text{min.}$) time point ($p<0.05$) (fig. 21D). Thus, the flattening of the interface and reduced interdigitation coincides with loss of the lamellar pattern and the peak of actin dynamics (fig. 21B). Treatment of cell conjugates with JASP reduced the interface length to diameter ratio at early time points to 1.5 ± 0.2 ($p<0.05$) similar to the late time point ratio under control conditions ($p>0.05$) (fig. 21C-D). Thus, actin dynamics were required for formation of a highly interdigitated early T cell:APC interface. Relating the undulating membrane topology to F-actin distributions, fixed 5C.C7:CH27 conjugates stained with phalloidin and imaged by STED microscopy revealed F-actin structures that were aligned with T cell protrusions perpendicular to the

interface plane, as opposed to a more diffuse network at late time points (fig 22A-B). The depth to width ratio of resolved (135% of cell background) F-actin structures at the early time points was 2.6 ± 0.3 compared to 0.7 ± 0.1 at the late ($p < 0.0001$) (fig. 22C). Early F-actin structures were also discrete and of limited size in contrast to more diffuse F-actin structures at late time points. The intensity to area ratio of the F-actin structures was 7.5 ± 0.8 at the early time point as opposed to 1.2 ± 0.1 at late time points ($p < 0.0001$) (fig. 22D). The force vector of actin polymerization is thus likely oriented perpendicular to the interface during early T cell activation and applied to relatively small areas of plasma membrane. This should contribute to an undulating and highly interdigitated T cell:APC interface by generating localized membrane projections that deform both the T cell and APC membrane. These data also establish that the depth of lamellar signaling does not have to be driven by events micrometers away from ligand engaged receptors at the plasma membrane but could be supported by plasma membrane folding deep into actin-dependent T cell invaginations, which is consistent with the lamellar accumulation of lipid sensors such as the PIP_2 sensor PLC δ PH-GFP.

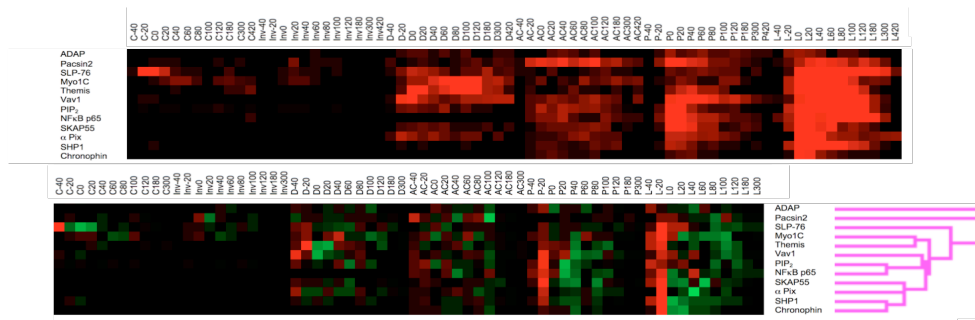


Figure 5. Cluster analysis of the spatiotemporal patterning of the T cell signaling system identifies a lamellar network of T cell signaling. The signaling intermediates with dominant lamellar patterning are shown as a subset of the T cell signaling system cluster analysis in Fig. 4.

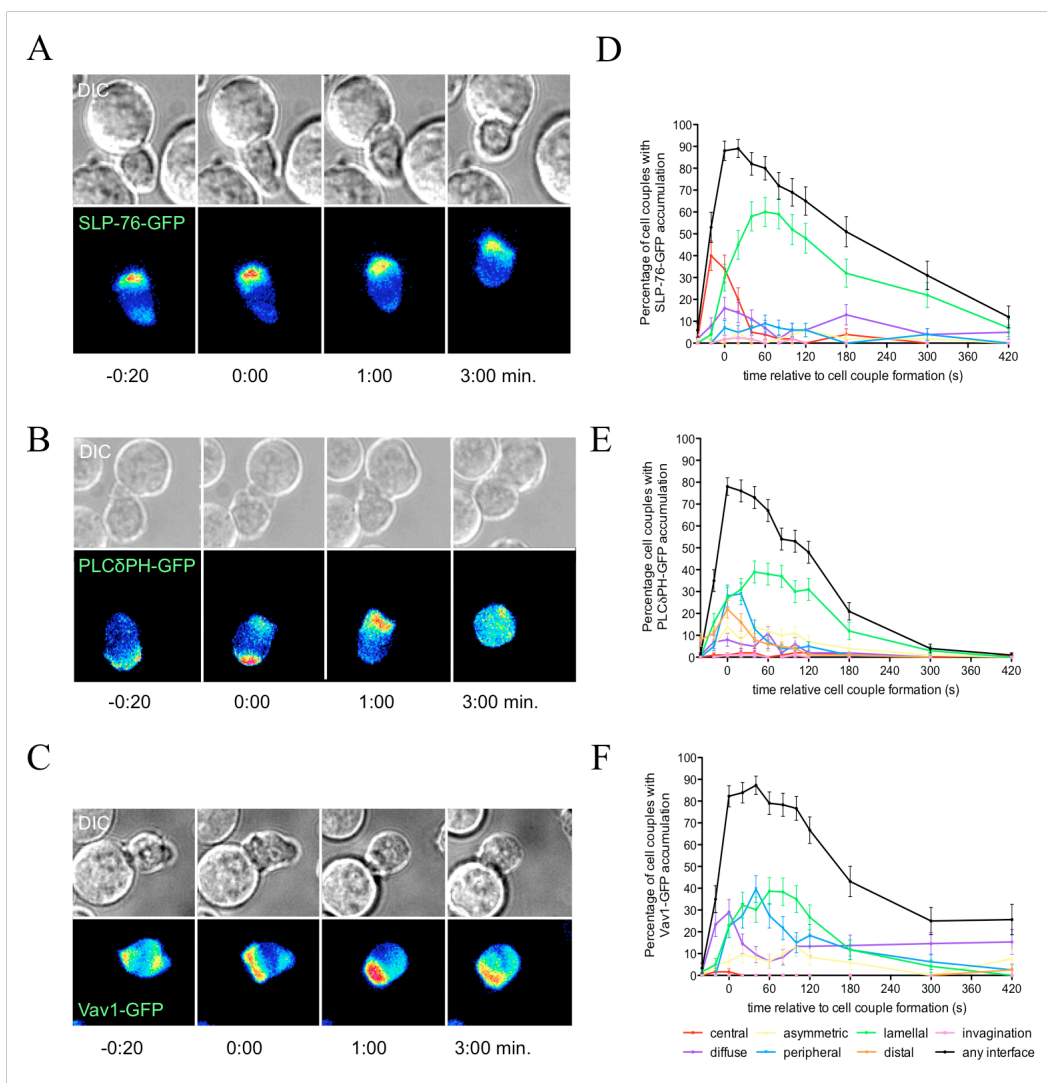


Figure 6. Critical regulators of T cell activation show transient localization to the T cell lamellum. Representative interactions of 5C.C7 T cells expressing **A**) SLP-76-GFP, **B**) PLCδPH-GFP (PIP₂ sensor) or **C**) Vav1-GFP with peptide-loaded CH27s (10μM MCC) over the indicated time relative to formation of a tight cell conjugate are given as in fig. 3A. The percentage of T cells showing accumulation in defined patterns are shown next to the representative images for **D**) SLP-76-GFP (n=56) **E**) PLCδPH-GFP (PIP₂ sensor) (n=63) and **F**) Vav1-GFP (n=63) as in fig 3B. Error bars are s.e.m.

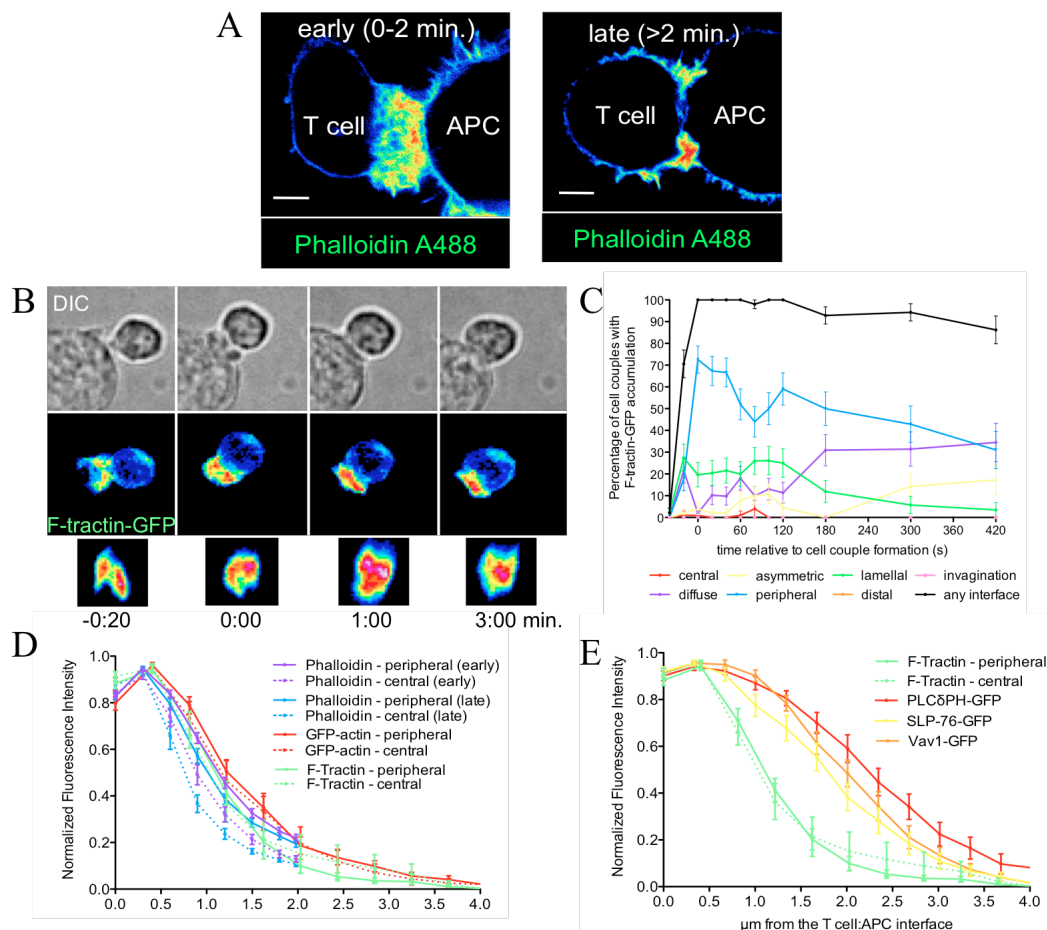


Figure 7. Actin and lamellar localized signaling intermediates distribute across the entire T cell:APC interface and extend several micrometers into the T cell. Phalloidin stained 5C.C7 T cell:CH27 APC conjugates imaged by STED **A**) 1 to 2 minutes (left) and >2 minutes (right) after cell conjugate formation are shown in a rainbow-like color scale (scale bars=2μm). **B**) A representative interaction of a 5C.C7 T cell expressing the F-actin sensor F-tractin (n=51) is given similar to Fig. 3A. In addition, an en face view of the T cell is shown at the bottom. **C**) The pattern classification graph is given for F-tractin-GFP similar to fig. 3B (n=51). **D**) T cell actin depth amounts relative to maximum as a function of the distance from the interface in the periphery (outer 25% of the interface diameter) and center (middle 50% of the interface) measured from fixed Phalloidin stained 5C.C7 T cell:CH27 APC conjugates at an early (<2 min, n=26) and late (>2min, n=16) time point by STED and live cell conjugates expressing actin-GFP (n=15) or F-tractin (n=19) (both measured at the 1 min. time point) are given. **E**) Depth of lamellar localized signaling intermediates PLCδPH (PIP₂) (n=18), SLP-76 (n=19), and Vav1 (n=18) measured across the entire interface in live 5C.C7 T cell:APC conjugates is given similar to panel D. F-tractin depth is shown as a reference. Error bars are s.e.m.

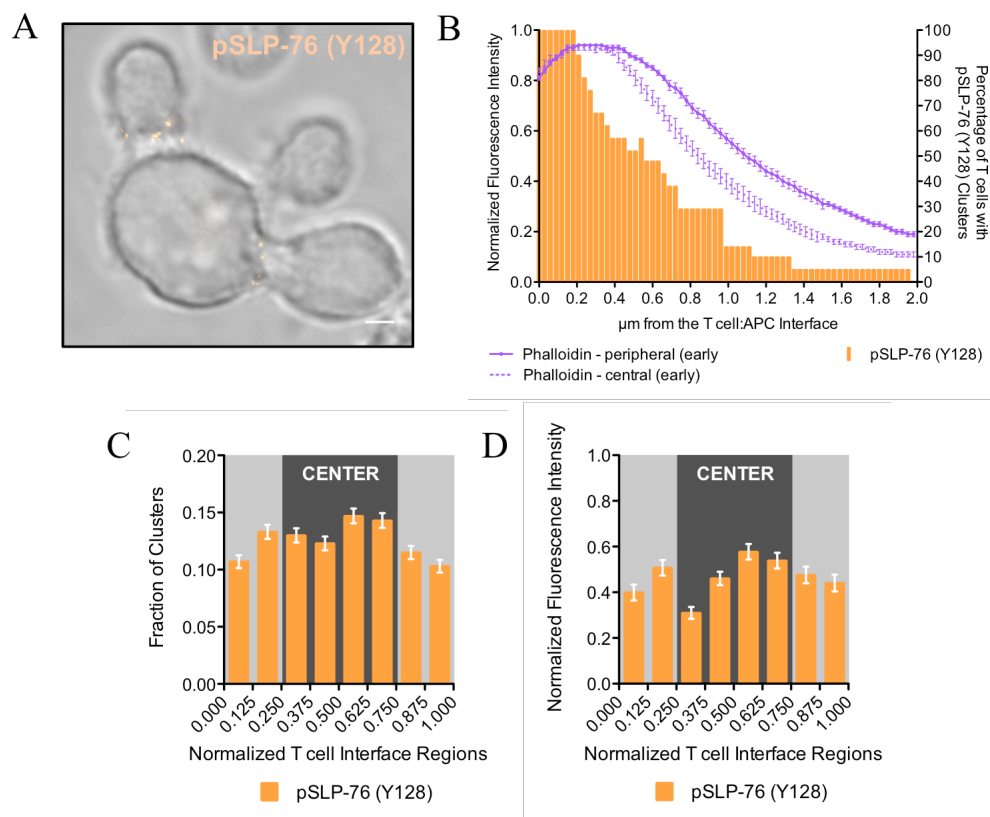


Figure 8. Activated SLP-76 localizes to the T cell lamellum. **A)** A representative STED image is given of two 5C.C7 T cells conjugated to a CH27 APC (10 μM MCC) stained for pSLP-76 (Y128) at a single central z-plane as a DIC and fluorescence overlay (scale bar=2 μm). **B)** F-actin depth measured from STED images is given for the early (<2min.) time point as in fig. 7D and plotted on the left y-axis (n=26). The percentage of 5C.C7:CH27 conjugates (10 μM MCC) imaged by STED with pSLP-76 (Y128) clusters is shown as a function of depth into the T cell and plotted on the right y-axis (n=21) (data from single color stains). **C)** The fraction of pSLP-76 clusters in each normalized interface region (interface diameter=1) across the T cell:APC interface diameter from the same cells as in panel B is given. **D)** The intensity distribution of pSLP-76 (Y128) is binned into normalized interface regions for the same cells as in panel B. Error bars are s.e.m.

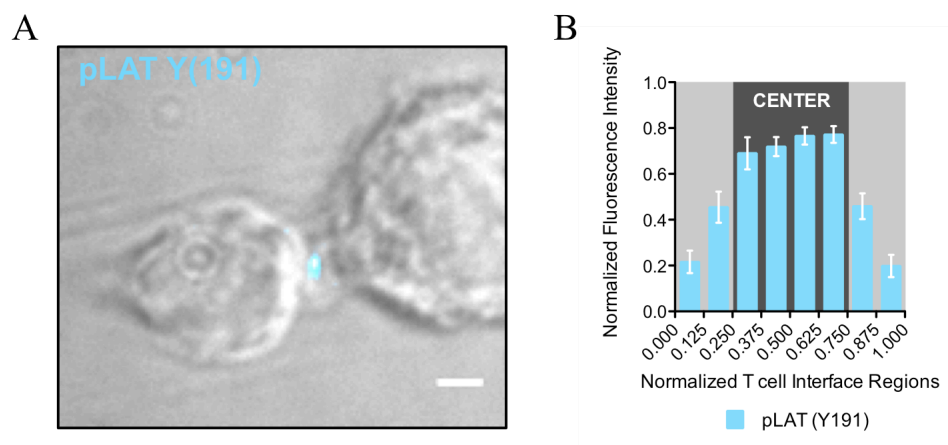


Figure 9. Activated LAT localizes to the T cell:APC interface center. A) 5C.C7:CH27 conjugates (10 μ M MCC) stained for pLAT (Y191) were imaged by deconvolution microscopy and a representative image is given (scale bar=2 μ m). **B)** The intensity distribution of pLAT (Y191) at the T cell:APC interface is given as in fig. 8D (n=12). Error bars are s.e.m.

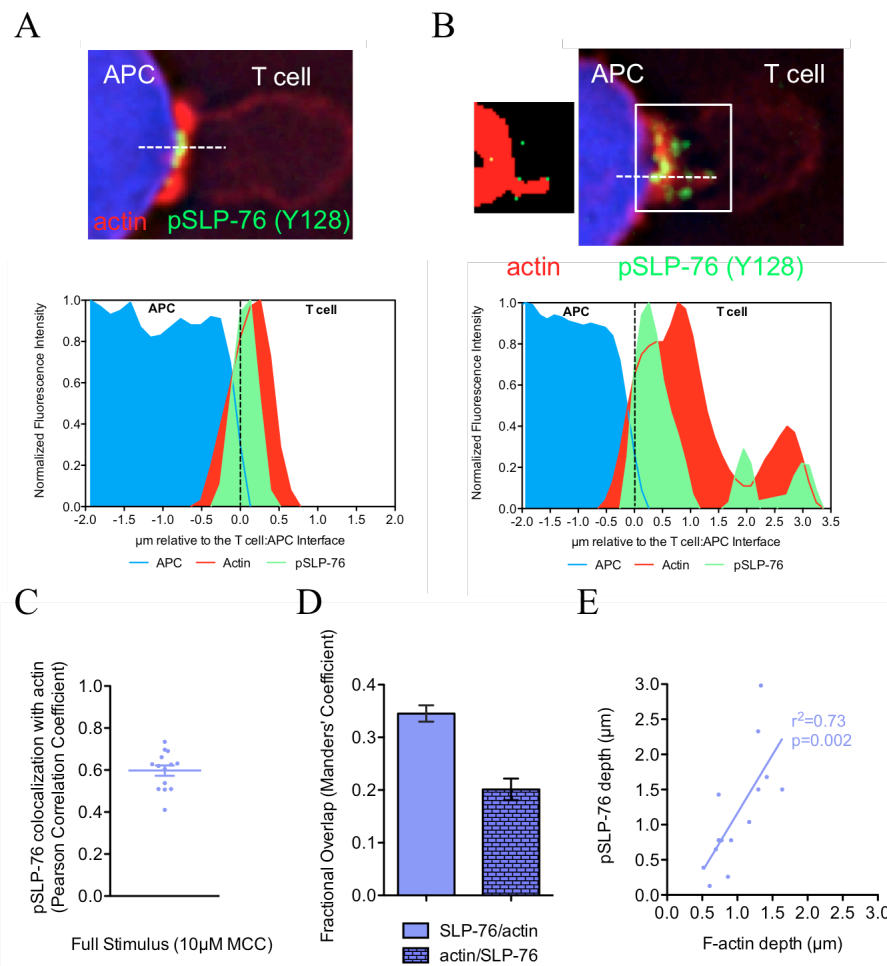


Figure 10. Activated SLP-76 localizes to lamellar F-actin structures. Fixed 5C.C7 T cell:CH27 APC conjugates were stained for F-actin (Phalloidin), pSLP-76 (Y128), and APCs with Cell Trace Violet. Representative images of **A)** APC proximal and **B)** lamellar localized pSLP-76 clusters are given. Representative images are shown on top while intensity line scans perpendicular to the interface (dotted white line) are shown below. A binary mask of above background F-actin (red) is shown with the centers of mass of pSLP-76 clusters (green) next to the representative image in panel B. **C)** Pearson's correlation coefficients for colocalization of pSLP-76 with F-actin were determined for 15 cell conjugates. **D)** Mander's coefficient reporting the percentage of pSLP-76 that overlaps with F-actin and vice versa was calculated for the same 15 cell conjugates as in panel C. **E)** The F-actin depth at the interface was measured at the point of half-maximal fluorescence (number represents the average of peripheral and central depth measurements) and plotted against the depth of the deepest pSLP-76 cluster with the Pearson's correlation coefficient for the same cell conjugates as in panel C. Error bars are s.e.m.

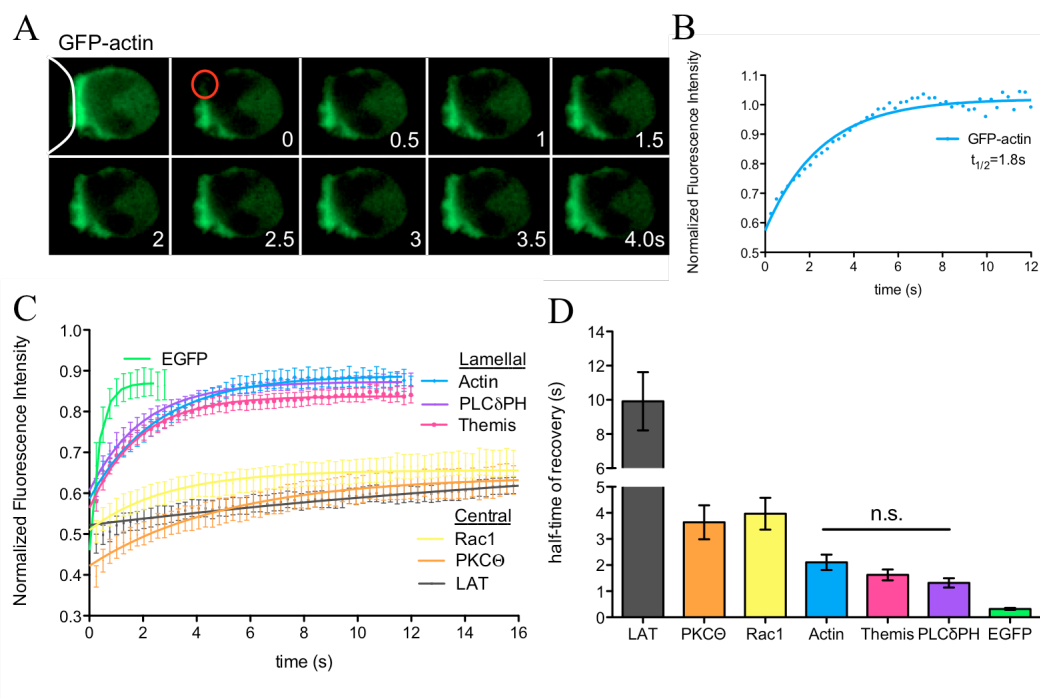


Figure 11. Lamellar signaling intermediates diffuse at similar rates as actin. **A)** A fluorescence recovery after photobleaching (FRAP) time series is shown for GFP-actin with an initial prebleached image and post-bleached images spaced 255ms (APC is represented by white line, bleach spot=red circle). **B)** The corresponding fitted recovery curve is given. **C)** Average fitted recovery curves for lamellar localized signaling intermediates PLC δ PH (n=11) and Themis (n=11) and centrally localized PKC θ (n=9), LAT (n=10), active Rac (n=13) plotted with actin (n=10) and GFP (n=10) control are shown. **D)** The average half-times of recovery for the same cell conjugates analyzed for panel C. (the line indicates significance by 1 way ANOVA, $p > 0.05$). Error bars are s.e.m.

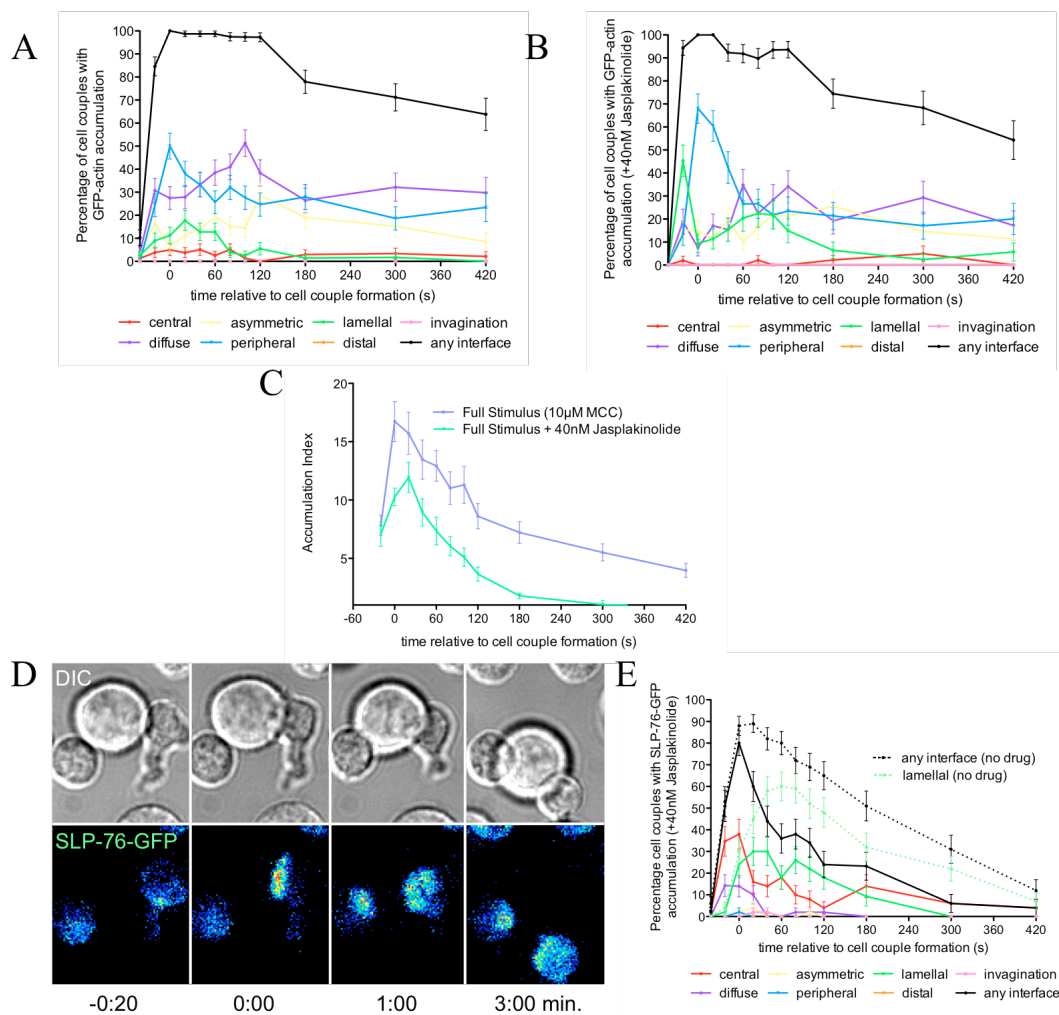


Figure 12. Diminished actin at the T cell:APC interface disrupts lamellar localization of SLP-76. The pattern classification graph is given for 5C.C7 T cells expressing GFP-actin under the **A**) control DMSO (n=80) or **B**) 40nM JASP (n=53) condition similar to fig. 3B. **C**) 5C.C7 T cells expressing GFP-actin were stimulated with peptide loaded CH27s (10μM MCC) in the presence of 40nM JASP (n=25) or DMSO (n=25). The accumulation index was calculated as described in the 'Materials and Methods' and is plotted relative to tight cell conjugate formation. **D**) A representative interaction of a 5C.C7 T cell expressing the SLP-76-GFP with 40nM JASP is given similar to Fig. 3A. **E**) The corresponding pattern classification graph is given upon treatment with 40nM JASP similar to Fig. 3B (n=50). Control 'any interface' and 'lamellar' accumulation curves are plotted as a reference (data also shown in Fig. 6D). Error bars represent s.e.m.

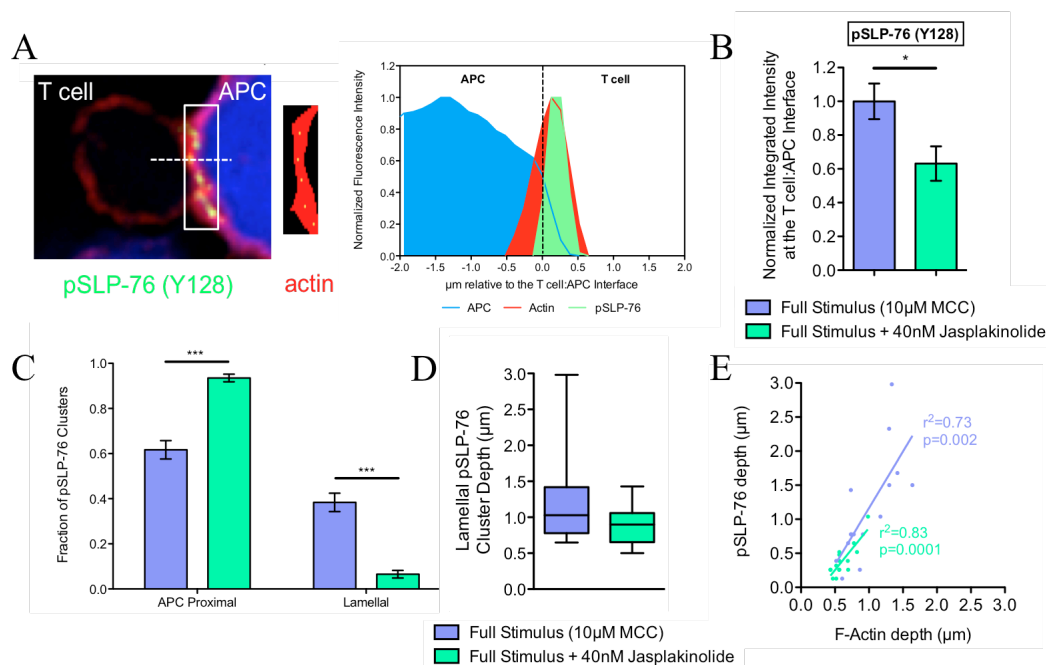


Figure 13. Diminished actin at the T cell:APC interface disrupts lamellar localization and activation of SLP-76. **A)** 5C.C7 T cell:CH27 APC conjugates treated with 40nM JASP were stained as in fig. 10A-B. **B)** pSLP-76 (Y138) cluster intensity measured in fixed 5C.C7 T cell:APC conjugates is given for DMSO control (n=17) and JASP (n=17) treated cell conjugates. **C)** Fixed 5C.C7 T cell:APC conjugates were treated with 40nM JASP (n=40) or DMSO (n=40) and the frequency of APC proximal (Fig. 10A) and lamellar clusters (Fig. 10B) are given. **D)** The depth of lamellar pSLP-76 clusters for DMSO control (32 clusters) and residual lamellar clusters in JASP treated cell conjugates (12 clusters) from same cells analyzed in panel E are plotted (whiskers=min and max). **E)** F-actin depth versus pSLP-76 depth is plotted as in Fig. 10E for JASP treated cell conjugates from same cells as in panel E. Non-treated control data (Fig. 10E) included for comparison. Significance was determined by Student's t-test and is indicated by asterisks (* $p<0.05$, ** $p<0.001$, *** $p<0.0001$).

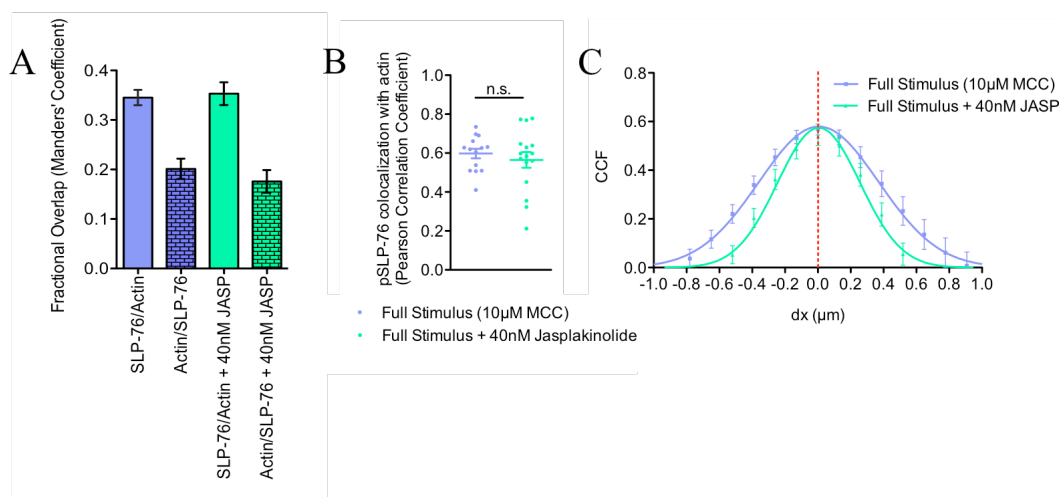


Figure 14. Activated SLP-76 associates with F-actin despite disruption of actin at the T cell:APC interface. **A)** Mander's coefficient reporting the percentage of pSLP-76 that overlaps with F-actin and vice versa was calculated for the same cell conjugates as in fig. 10 and 13. **B)** Pearson's correlation coefficients for colocalization of pSLP-76 with F-actin were determined for the same cells conjugates as in panel A. **C)** The Van Steensel's cross correlation coefficient described in the 'Material and Methods' for the same cells as in panel A. Error bars are s.e.m. Significance was determined by Student's t-test and is indicated by asterisks (* $p < 0.05$, ** $p < 0.001$, *** $p < 0.0001$).

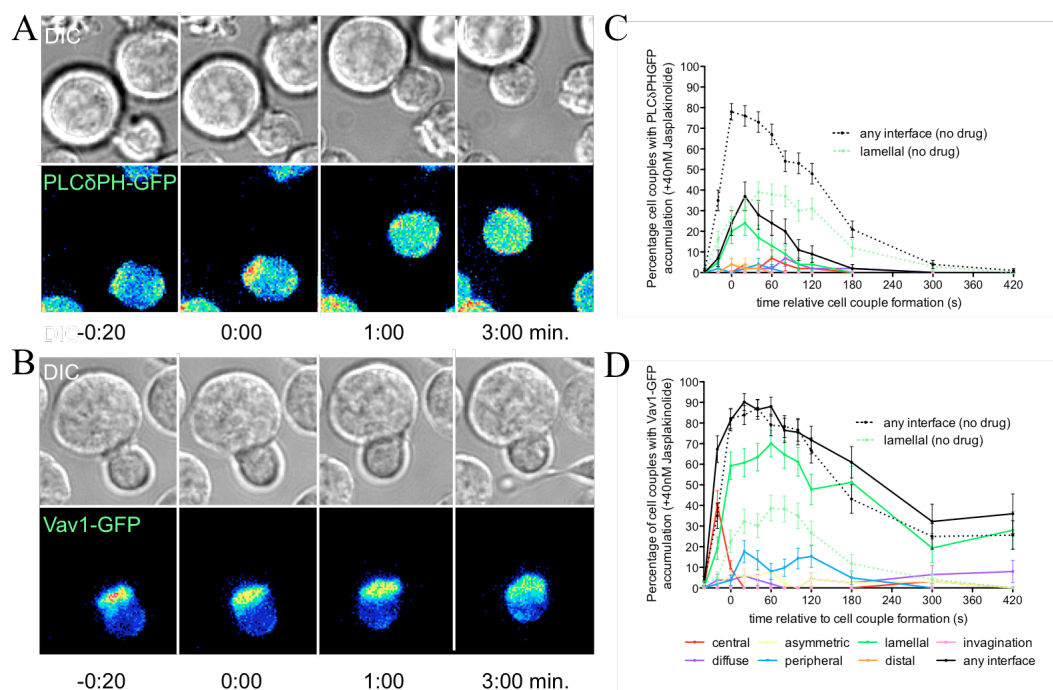


Figure 15. Diminished actin at the T cell:APC interface disrupts lamellar localization of PLCδPH and enhances lamellar localization of Vav1. A representative interaction of a 5C.C7 T cell expressing A) PLCδPH-GFP or B) Vav1-GFP with 40nM JASP treatment is given similar to fig. 3A. The corresponding pattern classification graphs for PLCδPH-GFP (n=46) and Vav1-GFP (n=50) is given similar to fig. 12E. Error bars represent s.e.m.

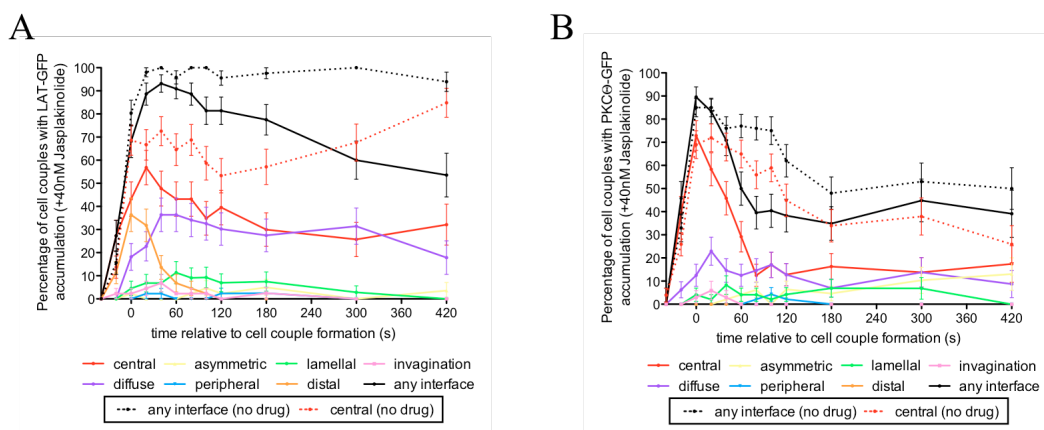


Figure 16. Disruption of actin dynamics diminishes sustained central localization of LAT and PKC θ . Pattern classification graphs are given for 5C.C7 T cells expressing **A)** LAT-GFP (n=44) or **B)** PKC θ -GFP (n=48) activated with CH27 APCs (10 μ M MCC) in the presence of 40nM JASP similar to Fig. 12E. Control ‘any interface’ and ‘central’ accumulation curves are plotted as a reference. Error bars are s.e.m.

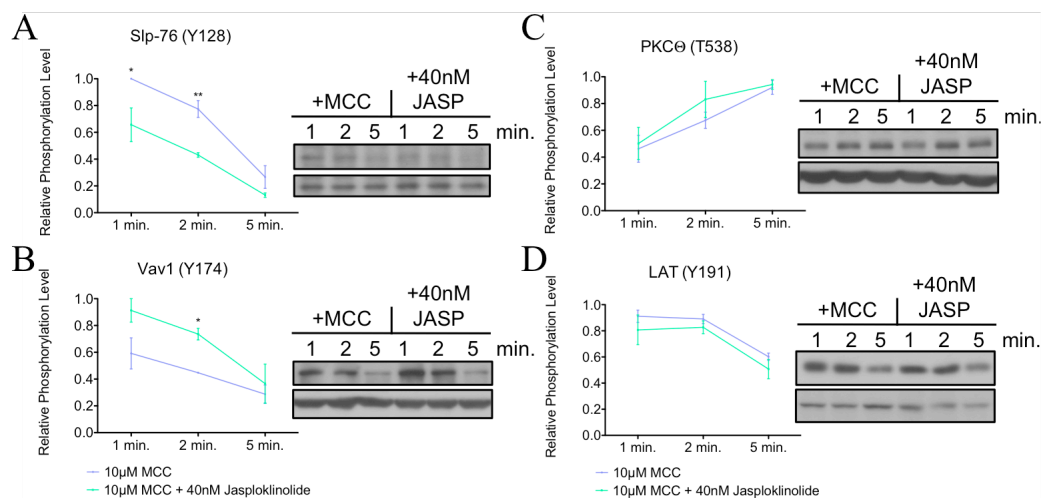


Figure 17. Disruption of actin dynamics with Jasplakinolide selectively modulates the activation of lamellar signaling intermediates. 5C.C7 T cells were activated with CH27 APCs (10μM MCC) in the presence of 40nM JASP. Phosphorylation levels for **A)** SLP-76, **B)** Vav1, **C)** PKCθ, and **D)** LAT were determined after 1, 2, and 5 minutes of stimulation by immunoblot. Graphs depict phosphorylation levels normalized to the max value (at least 3 independent experiments). Corresponding representative immunoblots are adjacent to each graph. Significance was determined by Student's t-test and is indicated by asterisks (*p<0.05, **p<0.001, ***p<0.0001).

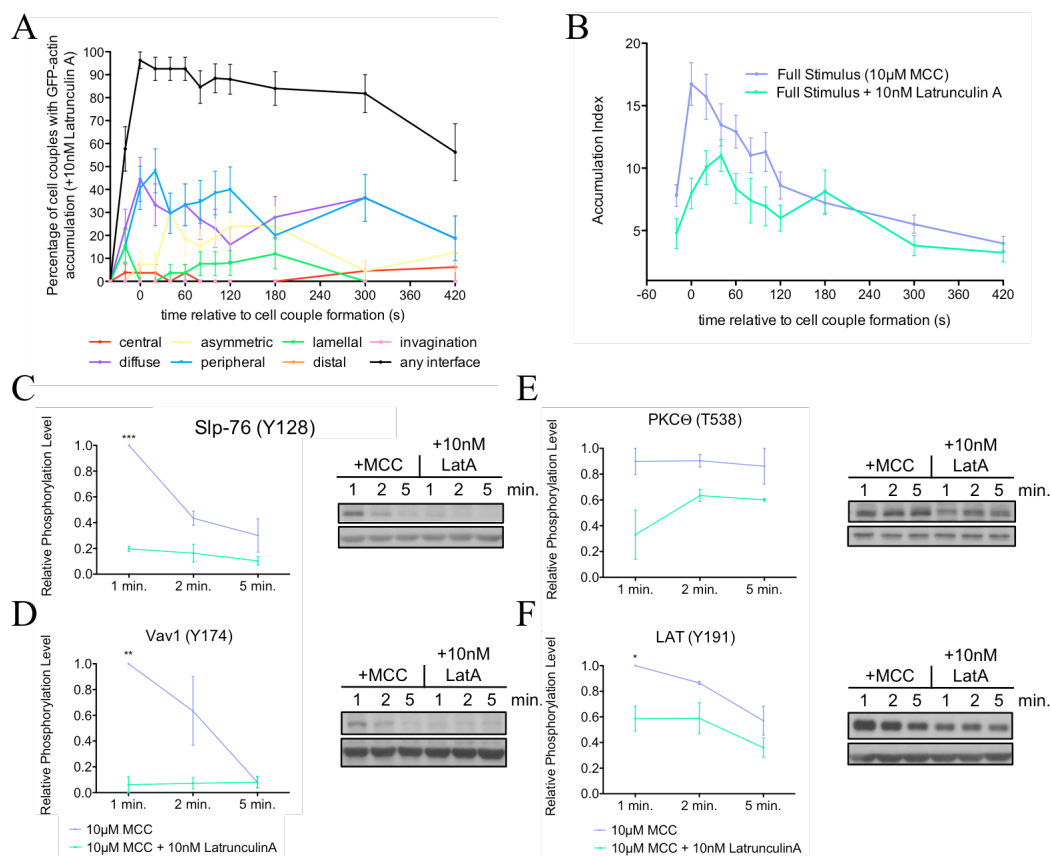


Figure 18. Disruption of actin with Latrunculin A severely diminishes T cell signaling. **A)** The pattern classification graph is given for 5C.C7 T cells expressing GFP-actin treated with 10nM LatA similar to fig. 3B ($n=27$). **B)** 5C.C7 T cells expressing GFP-actin were stimulated with peptide loaded CH27s ($10\mu\text{M}$ MCC) in the presence of 10nM LatA ($n=25$) or DMSO ($n=25$). The accumulation index was calculated as described in the 'Materials and Methods' and is plotted relative to tight cell conjugate formation. **C)** 5C.C7 T cells were activated with CH27 APCs ($10\mu\text{M}$ MCC) in the presence of 10nM LatA. Phosphorylation levels for SLP-76, **D)** Vav1, **E)** PKC θ , and **F)** LAT were determined after 1, 2, and 5 minutes of stimulation by immunoblot. Graphs depict phosphorylation levels normalized to the max value (at least 3 independent experiments). Corresponding representative immunoblots are adjacent to each graph. Error bar are s.e.m. Significance was determined by Student's t-test and is indicated by asterisks (* $p<0.05$, ** $p<0.001$, *** $p<0.0001$).

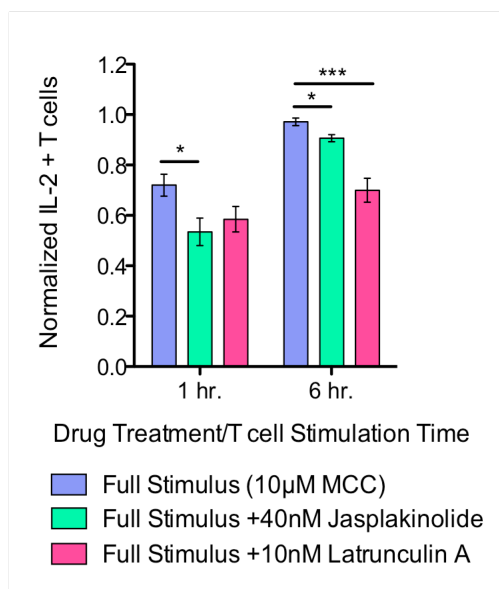


Figure 19. Selective disruption of actin dynamics during the first hour of T cell activation diminishes IL-2 production. IL-2 intracellular assays were performed with 5C.C7 T cells stimulated with CH27s (10µM MCC) in the presence of 40nM JASP, 10nM LatA or DMSO for 1 and 6 hours. The drugs were removed, a blocking MHC antibody was added and IL-2+ cells were measured at 24 hours. The percentage of IL-2+ cells is given normalized to the max percentage across the 1 and 6 hr. time points (3 independent experiments). Significance was determined by Student's t-test and is indicated by asterisks (* $p < 0.05$, ** $p < 0.001$, *** $p < 0.0001$).

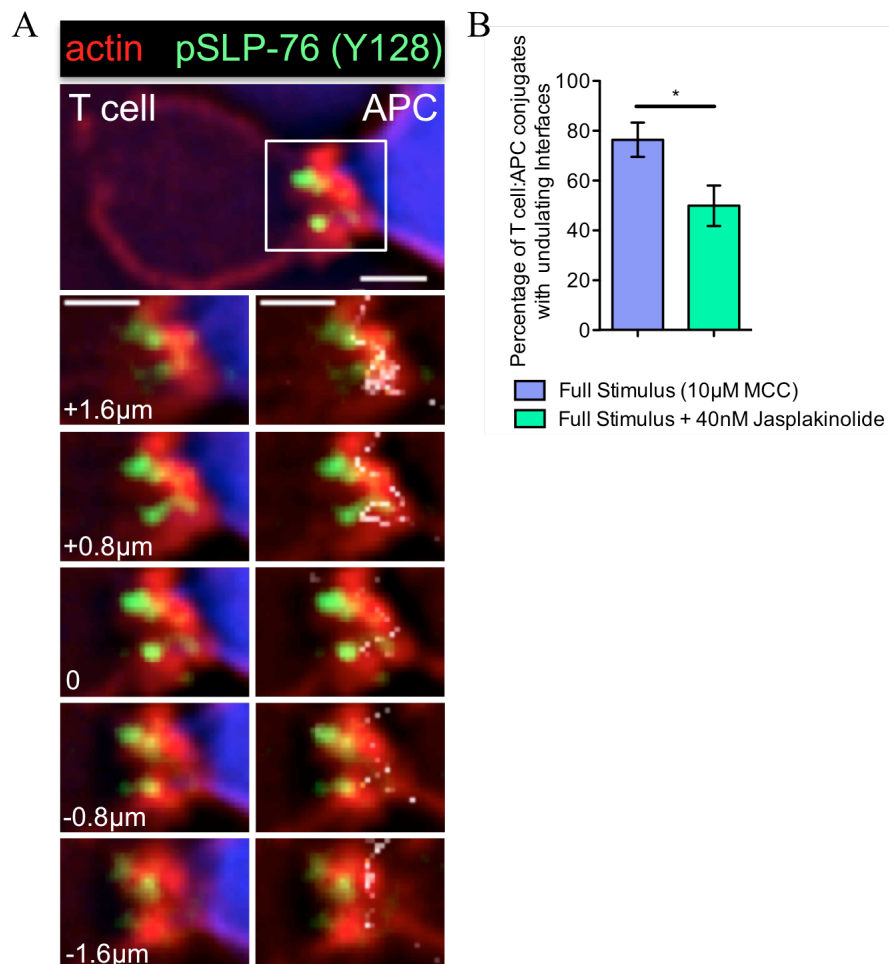


Figure 20. Deconvolution microscopy shows the early T cell:APC interface has an undulating and interdigitated architecture that is supported by actin. A) A representative image of a fixed 5C.C7 T cell:CH27 APC conjugate stained as in Fig. 10A-B is given. The whole T cell is shown on top at the center z plane. Below are zoomed in images of the interface at the z-planes indicated relative to the T cell center. The right column shows the APC outline as a white line (scale bars=2µm). **B)** Fixed 5C.C7 T cell:CH27 APC conjugates were control DMSO (n=38) or 40nM JASP (n=38) treated and the percentage of T cells with interdigitated membrane architecture was determined as described in the 'Materials and Methods' for the same cell conjugates as in Fig. 10 and 13.. Significance was determined by Student's t-test and is indicated by asterisks (*p<0.05, **p<0.001, ***p<0.0001).

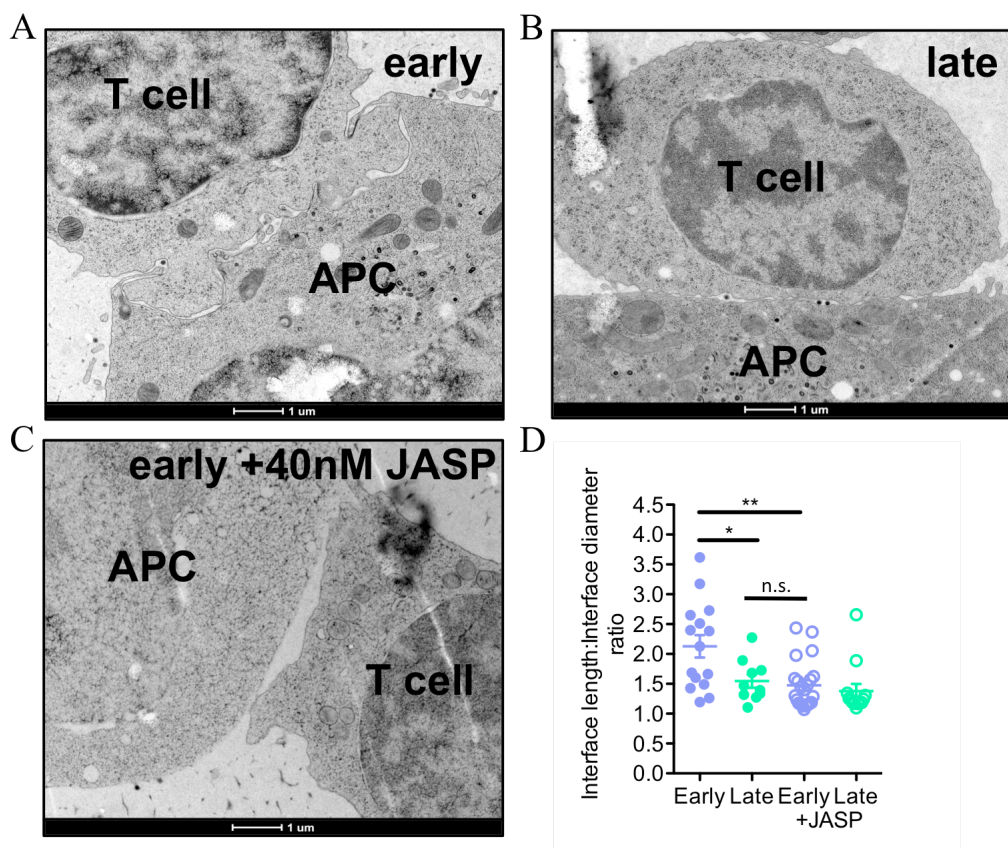


Figure 21. Electron microscopy shows the early T cell:APC interface has an undulating and interdigitated architecture that is supported by actin. A) A representative early (0-2min.), **B)** late (>2min.), and **C)** early (+40nM JASP) electron micrograph image of a 5C.C7:CH27 APC conjugate (10μM MCC) is given. **D)** The interface length to diameter ratio is given for early (n=15) and late (n=10) DMSO and early (n=22) and late (n=16) 40nM JASP treated cell conjugates (see fig. 2A for analysis details). Error bars are s.e.m. Significance was determined by Student's t-test and is indicated by asterisks (*p<0.05, **p<0.001, ***p<0.0001).

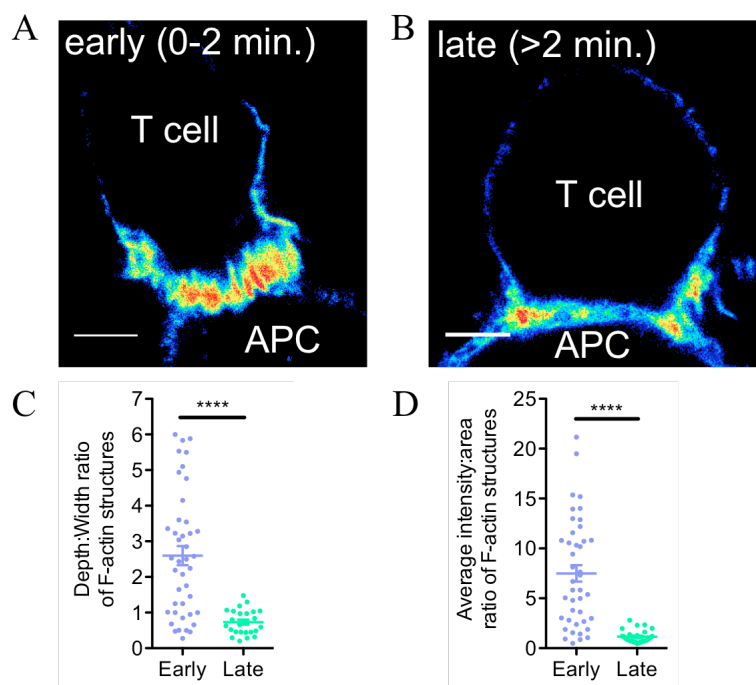


Figure 22. The early F-actin structures at the T cell:APC interface are discreet, limited in size, and oriented perpendicular to the interface plane. A) Representative phalloidin stained early (0-2min.) and **B)** late (>2min.) 5C.C7 T cell:CH27 APC conjugates imaged by STED similar to fig. 7A are given (scale bars=2μm). **C)** The depth to width ratio of resolved phalloidin stained F-actin structures (>135% above cellular background) in early (n=12) and late (n=12) STED imaged 5C.C7 T cell:CH27 APC conjugates is given. **D)** The average intensity to area ratio of F-actin structures from panel C is given. See fig. 2B for analysis details. Error bars are s.e.m. Significance was determined by Student's t-test and is indicated by asterisks (*p<0.05, **p<0.001, ***p<0.0001).

Systems-scale Integration of T cell Receptor and Co-stimulatory Signals Regulate Actin Dynamics Required for T cell Activation

Systems-scale assessment of actin regulation at the T cell:APC interface reveals the requirement of CD28 co-stimulation for sustained actin regulation

T cell actin dynamics are regulated through engagement of multiple receptors during early T cell activation including the co-stimulatory receptor CD28 [10]. Bone fide upstream initiators of actin regulation such as Vav1, Grb2, and Itk have been implicated in CD28 signaling [64], but it is unclear how CD28 contributes to polarized actin dynamics at the T cell:APC interface and subsequent T cell activation. A large-scale network of actin regulatory molecules are involved in F-actin nucleation, capping, and severing. To provide a quantitative and systems-level perspective of actin regulation in T cells, we have monitored the spatiotemporal dynamics of a group principle actin regulators that include NPFs, WASp and WAVE2, the branched actin nucleator ARP2/3, the F-actin stabilization factor HS1, the actin filament capping protein, the negative regulator of the ARP2/3 complex Coronin1A, the actin motor protein and destabilization factor Myosin II, and the F-actin severing protein Cofilin in primary T cells (fig. 23). These molecules together are able to recapitulate actin polymerization *in vitro* and disruption of any one of them impaired multiple aspects of T cell biology [19,74].

We used live cell fluorescence spinning-disk confocal microscopy to monitor the spatiotemporal patterning of the actin regulatory network in primary *ex vivo* primed 5C.C7 CD4⁺ TCR transgenic T cells activated with CH27 B cell lymphoma APCs pulsed

with 10 μ M MCC peptide. To isolate the contribution of CD28 co-stimulation to early T cell actin regulation, CD28 signaling was blocked with antibodies directed towards its cognate ligands, B7-1 and B7-2, on the APC (B7 blockade condition). The spatiotemporal organization of actin itself remained intact when CD28 signaling was blocked (fig. 24A-B). The characteristic peripheral ring of accumulation was maintained as 50.0 \pm 5.6% T cells that received full stimulation showed peripheral accumulation of actin at time 0 compared to 53.7 \pm 4.8% for the B7 blockade condition ($p>0.05$). Overall T cell:APC interface accumulation of actin was also retained with B7 blockade as the percentage was equivalent to full stimulation at all time points ($p>0.05$) (fig. 24A-B). Despite intact spatiotemporal organization of actin, the amounts of actin at the T cell:APC interface as measured by the 'accumulation index' were reduced without CD28 co-stimulation at time 0 from 16.7 \pm 1.7 to 10.5 \pm 0.9 ($p=0.003$) and the reduction was maintained at 1 minute (12.9 \pm 1.3 to 6.0 \pm 0.6, $p<0.0001$) (fig. 24C). This time period encompasses the peak of polarized actin polymerization. Thus, CD28 co-stimulation is required for initial and sustained actin enrichment at the T cell:APC interface.

The enrichment of the actin regulatory network at the T cell:APC interface coincided with actin polymerization and their spatiotemporal patterning was similar to actin with the exception of the active Myosin II sensor, Myosin II regulatory light chain (MRLC) (fig. 25-33). The actin regulators showed dominant peripheral and diffuse spatiotemporal organization at the interface. For example, ARP2/3 was localized to the periphery of 60.4 \pm 4.6% of T cells at time 0 and retained peripheral patterning during the first minutes of T cell activation. Diffuse and lamellar patterning occurred in parallel to peripheral patterning for ARP2/3 and the other actin regulatory proteins (fig. 25A). Actin

and the actin regulators showed sustained enrichment at the interface as between 90% and 100% of T cells maintained interface enrichment of the molecules during the first minute of activation and after 7 minutes between 50% and 90% of T cells showed enrichment depending on the protein (with the exception MRLC) (fig. 25-33).

While changes in spatiotemporal organization of the actin regulators occurred when CD28 co-stimulation was blocked, the most striking effect of co-stimulation blockade was the overall transience in the accumulation of the molecules at the T cell:APC interface compared to full stimulation (fig. 25-33). For example, WAVE2 and Cofilin were the most drastically affected. Cofilin retained accumulation at time 0, however, peripheral enrichment was diminished from $57.4 \pm 4.0\%$ to $24.4 \pm 4.0\%$ ($p < 0.0001$) (fig. 27). For WAVE2, even 'any interface accumulation' was diminished as of time 0 from 100% to $66.7 \pm 5.8\%$ ($p < 0.0001$) (fig. 27). By 2 minutes after cell conjugate formation nearly 100% of T cells retained accumulation of Cofilin and WAVE2 under control conditions, however, without co-stimulation only $44.0 \pm 5.0\%$ and $10.3 \pm 4.0\%$ showed interface enrichment, respectively ($p < 0.0001$ for both) (fig. 27 and 32). The other actin regulators also showed transient recruited to the interface without co-stimulation (fig. 25-33). Thus, CD28 signaling in part acted to maintain the activity of the actin regulatory network at the T cell:APC interface.

Interestingly, MRLC responded differently to co-stimulation blockade. While its recruitment was more transient as observed for the other actin regulators, it was more rapidly recruited to the T cell:APC interface when co-stimulation was blocked (fig. 30). The peak of MRLC recruitment (~83% of T cells with accumulation for both full stimulus and B7 blockade) was at 1 minute 40 seconds after cell conjugate formation and

at 40 seconds without co-stimulation (fig. 30). The more rapid recruitment of MRLC to the T cell:APC interface resulted in more transient accumulation as by 3 minutes $62.0 \pm 7.5\%$ of T cells under full stimulus conditions showed MRLC accumulation compared to $29.0 \pm 8.2\%$ without co-stimulation ($p < 0.0001$) (fig.30). Myosin II can mediate F-actin depolymerization [33] thus more rapid recruitment to the interface upon blockade of CD28 signaling may contribute the diminished actin levels.

Biochemical reactions involved in cellular signal transduction are concentration-dependent, thus the levels of enrichment of the actin regulatory network components in addition to their spatiotemporal organization are critical parameters controlling actin dynamics. Therefore, we measured the enrichment of the molecules at the T cell:APC interface in regions of accumulation compared to the average intensity of the molecule in the entire cell. We then further scaled the resultant fold-enrichment by multiplying it by the fraction of T cells with accumulation at the corresponding time point (enrichment index). Enrichment levels of the actin regulatory network were significantly affected by loss of CD28 signaling (fig. 33). As with the spatiotemporal patterning data, Cofilin and WAVE2 were the most drastically affected. The enrichment index for Cofilin at time 0 was reduced from 1.93 ± 0.05 to 1.80 ± 0.04 ($p = 0.04$) and by 1 minute from 1.87 ± 0.05 to 1.19 ± 0.03 ($p < 0.0001$) without CD28 signaling (fig. 33C). WAVE2 enrichment was even more reduced with a reduction from 3.20 ± 0.13 to 1.87 ± 0.11 ($p < 0.0001$) at time 0 and 2.72 ± 0.16 to 0.71 ± 0.03 ($p < 0.0001$) at 1 minute (fig. 33H). All other actin regulators with the exception of ARP2/3 also showed diminished enrichment at the 1 minute time point ($p < 0.05$ for all) (fig. 33). ARP2/3 surprisingly showed increased enrichment without CD28 signaling. The enrichment index for ARP2/3 increased at time 0 from 1.92 ± 0.02 to

3.02±0.09 ($p<0.0001$) and remained higher at 1 minute (1.96±0.03 vs. 2.77±0.08 $p<0.0001$) (fig. 33B). It is possible that ARP2/3 localization was retained, but it was not effectively activated by NPFs.

These data reveal a requirement for CD28 co-stimulation for retention of a large scale network of actin regulatory proteins at the T cell:APC interface and also identify the cytoskeletal regulators, WAVE2 and Cofilin, as highly dependent on CD28 co-stimulation. Furthermore, the enrichment levels of the different molecule differ greatly without CD28 signaling leading to altered stoichiometries of the actin regulatory network at the T cell:APC interface, which likely further contributes to the observed reduction in actin dynamics.

CD28 sustains recruitment and activation of regulators of the WAVE2 complex

WAVE2 is required for polarized actin polymerization at the T cell:APC interface [43] and here we have shown that co-stimulation is necessary for the support of initial and sustained recruitment of WAVE2 to the T cell:APC interface (fig. 32-33). Therefore, a major role of CD28 signaling may be to maintain WAVE2-mediated actin dynamics required for T cell signaling and activation. Given the drastic reduction in WAVE2 recruitment to the T cell:APC interface in the absence of CD28 signaling, we determined the effects of loss of co-stimulation on upstream regulators of WAVE2. Specifically, we assessed the spatiotemporal patterning of the critical Rho family GEF, Vav1, which among other functions activates the small GTPase required for WAVE2 activation, Rac1. Both Vav1 and Rac1 showed altered spatiotemporal organization and

impaired recruitment to the T cell:APC interface without CD28 signaling (fig. 34-35). At time 0, an equivalent percentage of T cells enriched Vav1 at the T cell:APC interface ($83.3 \pm 3.3\%$ versus $78.4 \pm 5.8\%$ without co-stimulation, $p > 0.05$). However, sustained recruitment of Vav1 was co-stimulation dependent as $83.7 \pm 3.9\%$ of fully stimulated T cells showed accumulation while only $47.9 \pm 7.2\%$ accumulated Vav1 without CD28 signaling at 1 minute ($p < 0.0001$). Co-stimulation mostly affected lamellar localization of Vav1, as there was a reduction in the percentage of T cells with lamellar patterning from $39.3 \pm 5.1\%$ to $16.7 \pm 5.4\%$ at 1 minute ($p = 0.01$). Loss of co-stimulation not only impaired the spatiotemporal organization of Vav1, but also enrichment levels at the T cell:APC interface. The enrichment index for Vav1 as of time 0 (2.75 ± 0.10 to 2.12 ± 0.08 , $p < 0.0001$), and at 1 minute the reduction was maintained (2.03 ± 0.05 vs. 1.24 ± 0.12 , $p < 0.0001$) (fig. 36B). Therefore, Vav1 localization and likely activity was diminished at the T cell:APC interface upon co-stimulation blockade

The active Rac1 sensor showed similar defects in sustained enrichment at the T cell:APC interface without CD28 signaling (fig. 35). Initial recruitment was intact as $46.8 \pm 6.3\%$ and $38.3 \pm 7.1\%$ of T cells showed accumulation at time 0 under control and B7 blockade conditions, respectively ($p > 0.05$). By 1 minute there was a severe defect in active Rac1 enrichment. $75.9 \pm 5.6\%$ of fully stimulated T cells enriched the active Rac1 sensor but only $39.1 \pm 7.2\%$ showed accumulation without co-stimulation. Sustained central accumulation was particularly impaired as the percentage of T cells with centrally localized active Rac1 was reduced from $41.4 \pm 6.5\%$ to $19.6 \pm 15.9\%$ without CD28 signaling ($p = 0.03$) (fig. 35). The enrichment index for the active Rac1 sensor was also reduced without co-stimulation from 0.92 ± 0.05 to 0.67 ± 0.02 at time 0 ($p < 0.0001$) and

1.52±0.09 to 0.75±0.03 at 1 minute ($p<0.0001$) (fig. 36C). Thus, Vav1 and Rac1 activity was impaired at the T cell:APC interface and likely contributed to loss of WAVE2 localization and decreased actin enrichment at the T cell:APC interface. These data also suggest that TCR signaling alone may support a substantial part of the initial activity of the actin regulatory network as enrichment was retained at the 0 time point, but co-stimulation is required for maintained signaling as enrichment was severely impaired by 1 minute.

System-scale assessment reveals a loss in coordinated spatiotemporal regulation of the actin regulatory network

To gain insight into the control of spatiotemporal patterning of the actin regulatory network and upstream regulatory molecules by CD28 signaling at the system-systems-scale, we hierarchically clustered the molecules based on their dynamic patterning data (fig. 22-32, 34-35) under control and co-stimulation blockade conditions (fig. 37). The actin regulators showed highly coordinated spatiotemporal dynamics under full stimulus conditions (fig. 37). However, without CD28 signaling the overall network of actin regulators showed less coordinated spatiotemporal dynamics revealed by the loss of the tightly correlated cluster of the principle actin regulators WAVE2, HS1, Cofilin, Coronin1A, ARP2/3, CPα1, and WASp. WAVE2 is completely absent from the actin regulatory network cluster without CD28 signaling (fig. 37). Myosin II (MRLC) showed the opposite change as blockade of CD28 signaling resulted in higher correlation with the actin regulatory network cluster (fig. 37). This further supports the notion that CD28 may

in part act to constrain Myosin II activity at the T cell:APC interface during initial T cell activation. Rac1 and PKC θ (centrally localized molecules) are less correlated with each other, likely due to a reduction in their sustained central localization (fig. 37). These data suggest that co-stimulation both controls the sustained recruitment and peripheral organization of the actin regulatory machinery and also contributes to the maintained central localization of signaling intermediates. Therefore, CD28 signaling controls the initial actin burst and sustained actin regulator dynamics required for the organization and maintenance of polarization of the T cell signaling system.

Constitutively active Rac1 and Cofilin restore actin enrichment at the T cell:APC interface and AKT activation despite inhibition of CD28 co-stimulation

The most severe effect of loss of CD28 signaling on the actin regulatory network was reduced recruitment of WAVE2 and Cofilin to the T cell:APC interface. Therefore, we attempted to restore WAVE2 and Cofilin activity under co-stimulation blockade conditions by treating T cells with cell permeable tat-tagged constitutively active Rac1 Q61L (Rac1CA) and Cofilin S3A (CofilinCA) before performing live cell imaging experiments. 5C.C7 T cells expressing actin-GFP were treated with 1 μ M Rac1CA and 0.25 μ M CofilinCA and activated by antigen pulsed CH27s under co-stimulation blockade conditions. The enrichment index for actin was restored in T cells pretreated with the proteins at all time points except for at 7 minutes (Full Stimulus vs. Reconstitution $p > 0.05$) (fig. 38A). WAVE2 was also imaged under the same conditions to assess whether sustained recruitment of WAVE2 was also restored. WAVE2 enrichment

showed complete restoration during the first two minutes of T cell activation (Full Stimulus vs Reconstitution $p>0.05$). Later time points were also restored but the enrichment index was slightly higher with Rac1CA and CofilinCA treatment (fig. 38B).

One of the hallmark signaling events downstream of CD28 is the phosphorylation of AKT, which controls T cell survival and proliferation [64]. Therefore, we determined whether reconstitution of actin with Rac1CA and CofilinCA not only restored actin dynamics but also AKT activity. 5C.C7 T cells treated with Rac1CA and CofilinCA were activated with CH27s under co-stimulation blockade conditions and restoration of AKT phosphorylation was assessed by immunoblot. Blockade of CD28 signaling caused a 27% reduction in phosphorylation of AKT T468 (pAKT) after 30 minutes of stimulation ($p=0.007$). Full stimulus levels of pAKT were restored when T cells were treated with Rac1CA and CofilinCA (fig. 39). Therefore, reconstitution Cofilin and WAVE2 activity under co-stimulation blockade conditions not only restored actin dynamics, but also restored critical proximal signaling steps required for T cell activation. However, IL-2 production was not restored by reconstitution of actin dynamics (fig. 40).

Quantification of the spatiotemporal organization of the actin regulatory machinery in live T cells

Cellular signaling requires coordinated regulation of large-scale networks of signaling intermediates in complex 3-dimensional cellular geometries [75]. To further quantify and assess the regulation of cellular signaling by spatiotemporal patterning, we have developed approaches to measure parameters required for 4D modeling of signaling systems in live cells. These parameters included: 1) the average T cell volume, 2) molar concentrations of component molecules, 3) diffusion characteristics of the molecules, and 4) time resolved whole T cell maps of local molar concentrations of fluorescently labeled signaling intermediate sensors (fig. 41). These parameters along with previously determined biochemical characteristics of the actin regulatory proteins can be utilized to build 4D models of cellular signaling systems. Here we have determined the parameters for the principle group of actin regulatory molecules described above to gain further insight into regulation of the actin network during early T cell activation and the contribution of CD28 signaling to the regulation of actin (fig. 23). While the more traditional cell biological experiments described in previous sections yielded critical insight into the systems-level control of actin dynamics by co-stimulation, they did not provide comprehensive mechanistic insight into how the group of actin regulators coordinate the generation and turn over of F-actin at the T cell:APC interface or how the global changes in actin regulation caused by loss of CD28 signaling led to diminished actin dynamics. These complex questions are best addressed by mathematical models, which can handle such multi-factorial systems in space and time.

Concentrations of the actin regulatory network in primary T cells

To assess molar concentration of the actin regulatory network in live primary T cells, we first made volumetric measurements of *ex vivo* primed 5C.C7 T cells. Live T cells were first labeled with SNARF-1 as a whole cell stain and Hoechst to delineate the nucleus. The live T cells were then imaged by confocal microscopy and volumetric measurements were made of the whole T cell and nucleus. The average T cell volume was $394.3 \pm 9.3 \mu\text{m}^3$ and the nucleus volume was $264.3 \pm 6.1 \mu\text{m}^3$. Thus, the cytoplasm volume was $130.1 \pm 5.6 \mu\text{m}^3$ or $32.4 \pm 1.3\%$ of the T cell volume (fig. 42). Molar concentrations of the actin regulatory network were determined by quantitative immunoblots and cell-to-cell variability in expression was assessed by flow cytometry. Representative quantitative immunoblots are shown in figure 43. The average mass (ng amount) of each molecule per individual T cell was calculated and converted to an average molar concentration based on the volume measurements of an average T cell. The actin regulators with the exception of Cofilin were predominantly localized in the cytoplasm. Therefore, calculated molar concentrations for Cofilin were based on the whole T cell volume while all others were based on the cytoplasmic volume. Cell-to-cell variability of expression was shown to inversely correlate with the expression level of the protein [76,77]. Therefore, we assessed the cell-to-cell variability in expression of a high (Coronin1A), middle (Cofilin), and low (WAVE2) expressed actin regulator by flow cytometry. The variability in expression of the actin regulators was log-normally distributed and did not significantly differ for the three proteins ($\text{CV} = 0.33 \pm 0.04$ - 0.44 ± 0.01) (fig. 44A-F). The 5th to 95th percentile range of single cell molar

concentrations was determined based on the average molar concentration determined by quantitative immunoblotting and the corresponding log-normal distribution (fig. 44G). The average concentration of the actin regulators ranged from 4.2 μ M for Cofilin to 88.3 μ M for Coronin1A and by far the most highly expressed protein was actin itself with an average concentration of 293.5 μ M (fig. 45). Given that our experiments were done by retroviral transduction, overexpression levels were carefully assessed. Other than CP α 1, the mean overexpression level of the actin regulators fell within the endogenous range of expression. For CP α 1 the overexpression mean was 2-fold higher than the endogenous mean (fig. 45). However, CP α 1-expressing T cells showed no impairment in T cell:APC conjugate formation or interface spreading, which are sensitive parameters that help determine whether there is overexpression-mediated perturbation of T cell signaling.

Our data and others have shown that the cell-to-cell variability in protein expression is log-normally distributed [76,78], however, the size of cells at the high end of expression was not assessed. This was a critical question as if the high expressing cells were simply larger cells, the molar concentration range would vary less than the distribution would suggest. To obtain a rough estimate of cell size, forward scatter characteristics were measured for the low, middle, and high WAVE2, Cofilin, and Coronin1A-expressing T cells. For all three actin regulators the expression level roughly scaled with cell size (fig. 46). Therefore, the actual single cell molar concentration range was narrower than the log-normal distribution suggested.

Actin regulation at the T cell:APC interface is highly dynamic

Biochemical reactions in live cells are not only dependent on concentration, but also depend on the diffusion of molecules within the cellular space. To determine the diffusion characteristics of the actin regulatory network, we performed FRAP in 5C.C7 T cells during the first minutes of activation with antigen-pulsed CH27s. The half-times of recovery for the actin regulatory molecules and actin were rapid, ranging from 0.8 ± 0.2 s for Cofilin to 2.8 ± 0.4 s for ARP2/3 and showed on average 70% recovery over a timescale of 10s (fig. 47A-B). Furthermore, the actin regulators showed from 1.7 to 3.6-fold slower diffusion in regions of accumulation at the T cell:APC interface compared to other areas of the T cell where the molecules were not enriched (with the exception of Cofilin) (fig. 47C). Centrally localized molecules such as LAT, PKC θ , and Rac1, had longer half times of recovery ranging from 3.6 ± 0.6 s for PKC θ to 10.0 ± 1.7 s for LAT and on average only 30% recovery over a timescale of 20 to 40s (fig. 47A-B). These data showed that actin regulation was highly dynamic whereas centrally localized signaling complexes were more stable and may be highly cross-linked. Thus, the continual recruitment of the more dynamic actin regulatory machinery to the T cell:APC interface is likely necessary to support the longer lived signaling complexes involved in proximal T cell signal transduction.

High-throughput assessment of dynamic local concentrations of fluorescently labeled molecules in live T cells

To quantitatively define the spatiotemporal distribution T cell signaling intermediates for 4D modeling of signaling systems, we have developed software in collaboration with Dr. Robert Murphy's group at Carnegie Mellon University that allows for high-throughput assessment of dynamic local molar concentrations in live T cells (see fig. 48 details). The software has recently been optimized and is currently being used to build whole T cell time-resolved maps of the local molar concentration of the actin regulatory network under full stimulus and co-stimulation blockade conditions. These data combined with the above set of parameters will be used to build a 4D model of actin regulation at the T cell:APC interface and provide more comprehensive insight into the control of actin by CD28 signaling.

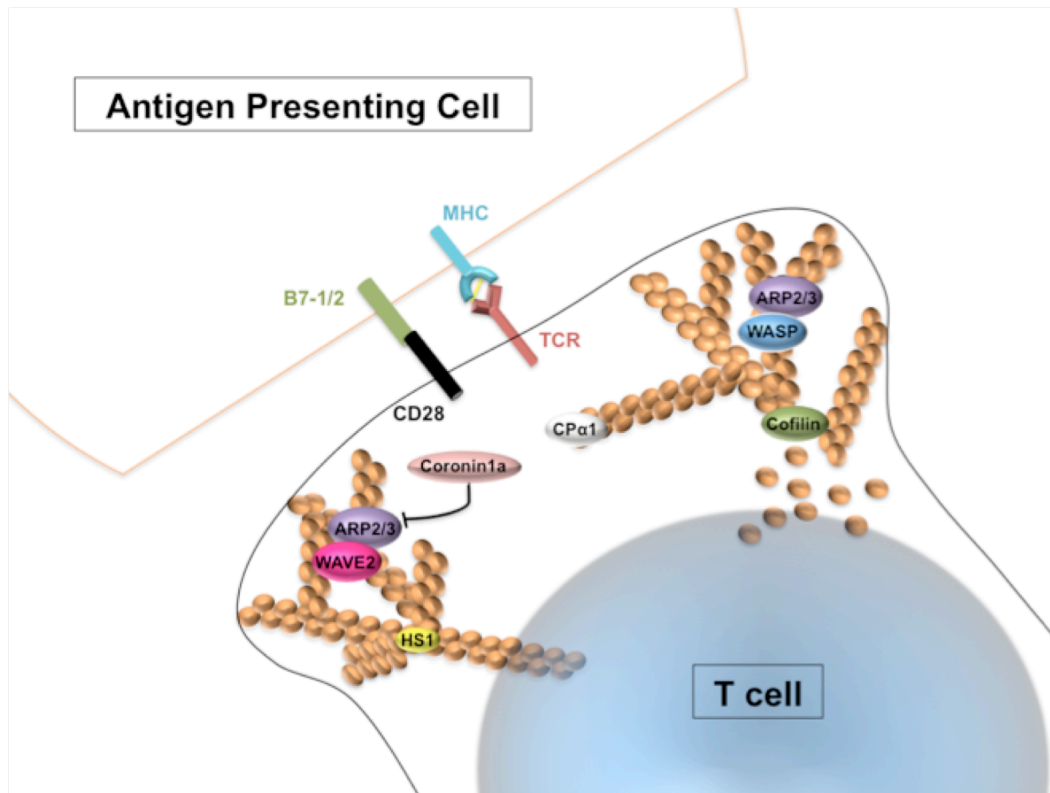


Figure 23. A systems-level view of actin regulation during early T cell activation. Actin dynamics are regulated by coordinated nucleation, polymerization, capping, stabilization, and severing of actin filaments. These processes are controlled by a group of key actin regulators shown above. ARP2/3 is the principal branched actin nucleation factor, which is activated by nucleation promoting factors WAVE2 and WASP. Coronin1A is a negative regulator of ARP2/3 nucleation. Capping protein $\alpha 1$ (CP $\alpha 1$) caps growing actin filaments and Cofilin is a severing factor. HS1 stabilizes actin filaments. The concerted regulation of actin dynamics by these factors is required for efficient T cell activation and controlled by both TCR stimulation and other cell surface receptors such as CD28.

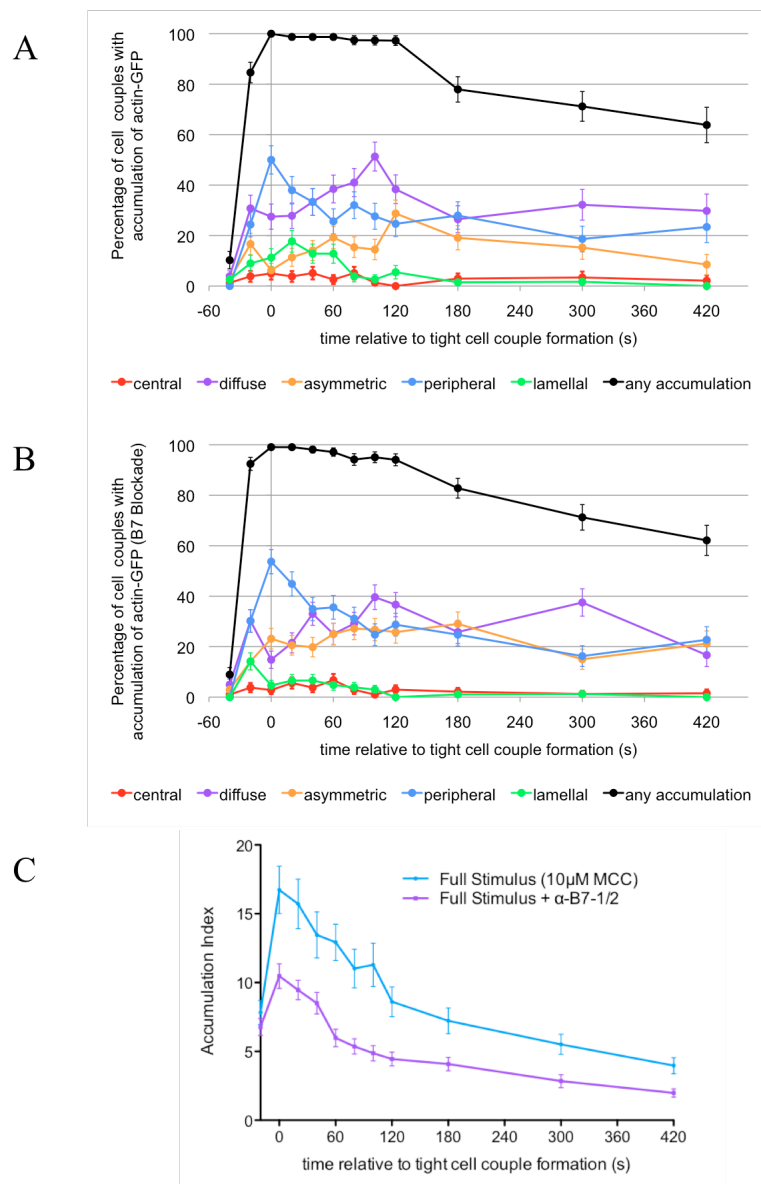


Figure 24. Spatiotemporal patterning of actin-GFP is retained without CD28 co-stimulation but the amount actin at the T cell:APC interface is reduced. Primed primary 5C.C7 T cells expressing actin-GFP were imaged with CH27 APCs under **A**) full stimulus (10μM MCC) or **B**) full-stimulus plus CD28:B7 co-stimulation blockade (10μg/mL α-B7-1/2). The time series is relative to formation of a tight cell couple. The percentage of T cells showing each spatiotemporal pattern is reported as a separate curve (n=>100 cell couples for each condition). **C**) The 'Accumulation Index' for actin-GFP under full-stimulus and B7-blockade conditions is given similar to fig. 12C. Error bars represent s.e.m.

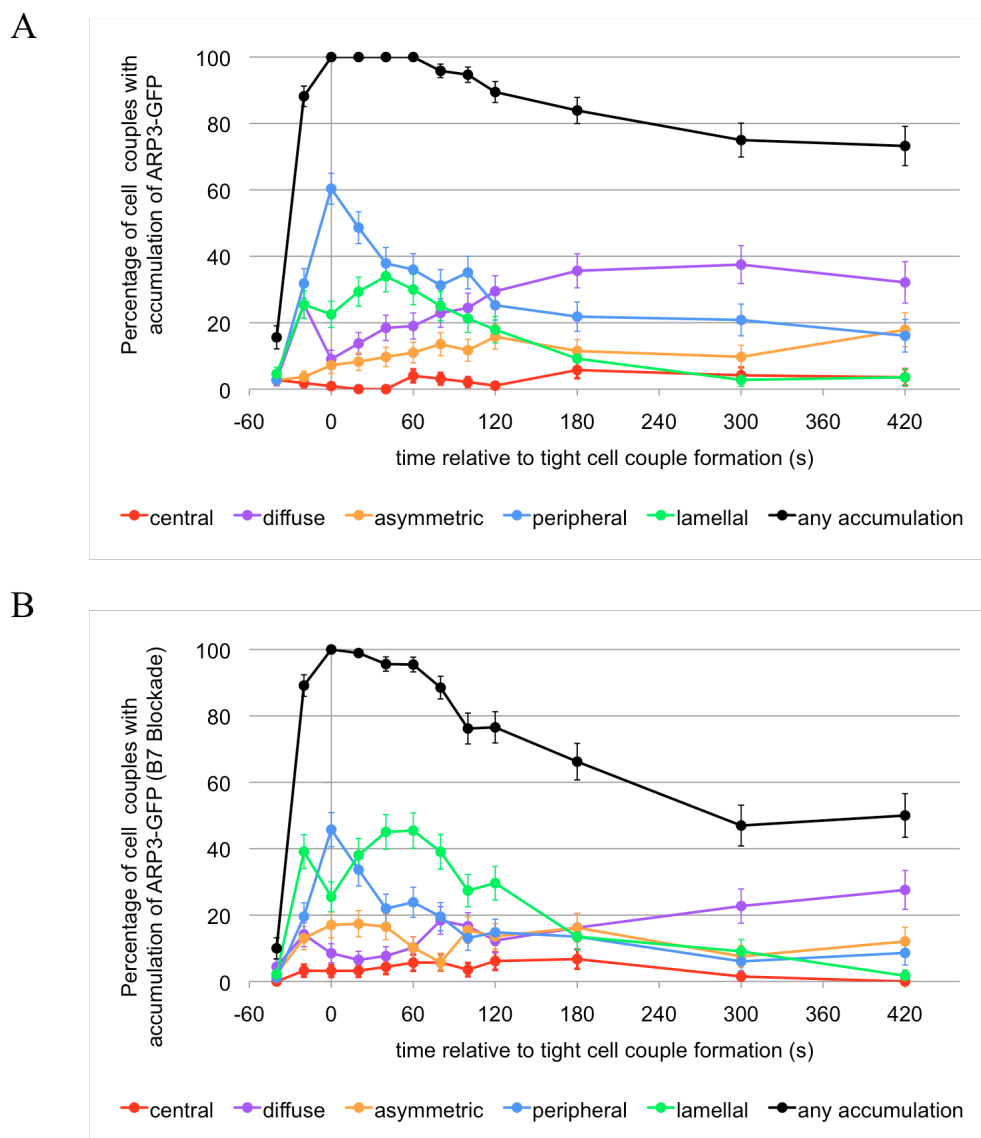
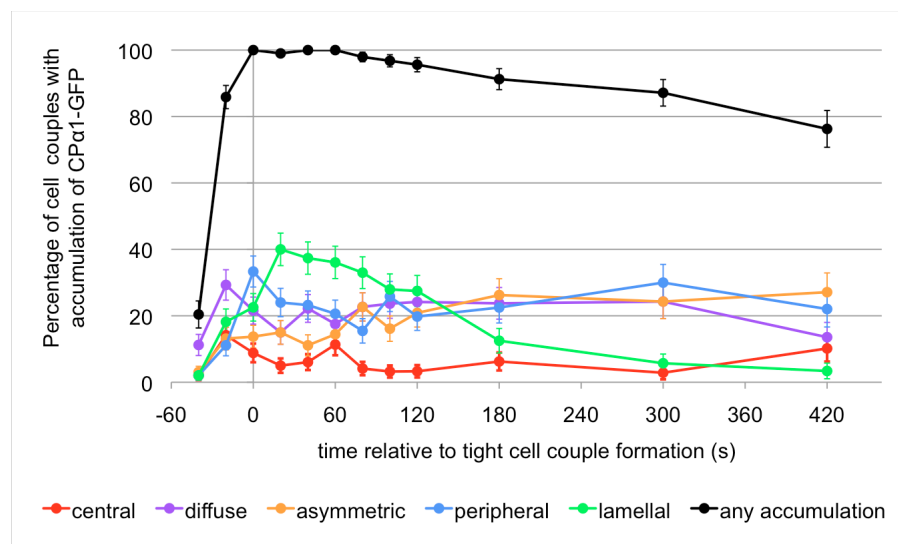


Figure 25. Spatiotemporal patterning of ARP3-GFP at the T cell:APC interface is more transient without CD28 co-stimulation. Primed primary 5C.C7 T cells expressing ARP3-GFP were imaged with CH27 APCs under **A**) full stimulus (10 μ M MCC) or **B**) full-stimulus plus CD28:B7 co-stimulation blockade (10 μ g/mL α -B7-1/2). The time series is relative to formation of a tight cell couple. The percentage of T cells showing each spatiotemporal pattern is reported as a separate curve. Error bars represent s.e.m. (n>=100 cell couples for each condition).

A



B

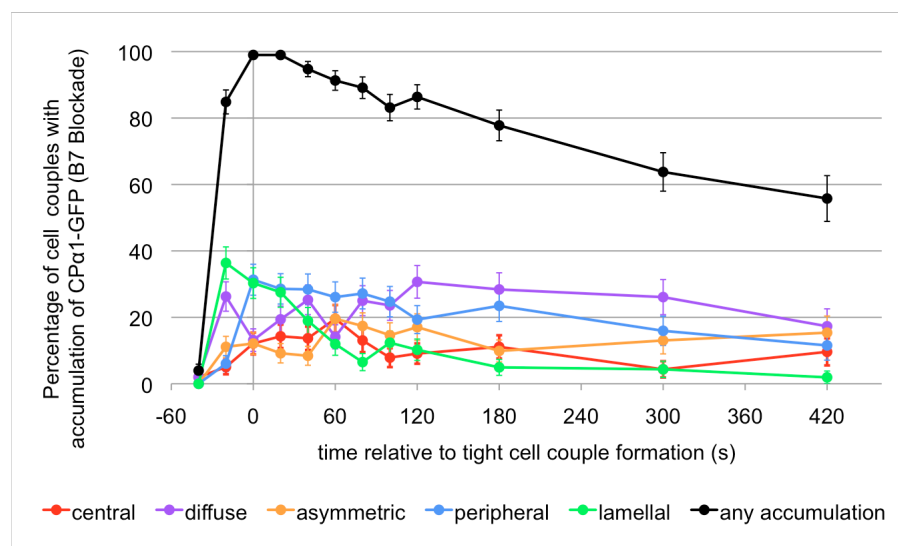
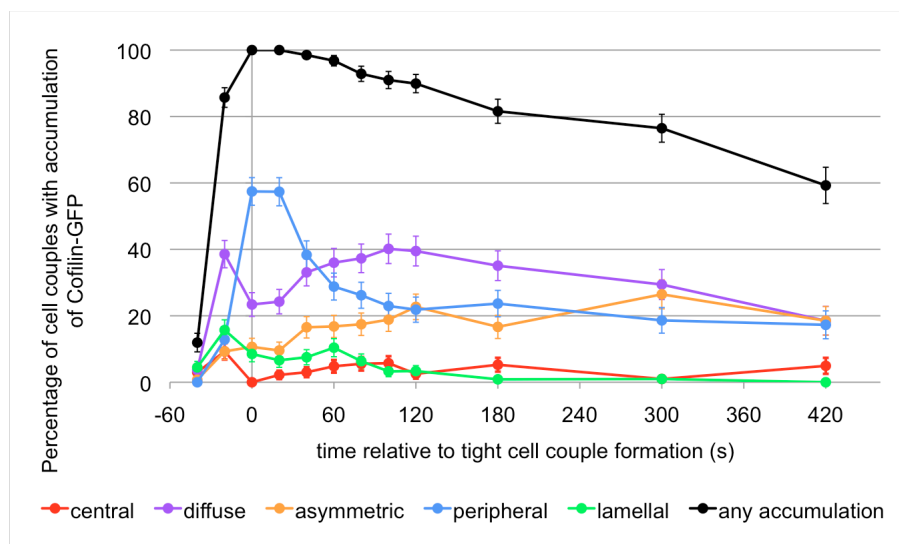


Figure 26. Lamellar localization of CPα1-GFP is more transient without CD28 co-stimulation. Primed primary 5C.C7 T cells expressing CPα1-GFP were imaged with CH27 APCs under **A)** full stimulus (10μM MCC) or **B)** full-stimulus plus CD28:B7 co-stimulation blockade (10μg/mL α-B7-1/2). The time series is relative to formation of a tight cell couple. The percentage of T cells showing each spatiotemporal pattern is reported as a separate curve. Error bars represent s.e.m. (n>100 cell couples for each condition).

A



B

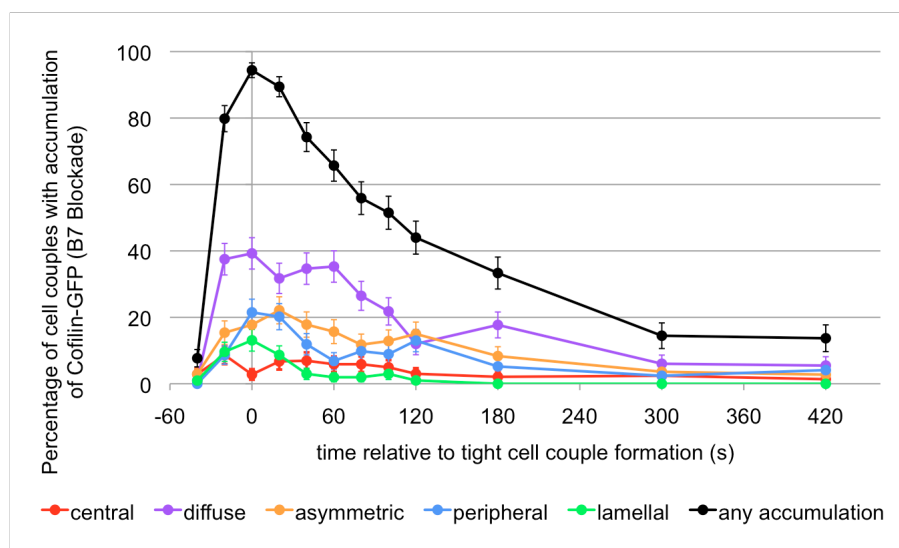


Figure 27. Peripheral localization of Cofilin-GFP at the T cell:APC interface is lost and overall enrichment is more transient without CD28 co-stimulation. Primed primary 5C.C7 T cells expressing Cofilin-GFP were imaged with CH27 APCs under **A**) full stimulus (10μM MCC) or **B**) full-stimulus plus CD28:B7 co-stimulation blockade (10μg/mL α-B7-1/2). The time series is relative to formation of a tight cell couple. The percentage of T cells showing each spatiotemporal pattern is reported as a separate curve. Error bars represent s.e.m. (n>100 cell couples for each condition).

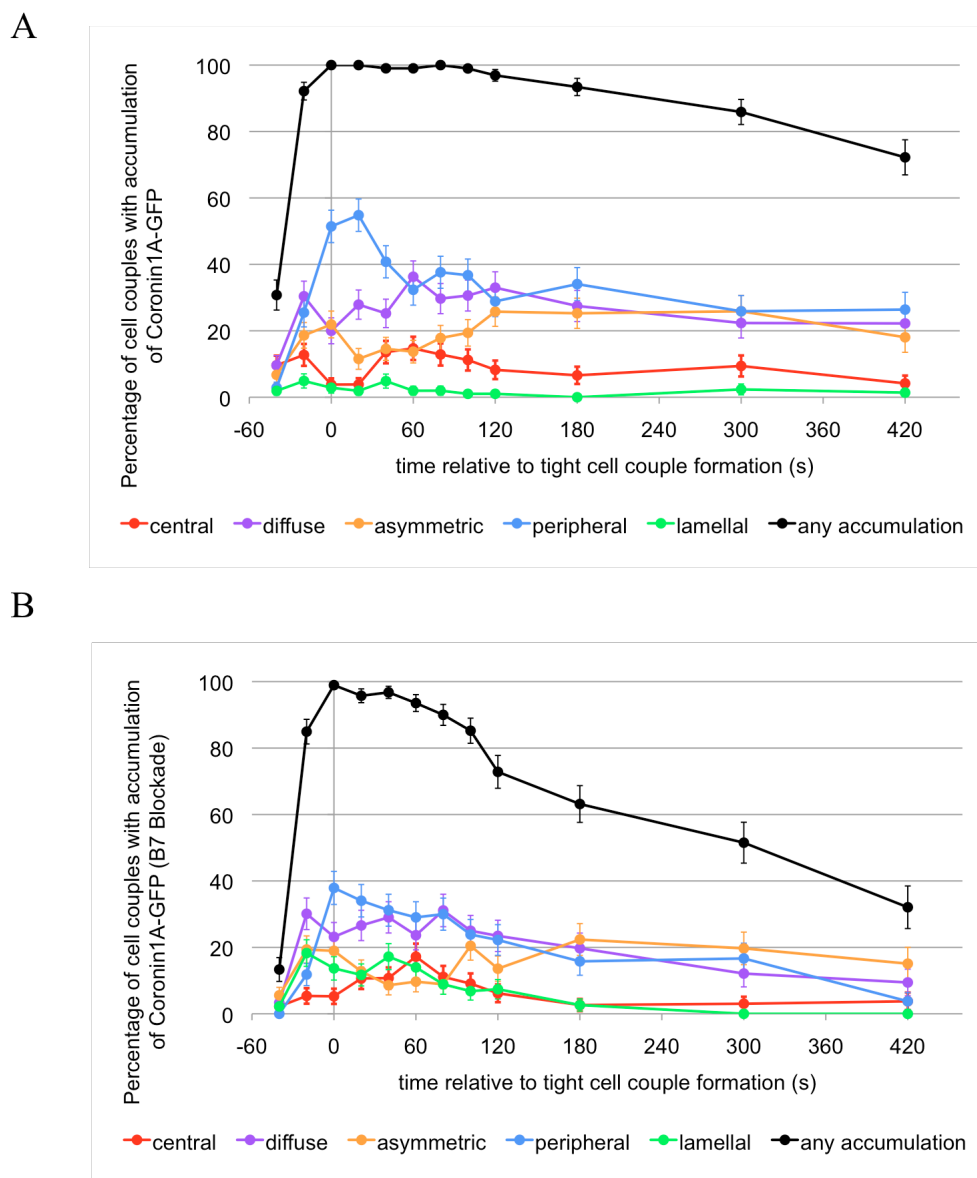


Figure 28. Spatiotemporal organization of Coronin1A-GFP at the T cell:APC interface is more transient without CD28 co-stimulation. Primed primary 5C.C7 T cells expressing Coronin1A-GFP were imaged with CH27 APCs under **A)** full stimulus (10 μ M MCC) or **B)** full-stimulus plus CD28:B7 co-stimulation blockade (10 μ g/mL α -B7-1/2). The time series is relative to formation of a tight cell couple. The percentage of T cells showing each spatiotemporal pattern is reported as a separate curve. Error bars represent s.e.m. (n>100 cell couples for each condition).

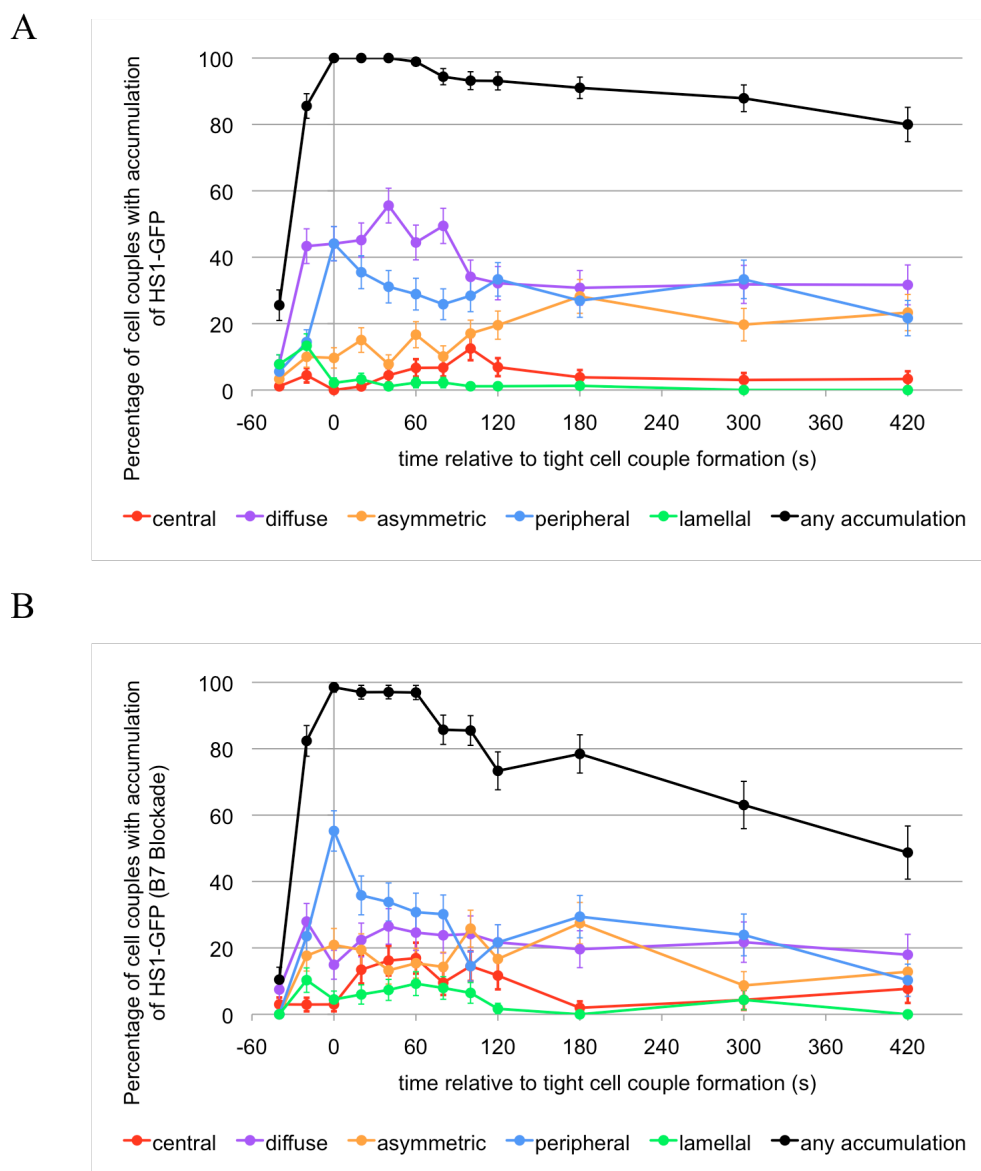


Figure 29. Spatiotemporal organization of HS1-GFP at the T cell:APC interface is more transient without CD28 co-stimulation and diffuse localization is reduced at early time points. Primed primary 5C.C7 T cells expressing HS1-GFP were imaged with CH27 APCs under **A**) full stimulus (10 μ M MCC) or **B**) full-stimulus plus CD28:B7 co-stimulation blockade (10 μ g/mL α -B7-1/2). The time series is relative to formation of a tight cell couple. The percentage of T cells showing each spatiotemporal pattern is reported as a separate curve. Error bars represent s.e.m. (n>100 cell couples for each condition).

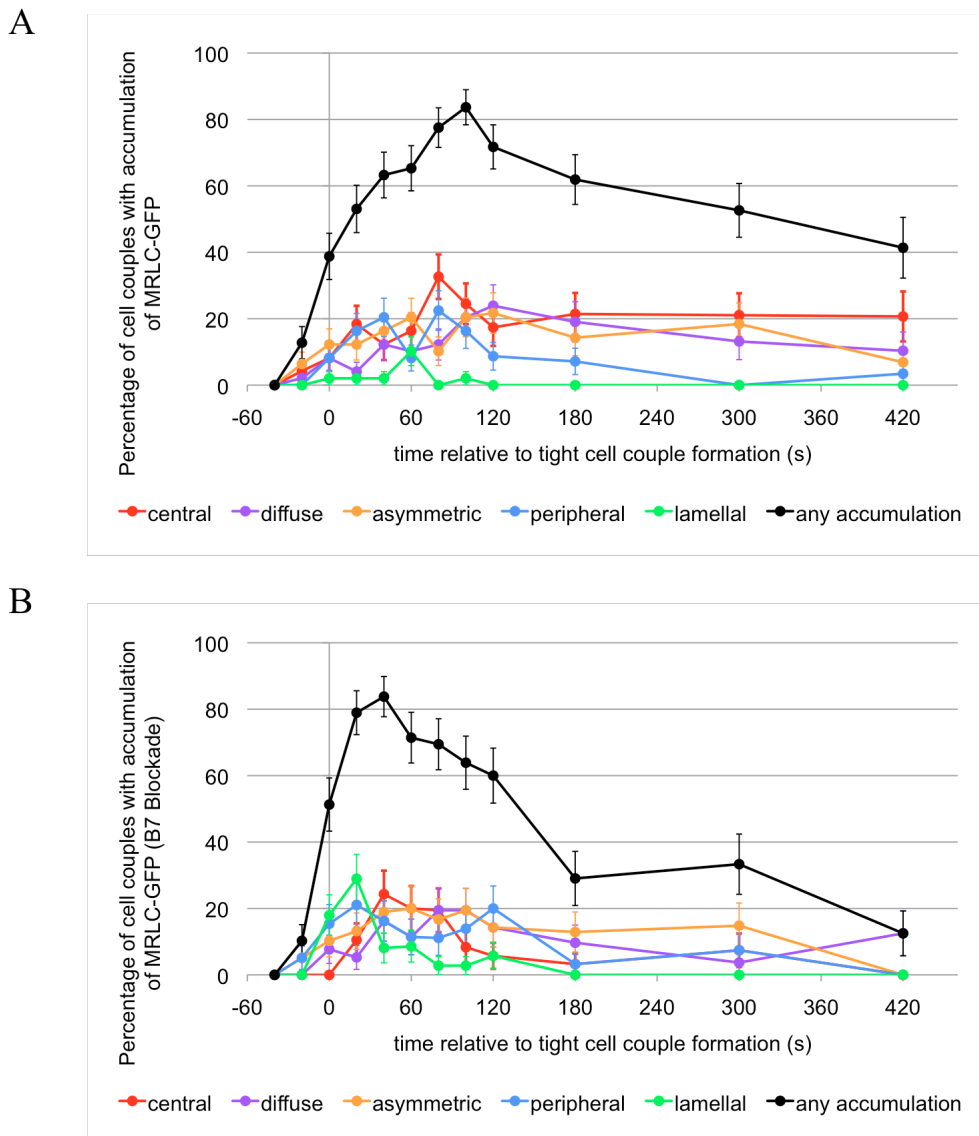
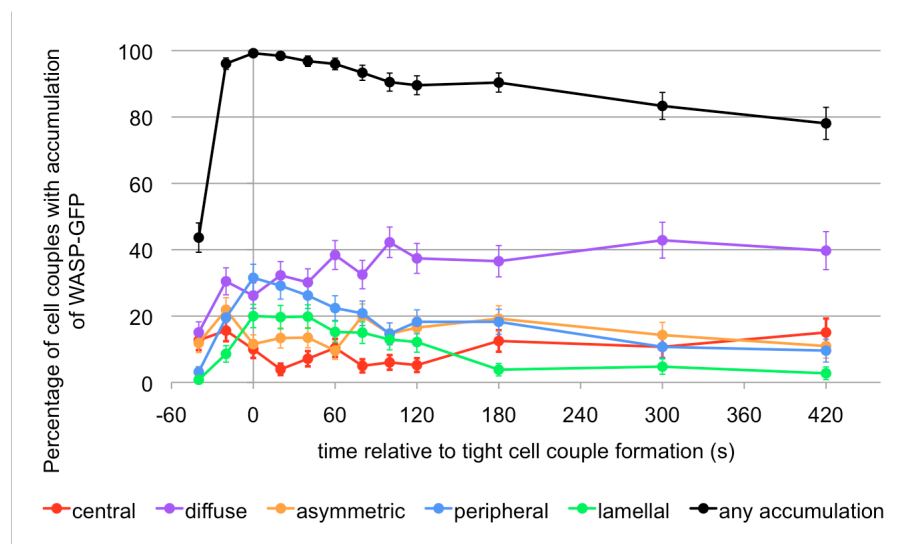


Figure 30. Myosin regulatory light chain-GFP is more rapidly recruited to the T cell:APC interface but more transient without CD28 co-stimulation. Primed primary 5C.C7 T cells expressing MRLC-GFP were imaged with CH27 APCs under **A**) full stimulus (10 μ M MCC) or **B**) full-stimulus plus CD28:B7 co-stimulation blockade (10 μ g/mL α -B7-1/2). The time series is relative to formation of a tight cell couple. The percentage of T cells showing each spatiotemporal pattern is reported as a separate curve. Error bars represent s.e.m. (n=49 for full stimulus and n=39 for B7 Blockade).

A



B

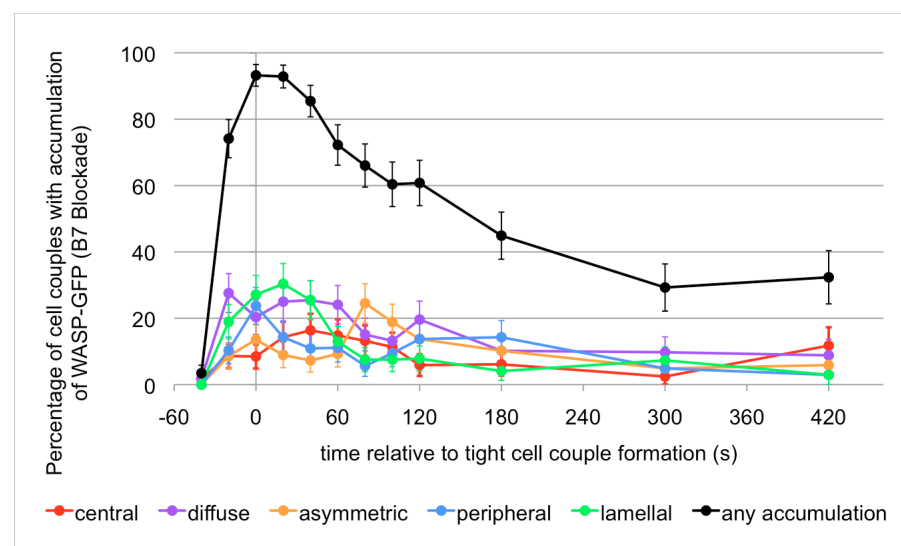
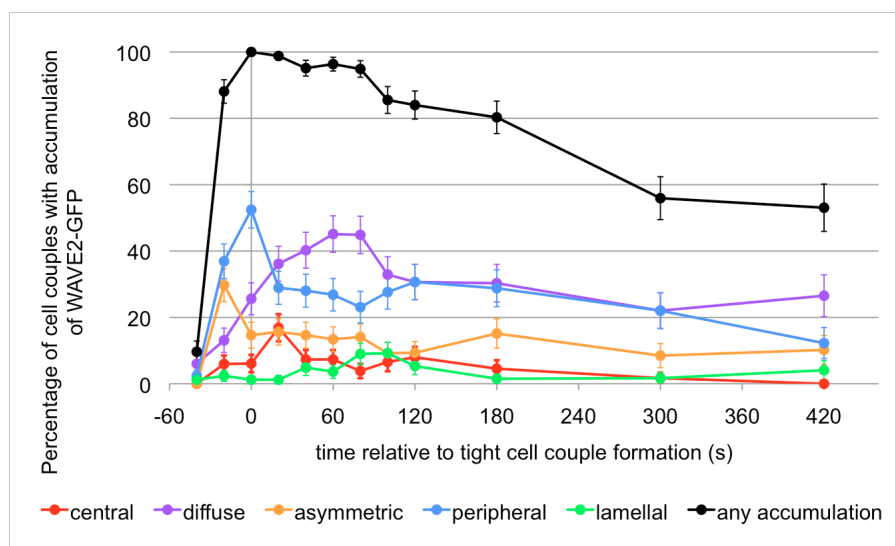


Figure 31. Spatiotemporal organization of WASp-GFP at the T cell:APC interface is more transient without CD28 co-stimulation. Primed primary 5C.C7 T cells expressing WASP-GFP were imaged with CH27 APCs under full stimulus (10 μ M MCC) or (B) full-stimulus plus CD28:B7 co-stimulation blockade (10 μ g/mL α -B7-1/2). The time series is relative to formation of a tight cell couple. The percentage of T cells showing each spatiotemporal pattern is reported as a separate curve. Error bars represent s.e.m. (n>100 cell couples for each condition).

A



B

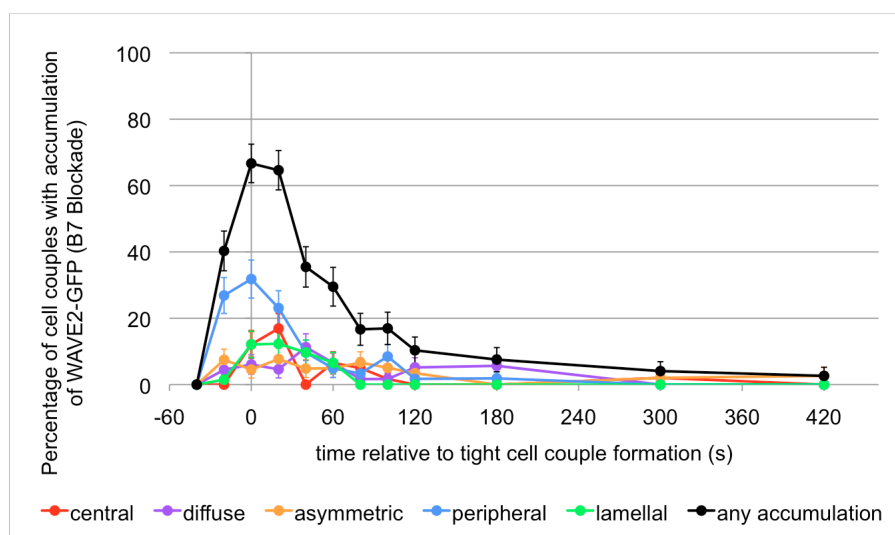


Figure 32. Spatiotemporal features of WAVE2-GFP at the T cell:APC interface are lost and are more transient without CD28 co-stimulation. Primed primary 5C.C7 T cells expressing WAVE2-GFP were imaged with CH27 APCs under **A)** full stimulus (10μM MCC) or **B)** full-stimulus plus CD28:B7 co-stimulation blockade (10μg/mL α-B7-1/2). The time series is relative to formation of a tight cell couple. The percentage of T cells showing each spatiotemporal pattern is reported as a separate curve. Error bars represent s.e.m. (n>100 cell couples for each condition).

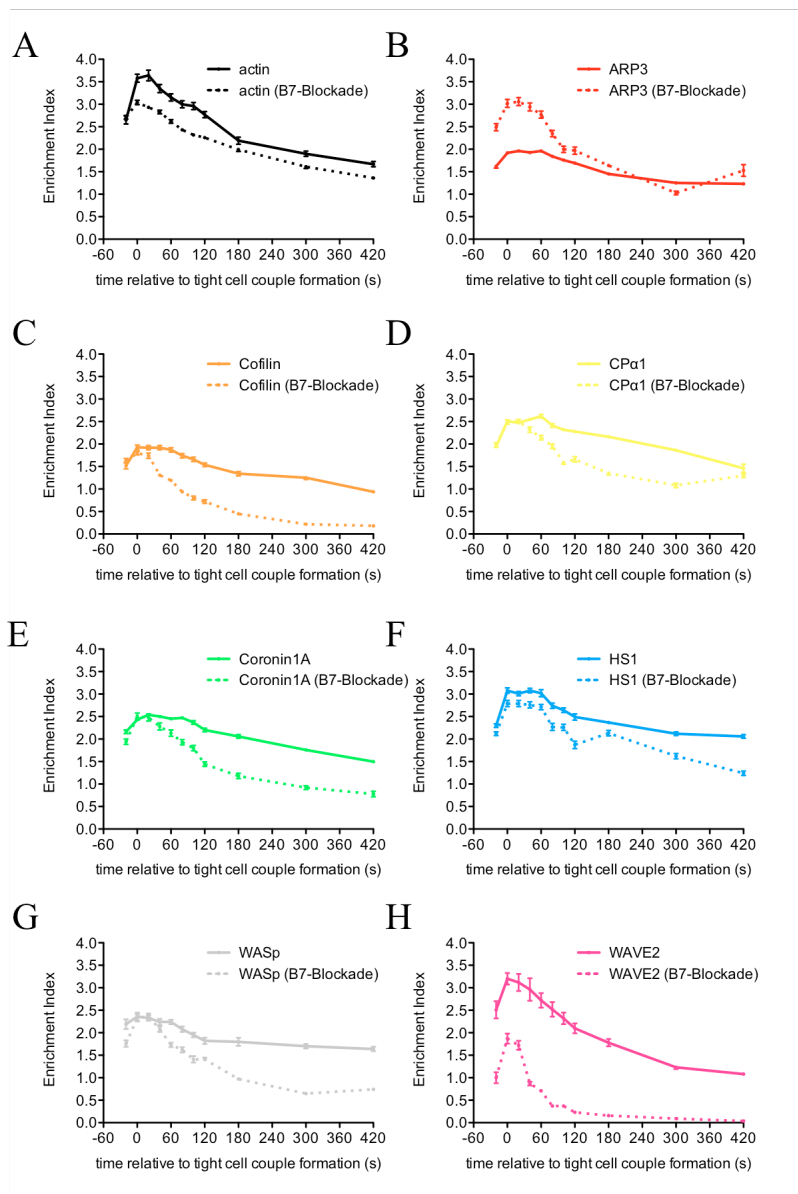


Figure 33. Most actin regulators show reduced enrichment at the T cell:APC interface without CD28 co-stimulation. A-H) Primed primary 5C.C7 T cells expressing the indicated actin regulatory proteins as GFP fusions were imaged with CH27 APCs under full stimulus (10 μ M MCC) or full-stimulus plus CD28:B7 co-stimulation blockade (10 μ g/mL α -B7-1/2, dotted line). The time series is relative to formation of a tight cell couple. See Materials and Methods section for detailed calculation of the enrichment index. Error bars represent s.e.m. (n=25 cell couples for each condition).

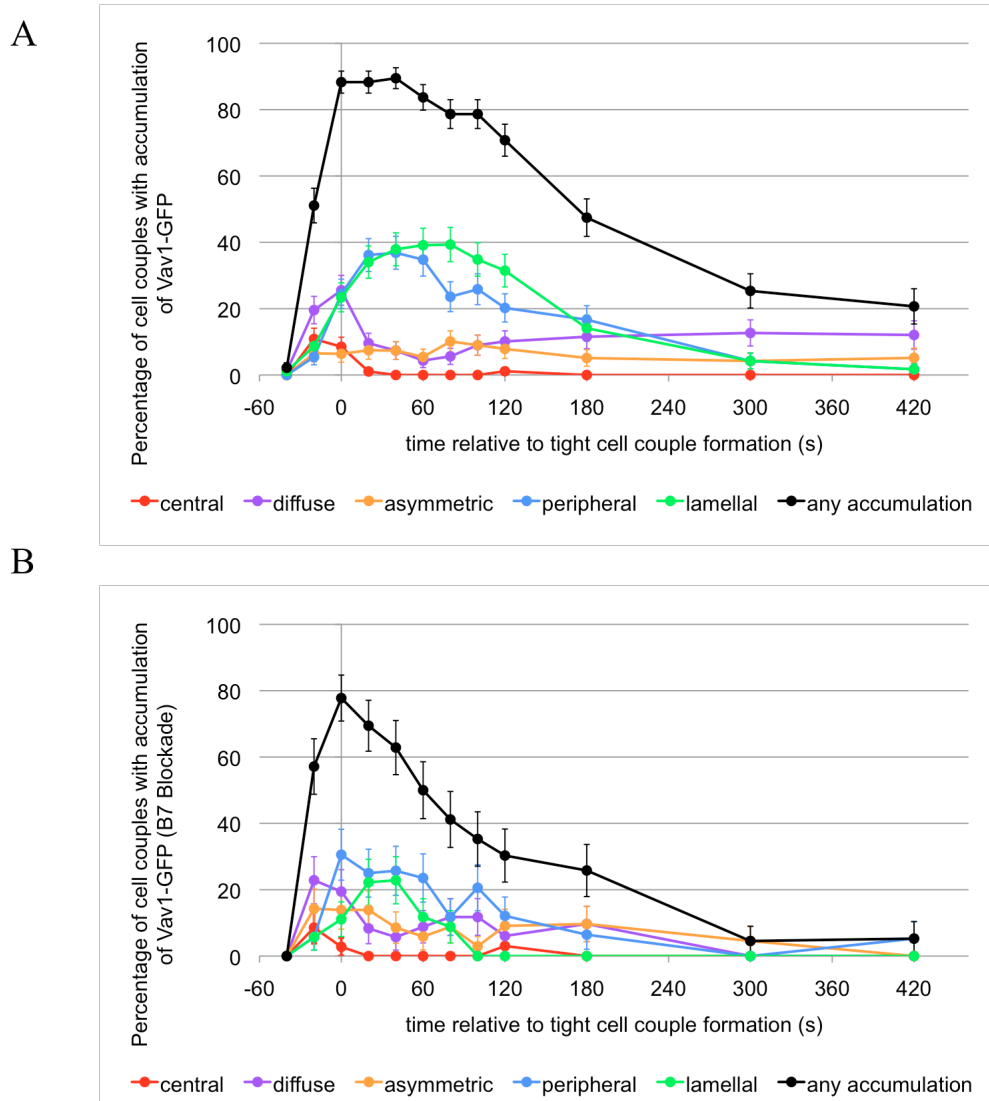


Figure 34. Spatiotemporal features of Vav1-GFP at the T cell:APC are diminished and more transient without CD28 co-stimulation. Primed primary 5C.C7 T cells expressing Vav1-GFP were imaged with CH27 APCs under **A)** full stimulus (10 μ M MCC) or **B)** full-stimulus plus CD28:B7 co-stimulation blockade (10 μ g/mL α -B7-1/2). The time series is relative to formation of a tight cell couple. The percentage of T cells showing each spatiotemporal pattern is reported as a separate curve. Error bars represent s.e.m. (n>50 cell couples for each condition).

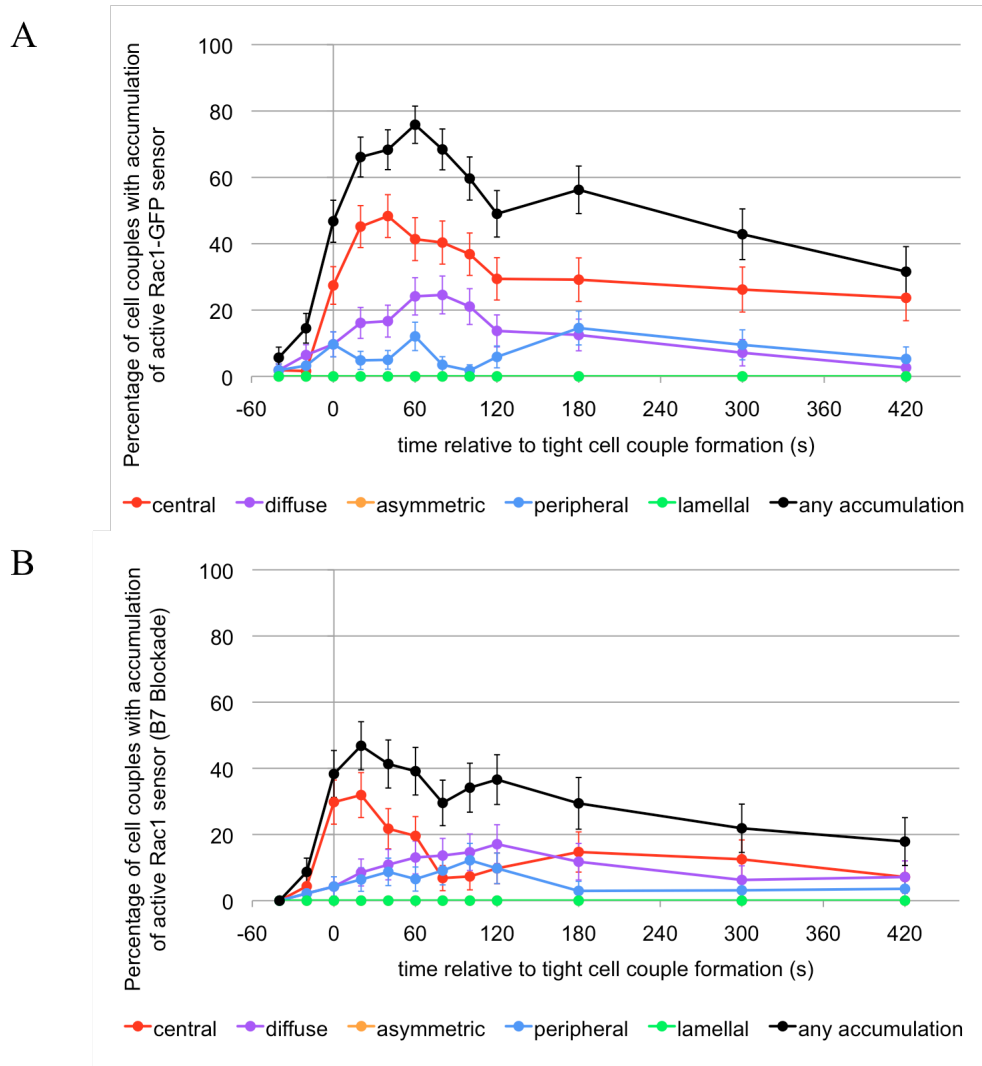


Figure 35. Activated Rac1 sensor recruitment to the T cell:APC interface is more transient without CD28 co-stimulation. Primed primary 5C.C7 T cells expressing active Rac1-GFP sensor were imaged with CH27 APCs under **A**) full stimulus (10 μ M MCC) or **B**) full-stimulus plus CD28:B7 co-stimulation blockade (10 μ g/mL α -B7-1/2). The time series is relative to formation of a tight cell couple. The percentage of T cells showing each spatiotemporal pattern is reported as a separate curve. Error bars represent s.e.m. (n=62 cell couples for full stimulus and, n=47 for B7 Blockade condition)

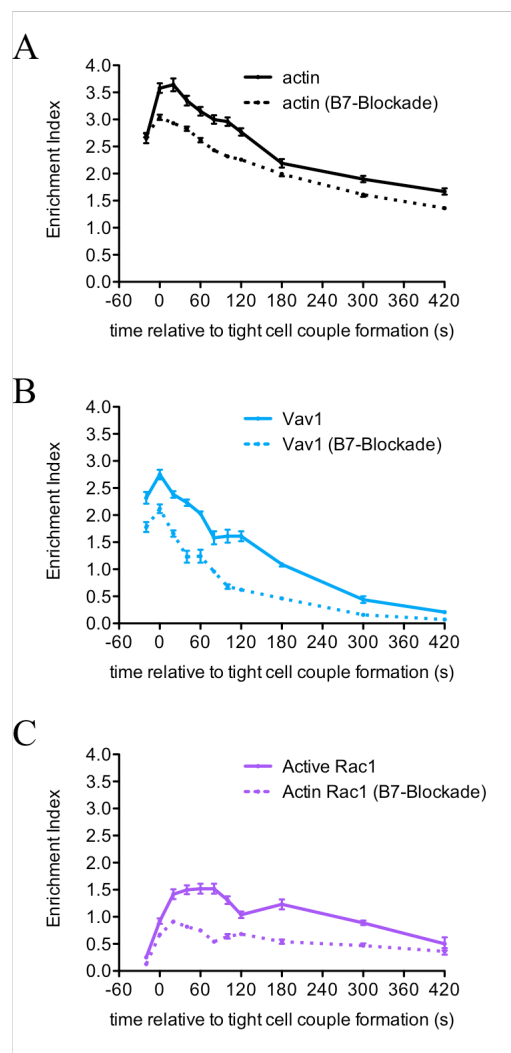


Figure 36. Enrichment of Vav1 and the active Rac1 sensor at the T cell:APC interface is reduced and less sustained without CD28 co-stimulation. Primed primary 5C.C7 T cells expressing **A)** actin-GFP, **B)** Vav1-GFP, and **C)** active Rac1 sensor-GFP were imaged with CH27 APCs under full stimulus (10 μ M MCC) or full-stimulus plus CD28:B7 co-stimulation blockade (10 μ g/mL α -B7-1/2, dotted line). The time series is relative to formation of a tight cell couple. See Materials and Methods section for detailed calculation of the enrichment index. Error bars represent s.e.m. (n=25 cell couples for each condition).

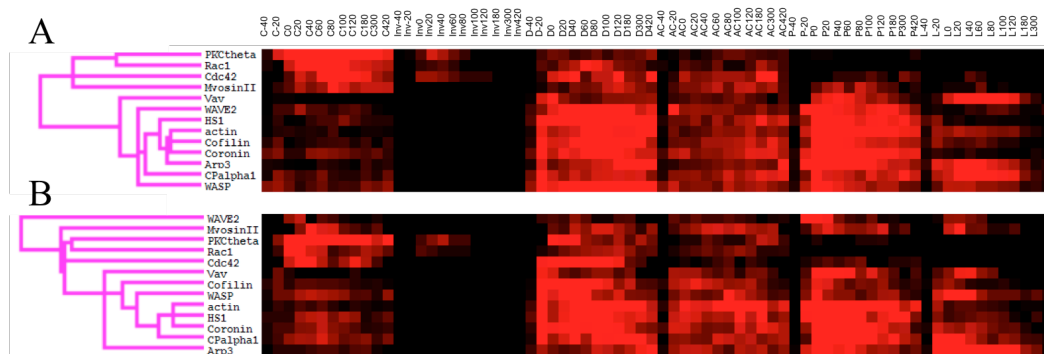


Figure 37. Systems-scale changes in spatiotemporal organization of the actin regulatory machinery without CD28 co-stimulation. A) 5C.C7 T cells expressing the indicated sensors were activated under full stimulus (10μM MCC) or **B)** B7 blockade conditions with CH27 APCs. Actin regulators were clustered based on previously described criteria (refer to fig. 4). These data consist of >2,500 cell couples and >30,000 time points.

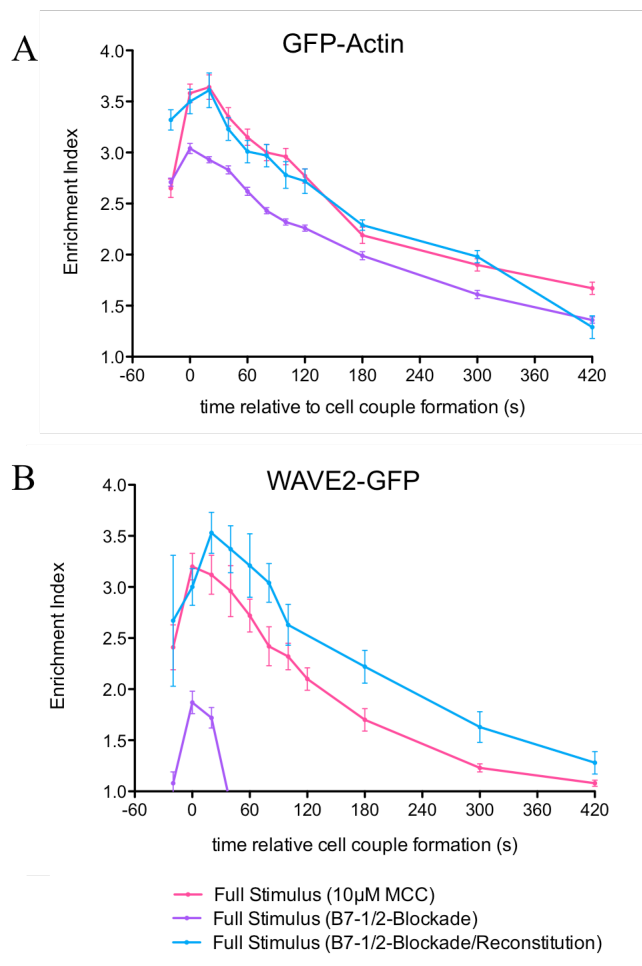


Figure 38. Constitutively active Rac1 and Cofilin restore actin and WAVE2 enrichment at the T cell:APC interface when CD28 co-stimulation is blocked. The enrichment index (see material and methods) at the T cell:APC interface for 5C.C7 T cells expressing **A)** GFP-actin or **B)** WAVE2-GFP imaged with peptide pulsed CH27 APCs under full stimulus (10µM MCC), full stimulus + B7 Blockade (10µg/mL α -B7-1/2), and full stimulus + B7 Blockade + 1µM Rac1CA/0.25µM CofilinCA (reconstitution) conditions is given. Error bars are s.e.m.

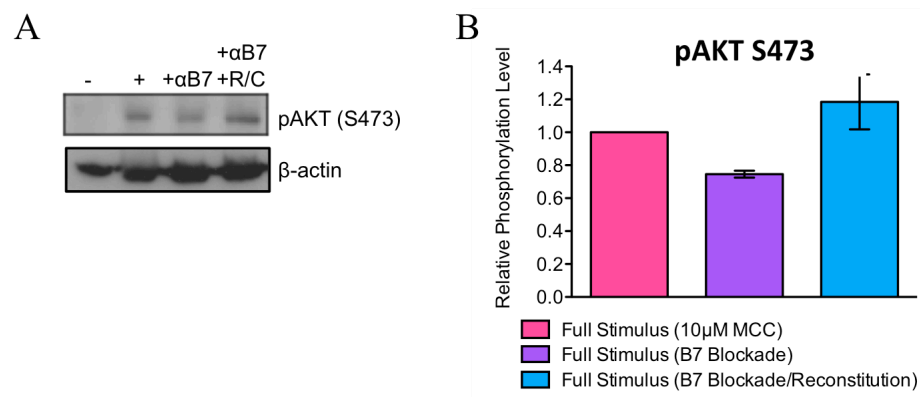


Figure 39. Constitutively active Rac1 and Cofilin restore AKT phosphorylation when CD28 co-stimulation is blocked. **A)** Representative pAKT (S473) immunoblot of 5C.C7 T cells stimulated with CH27 APCs for 30 minutes without peptide (-), with 10μM MCC (+), with MCC/α-B7-1/2 (+α-B7), and with MCC/α-B7-1/2/1μMRac1CA/0.25μMCoilinCA (+α-B7 +R/C) is shown. **B)** pAKT(S473) levels normalized to full stimulus (10μM MCC) calculated from immunoblots by densitometry are given. Data represents two independent experiments. Error bars are s.e.m.

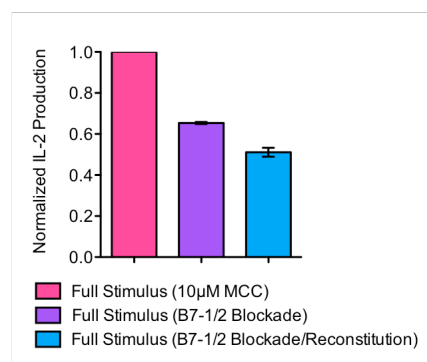


Figure 40. Constitutively active Rac1 and Cofilin dose not restore IL-2 production when CD28 co-stimulation is blocked. 5C.C7 T cells were activated under full stimulus conditions with antigen pulsed CH27 APCs (10µM MCC), full stimulus with 10µg/mL α -B7-1/2 (B7 Blockade), and B7 Blockade with 1µM Rac1CA and 0.25µM CofilinCA. Data represents two independent experiments. Error bars are s.e.m.

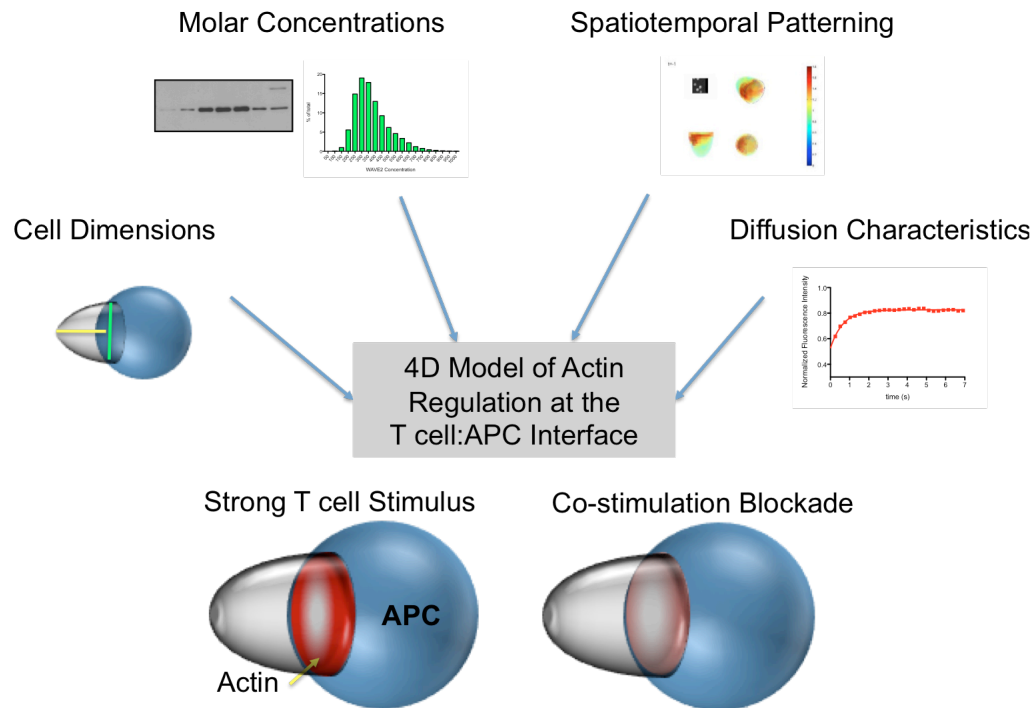


Figure 41. Outline of parameters required for generation of 4D models to quantify contribution of CD28 costimulation to actin dynamics during early T cell activation. To further understand how spatiotemporal organization of signal transduction contributes to activation of T cells a framework to build 4D models was devised. The T cell cellular space was determined by confocal microscopy (fig. 45). Single cell molar concentrations and cell-to-cell variability in expression for the actin regulators were determined by quantitative immunoblotting and flow cytometry (fig. 46-49). Software to track changes in local molar concentrations in 4D has been developed (fig. 51). Diffusion characteristics of actin regulatory molecules have been determined by FRAP (fig. 50). These parameters combined with previously characterized biochemical constants for the actin regulators will be combined for more comprehensive understanding of how actin is regulated with and without costimulation by CD28.

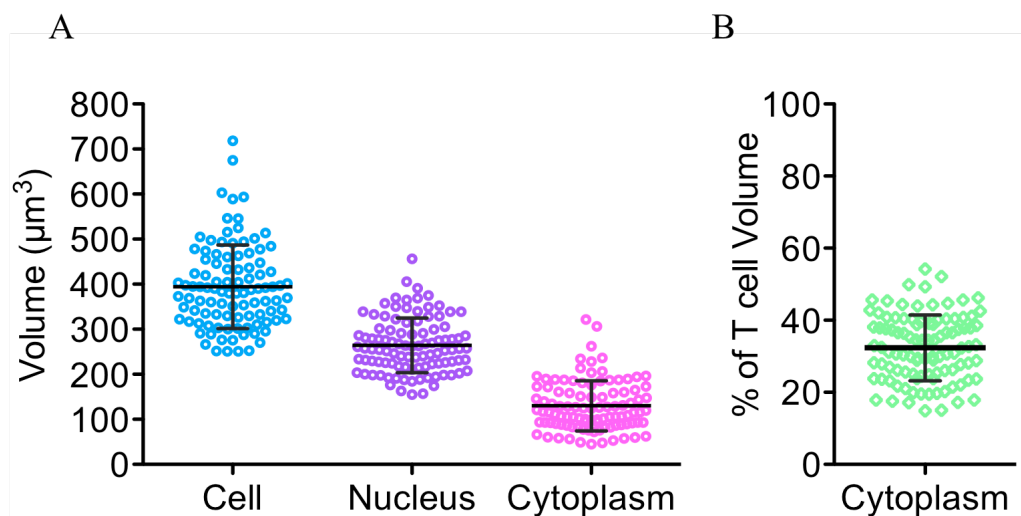


Figure 42. Volume measurements of 5C.C7 T cells. **A)** Primed 5C.C7 T cells were labeled with SNARF-1 (whole cell stain) and Hoechst (nuclear stain), imaged, and volumes of the T cell and nucleus were measured as described in the 'Materials and Methods' (n=100). **B)** The percentage of the T cell volume was calculated from values in panel A. Error bars are s.e.m.

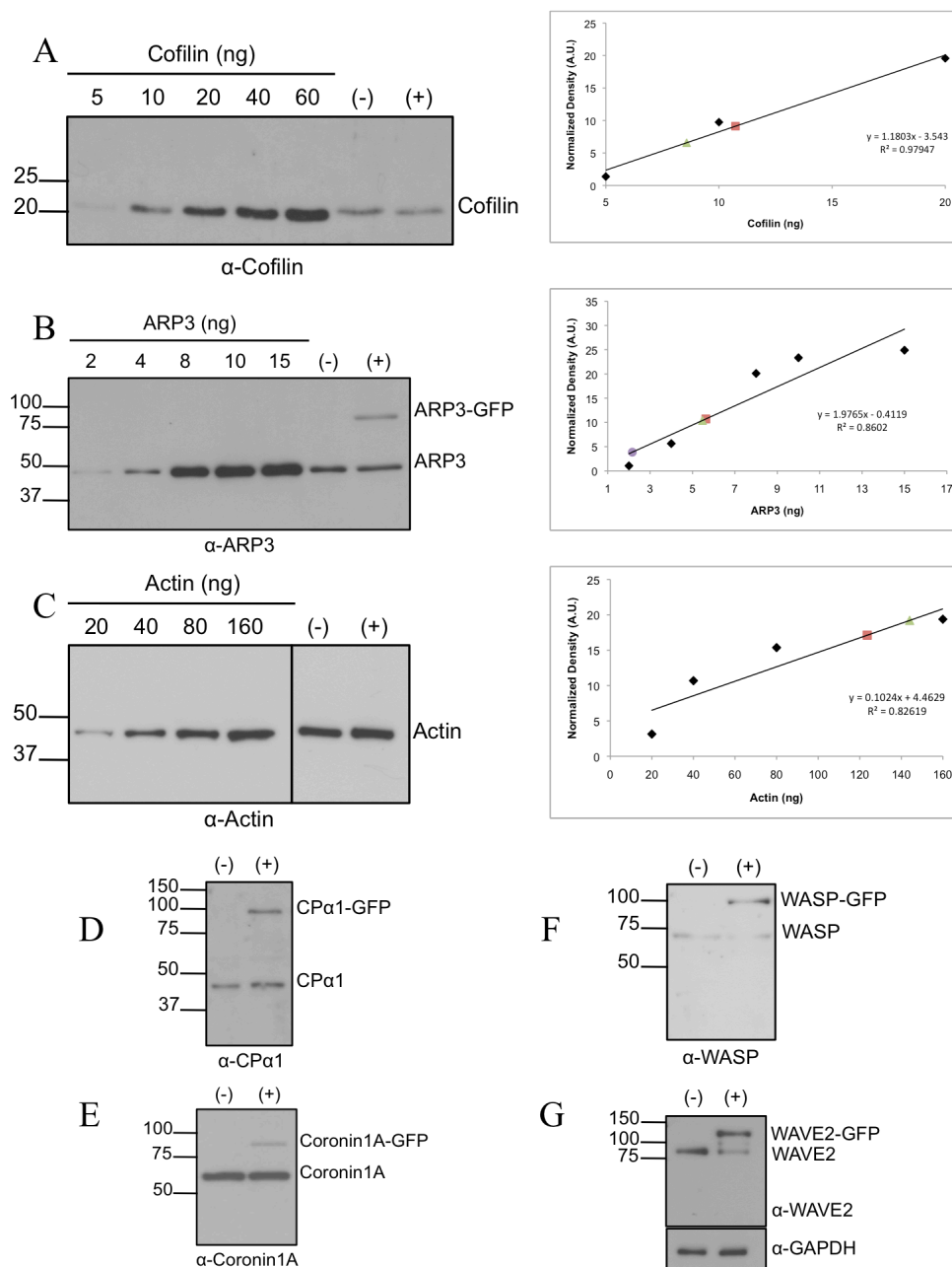


Figure 43. Quantitative immunoblots of actin regulators. (A-C) Actin regulator expressing 5C.C7s (+) and non-transduced controls (-) were sorted and run against protein standards. Standard curves are provided with calculated unknown values plotted for controls (-) red square, transduced endogenous (+) green triangle, and GFP-tagged purple circle. (D-G) Actin regulators for which purified proteins were not available were quantified based on the density measurement of the GFP tagged protein band (2.6μM).

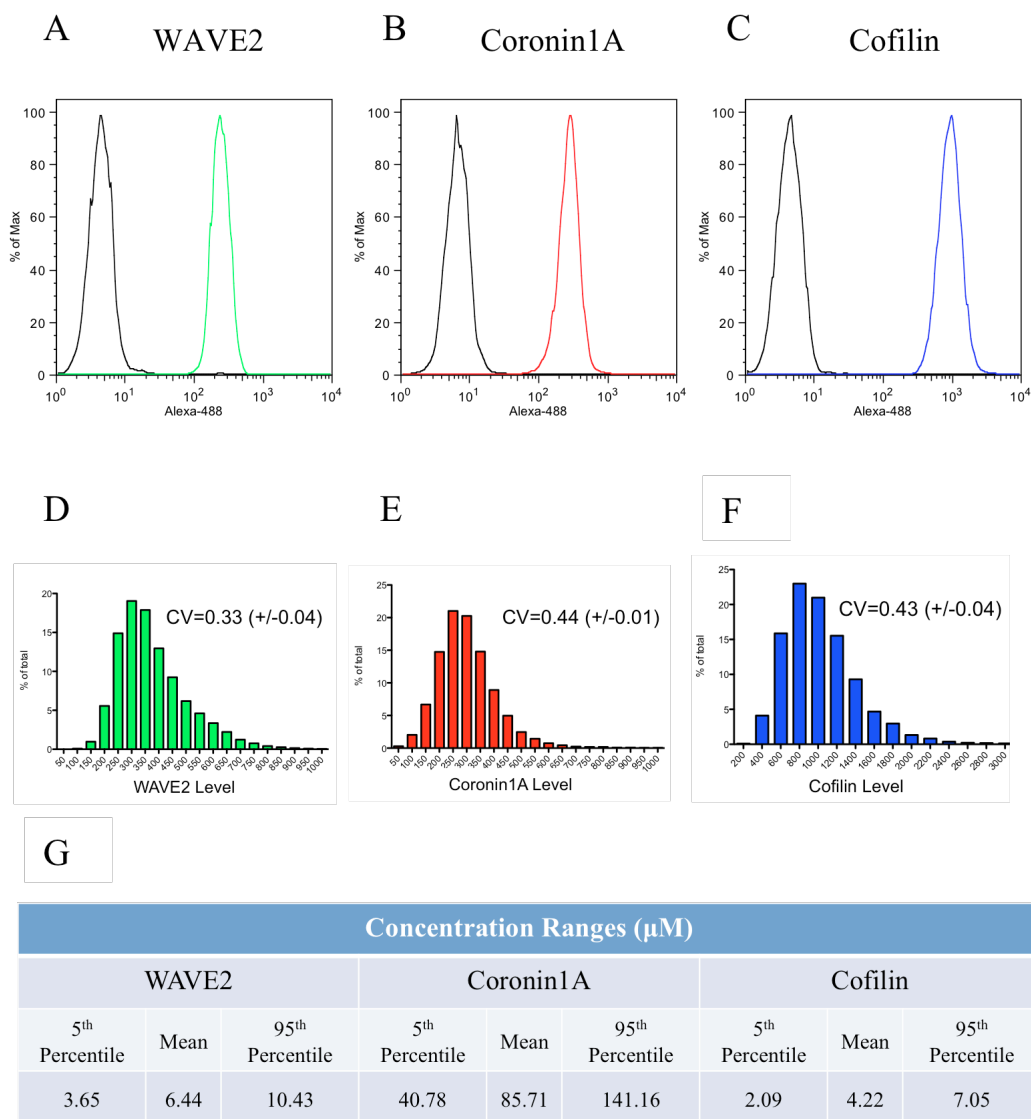


Figure 44. Cell-to-cell variability in actin regulator expression. 5C.C7 T cells were stained for endogenous levels of **A)** WAVE2, **B)** Coronin1A, and **C)** Cofilin and single cell levels were assessed by flow cytometry. **D-F)** Frequency distribution of single cell protein levels is given with the coefficient of variation (CV). **G)** Based on the frequency analysis, the 5th to 95th percentile molar concentrations were determined and given.

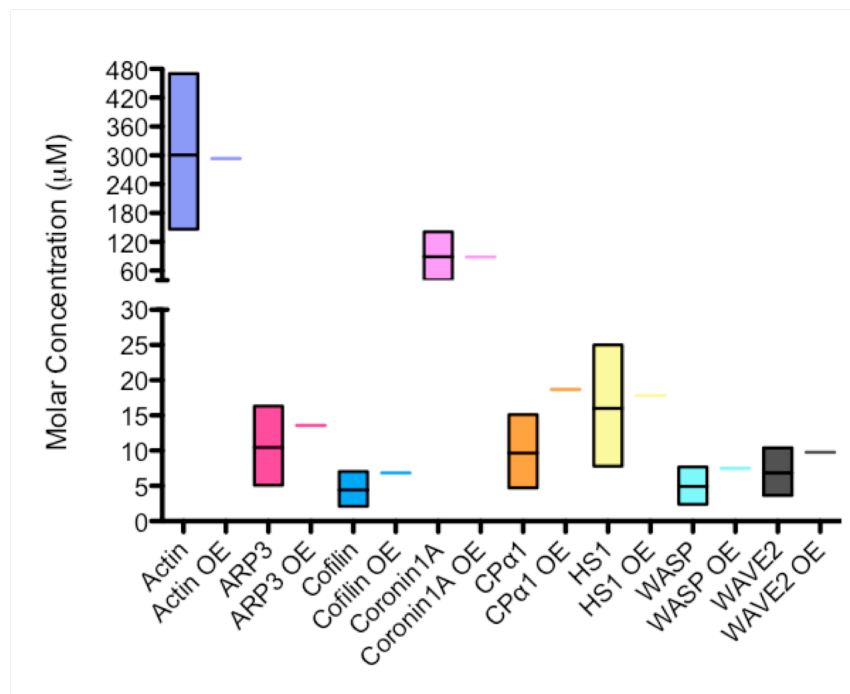


Figure 45. Cell-to-cell variability in expression of actin regulatory proteins plotted against the mean expression level in transduced T cells. The range of endogenous concentrations of the actin regulatory proteins is plotted (5th to 95th percentile of expression). Next to each endogenous range is the corresponding overexpression (OE) mean measured in retrovirally transduced 5C.C7 T cells. This graph combines data from quantitative immunoblots and flow cytometry (fig. 46-47).

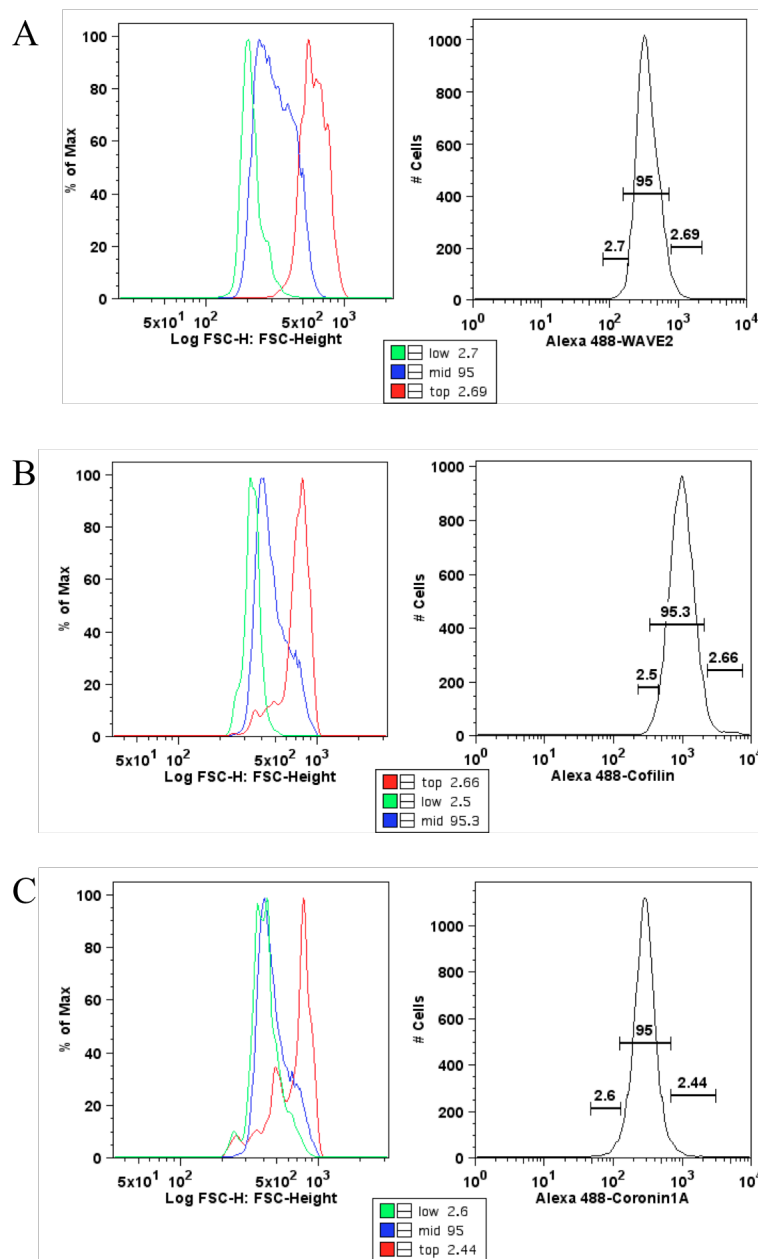


Figure 46. Protein expression scales with T cell size. 5C.C7 T cells with high (red), mid (blue), and low (green) levels of expression of **A)** WAVE2, **B)** Cofilin, and **C)** Coronin1A were gated on (right column) and forward scatter characteristics were plotted (left column).

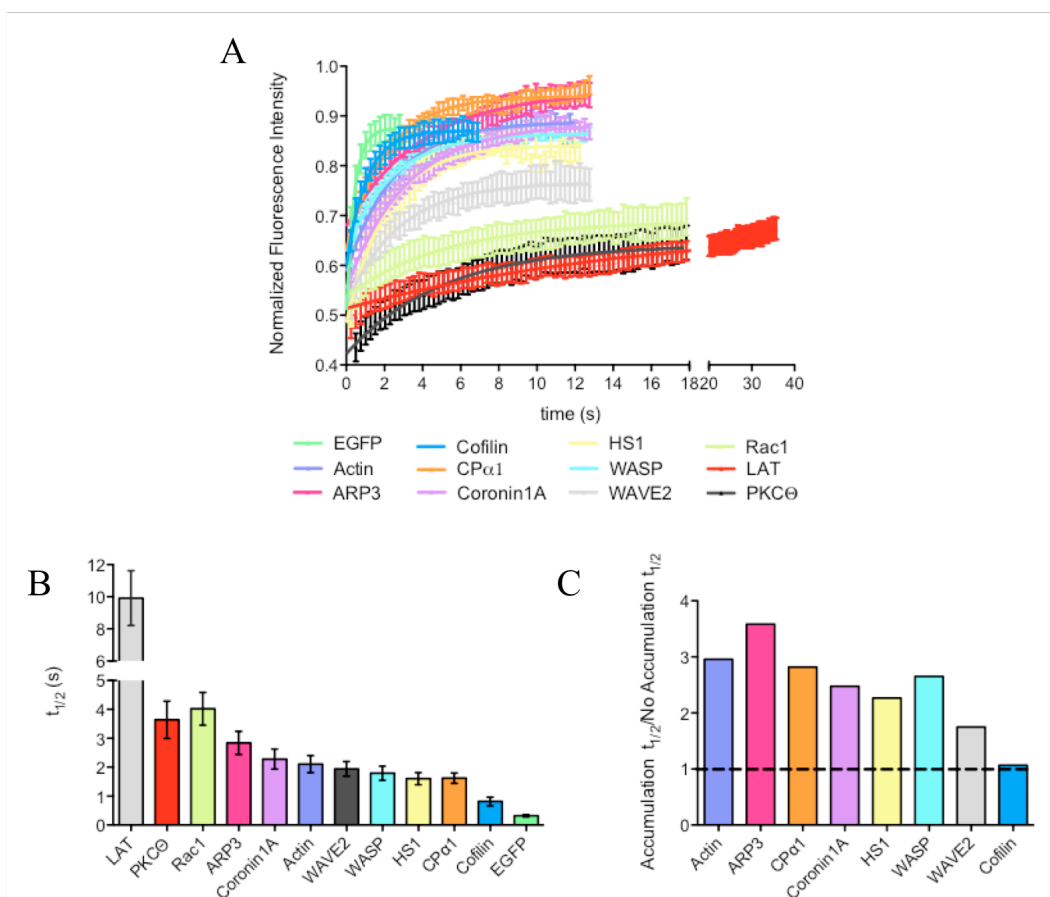


Figure 47. Actin regulation is highly dynamic during early T cell activation. A) Fitted recovery curves from FRAP of actin regulators, actin, and proximal signaling molecules downstream of the TCR are given similar to fig. 11A-C). **B)** The half-time of recovery for each actin regulator, actin, and several proximal signaling intermediates calculated from at least 10 recovery curves is given. **C)** The ratio of the half-time of recovery in an area of accumulation versus a region of no accumulation is given for each actin regulator and actin.

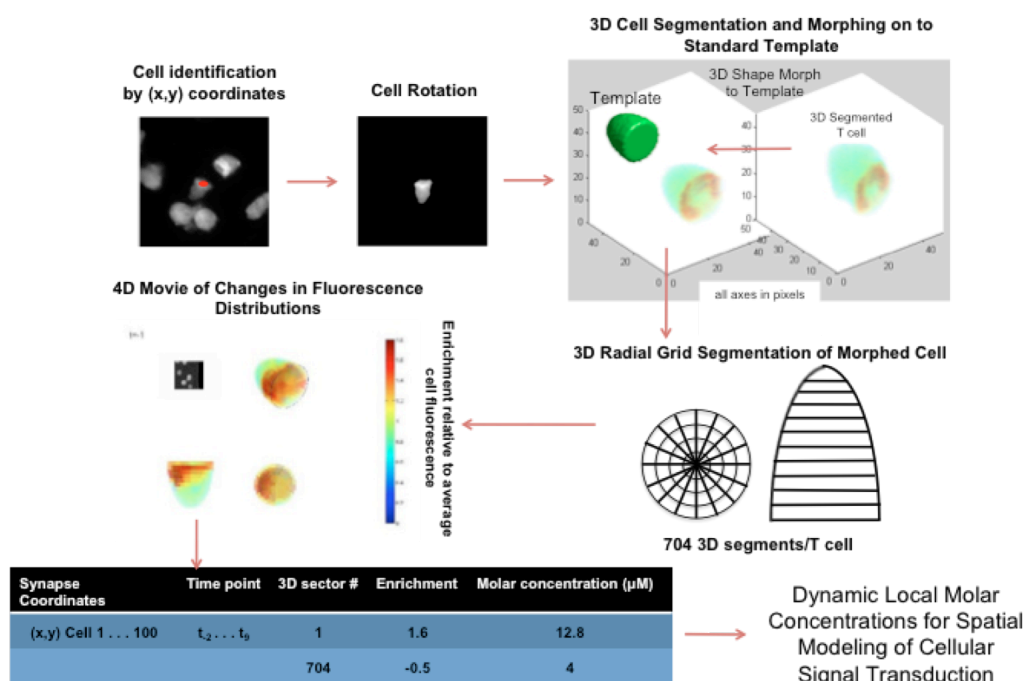


Figure 48. High-throughput determination of dynamic local molar concentrations of molecules in live cells for modeling of spatial regulation of cellular signal transduction. The T cell is identified by its (x,y) coordinates. After identification, all cells are segmented in 2D and rotated according to their medial axis so that the synapse is in a consistent orientation. The T cell is then segmented in 3D and morphed onto a template that is based on high-resolution measurements of T cells (template is a half ellipsoid with a diameter=9 μm). The intracellular space of the morphed T cell is then aligned to a 3D radial grid (704 3D segments). This grid is then applied to the original 3D segmented T cell (cell prior to morph) and fluorescence enrichment values are calculated for each segment. 4D movies are generated for each T cell to visualize distribution changes and enrichment values and molar concentrations of molecules in each segment are calculated.

CHAPTER FOUR

DISCUSSION

Spatiotemporal Patterning of T cell Activation is Highly Diverse

Spatiotemporal patterning of the T cell signaling was assessed at the systems-scale and the principle finding was that it was highly diverse. Over 50 signaling sensors were imaged in live primary T cells activated with APCs under a variety of stimulation conditions and no two signaling intermediates showed the same dynamic localization. Given the changing diversity in dynamic local enrichment of molecules under varying T cell activation conditions, interaction probabilities of these molecules will vary across time and space. Thus, spatiotemporal patterning of T cell signaling is a critical determinant of T cell signaling and activation. In support of this, we further showed that specific spatiotemporal features of T cell signaling were correlated with the strength of T cell signaling and activation [7].

Up until this study, molecules involved in signaling at the T cell:APC interface have been largely studied via a traditional single gene/protein approach in which contribution of individual molecules were determined by genetic manipulation or various inhibition approaches [79]. These studies often provide detailed mechanistic insight, but do not allow for a global view of changes in the signaling system. As cellular signaling is dependent on dozens of interconnected multifunctional molecules, cell biologists must begin to address systems in live cells to better understand input-output relations that result from experimental perturbation or disease [80].

A Deep and Transient Actin Network Controls T cell Activation

Here we describe a hitherto unappreciated structure supporting early T cell signaling, a large transient lamellum with a F-actin network extending from an interdigitated T cell:APC interface several micrometers deep into the T cell. A large group of signaling intermediates shares the spatial, temporal, and mobility features of the F-actin network and require both actin and defined molecular interactions for lamellar localization and their activity. These data strongly suggest that the transient F-actin network by controlling lamellar localization modulates the activity of a substantial part of the T cell signal transduction system.

Another region rich in proximal signaling with overlapping but distinct composition is the interface center, enriched with molecules such as the TCR, lymphocyte specific protein kinase (Lck), LAT, active Rac1, and PKC θ [4,5,7]. Molecule behavior in the lamellum is distinct from that of the center. Lamellar accumulation is transient on the scale of 1 to 3 minutes and enriched molecules are mobile, suggesting small signaling assemblies. In contrast, central accumulation is sustained over minutes if not more and enriched molecules are close to immobile, suggesting a highly cross-linked micrometer scale protein assembly [81]. As T cells must detect low doses of antigen [82,83,84] with only modest distinction from self [85,86], stable central signaling as suggested by effective central PKC θ accumulation even at limiting peptide concentrations [7], may provide a robust hub for signal propagation ensuring sensitivity. We speculate that the lamellum with smaller more dynamic complexes may be better suited to discriminate accidental or short-term receptor

triggering from strong sequential engagement over minutes, a time period several fold longer than that of the engagement of individual receptors [87,88,89], thus supporting specificity. In this scenario, actin dynamics elicited by the TCR and co-stimulatory receptors may be critical for ligand discrimination by providing positive feedback through structural support of proximal signaling complexes [10,90]. This is consistent with a prominent role of co-stimulation in autoimmune disease [64,91]. A structure allowing for rapid ligand strength discrimination may also be critical for T cells to respond flexibly in environments with APCs harboring peptides at varying doses *in vitro* and *in vivo* [92,93].

The size range of lamellar signaling assemblies is difficult to precisely resolve. Fixed cell staining for active pSLP-76 revealed distinct punctate structures implicating larger clusters while in live cell imaging, total SLP-76 was distributed evenly across the lamellum, implicating smaller ones. The absence of clusters in the live cell imaging is not due to inadequate resolution as we have observed punctate structures for other signaling intermediates such as active Arf6 and various TCR mutants [94,95]. Potentially contributing to the differences between the live and fixed cell data, fixation and detergent extraction required for fixed cells stains may extract smaller clusters leaving only larger ones [96]. It is thus plausible that the lamellar region consists of smaller signaling clusters of a range of sizes. Precedence for the importance of cellular control of signal complex size is evident in bacterial chemotaxis where receptor clustering across a defined size range provides both ligand sensitivity and a dynamic range spanning six orders of magnitude [97].

Here we show that the T cell:APC interface is an undulating and interdigitated cellular junction most prominent during the first minutes of T cell conjugate formation. This complex interface architecture occurs at a critical time in T cell activation, as it is coincident with the peak of proximal signaling and translocation of nuclear factor of activated T cells (NFAT) and NF κ B into the nucleus [7]. Such membrane topology is likely to have substantial consequences for the organization and function of the T cell signaling system. The approximate six-fold increase in contact area resulting from the undulations should enhance signal initiation. Theoretical and experimental evidence in neurons suggest that the dramatically increased membrane surface to cytoplasm volume ratio in T cell invaginations could alter signal progression [98,99]. In addition, a deep lamellal actin network may transmit cell surface signals via mechanotransduction along rigid actin filament assemblies to distant cellular compartments such as the nucleus at millisecond timescales [100]. The deep T cell plasma membrane undulations are also highly deformed membrane structures that could affect molecular interactions at the membrane as Bin/Amphiphysin/Rvs (BAR) proteins maintain curved membrane structures and provide a link to various actin regulators that are critical for T cell activation [101]. Moreover, the early T cell lamellum likely constrains actin-mediated transport. Retrograde actin flow during initial T cell activation is likely directed towards the base of T cell invaginations without much centripetal actin flow and invaginations may obstruct F-actin assemblies and cortical receptor movement towards the interface center. In fact, the central localization of molecules during initial cell conjugate formation was seemingly actin independent as SLP-76, LAT, and PKC θ all were enriched at the center when actin was perturbed by JASP. Only at later time points when the interface

becomes more planar and F-actin is less discrete does signaling intermediate accumulation at the interface centre become actin dependent.

The complexity of the interdigitated T cell:APC interface formed at the peak of T cell signaling in the first minutes of activation is likely to shape T cell activation. As such membrane architecture cannot be recapitulated by planar APC substitutes, actin dynamics and the regulation of the spatiotemporal organization of signaling with their consequences for T cell function should differ: e.g. centripetal actin flow, a hallmark of the spatiotemporal control of T cell signaling on bilayers [16], is likely restricted during early T cell activation on APCs. Therefore, it is unclear whether the actin-dependent microclusters observed on planar surfaces directly correspond to the clusters found here. Nevertheless, at later time points the T cell:APC interface more resembles a planar surface and biochemical principles of the T cell activation are likely to apply equally to activation on APCs and substitutes thereof.

Systems-scale Integration of T cell Receptor and Co-stimulatory Signals Regulate Actin Dynamics Required for T cell Activation

Here we provided a systems-scale quantitative overview of actin regulation at the T cell:APC interface and assessed the contribution of CD28 signaling to actin regulation. Blockade of CD28 resulted in modest changes to the spatiotemporal organization of actin, however, the level of actin enrichment was substantially decreased. Therefore, CD28 amplified and sustained actin polymerization important for regulation and maintenance of signaling at the T cell:APC interface.

CD28 signaling was important for sustained recruitment of the actin regulatory machinery to the T cell:APC interface with WAVE2 and Cofilin the most sensitive to co-stimulation loss. WAVE2 relies on multiple signals for activation including acidic phospholipids such as PIP₃, phosphorylation, and activated Rac1 [26,49]. CD28 signaling regulates PIP₃ levels through activation of PI3K, and Rac1 activity by stimulation of Vav1 [64]. However, CD28 dependent WAVE2 phosphorylation at important activation sites (e.g. Y150) has not been determined. Therefore, the loss of co-stimulation affects at least two of the signals important for WAVE2 activation, Rac1 activity and PIP₃ availability. In support of a defect signaling required for WAVE2 activation, we observed both reduced Vav1 and active Rac1 at the T cell:APC interface with blockade of CD28 ligation.

WAVE2 is indispensable for actin polymerization at the T cell:APC interface and calcium release activated channel (CRAC) mediated Ca²⁺ uptake into T cells [43]. In addition, reduction of Ca²⁺ entry through CRAC channels was observed when CD28:B7-1 ligation was blocked [102]. In light of these findings, loss of WAVE2 initial and sustained recruitment to the T cell:APC interface without CD28 signaling may contribute to loss of Ca²⁺ entry. WAVE2 may elicit actin dynamics important for the control of stromal interaction molecule (STIM) interaction with CRAC channels at the plasma membrane or regulation Ca²⁺ flux through the channels [103].

Cofilin is negatively regulated by phosphorylation at serine 3 and interaction with PIP₂ [30]. CD28 and other T cell accessory receptor (e.g. CD2, CD4, CD8) ligation activate phosphatases such as protein phosphatase 1 and protein phosphatase 2a that dephosphorylate and activate Cofilin [104,105]. Furthermore, CD28 along with the TCR

activates PLC γ 1, which results in rapid turn over of PIP₂ [1]. Therefore, loss of Cofilin activity upon blockade of CD28 signaling may be primarily caused by concomitant loss of phosphatase activity and reduced PIP₂ hydrolysis.

Coupled changes in WAVE2 and Cofilin activity has the potential to drastically decrease actin dynamics at the T cell:APC interface. Net production of F-actin depends heavily on balanced activity of NPFs such as WAVE2 and WASp and severing activity by molecules such as Cofilin. Imbalance in activity of WAVE2 and Cofilin thus has the ability to either rapidly promote or collapse actin networks. Loss of WAVE2 activity at the interface may reduce polymerization due to loss of ARP2/3 activation and Cofilin may quickly sever filaments. In the absence of sustained recruitment of NPFs as is the case for co-stimulation blockade conditions; Cofilin enrichment may be lost due to a reduction in F-actin substrate for severing.

Reconstitution of WAVE2 recruitment and Cofilin activity by treatment of T cells with Rac1CA and CofilinCA bypassed the requirement of CD28 signaling for normal actin enrichment and co-stimulation dependent AKT activation. While initial steps in T cell activation were restored, IL-2 production was not. This may be due to the inability of Rac1CA and CofilinCA to fully restore Grb2, PI3K, Itk, and PKC θ signaling, which culminates in the regulation of NFAT and NF κ B dependent IL-2 production. IL-2 production is also dependent on stabilization of the IL-2 mRNA through CD28 ligation [106] mediated Grb2 binding and JNK activation [64]. Our reconstitution does not conceivably restore such signaling events. T cell survival through AKT activation may be restored but cytokine production may remain at lower levels.

Given the paucity of quantitative time-resolved spatial data for signaling systems acquired from live cell imaging experiments [107], we have measured parameters necessary for 4D modeling of the actin regulatory system in live cells under full stimulus and co-stimulation blockade conditions. The entire actin regulatory network changed in response to loss of CD28 signaling as local concentrations at the T cell:APC interface differed and relative levels of proteins were altered. Mathematical modeling is best able to evaluate such complex changes in network relations. Thus, we have defined the parameters necessary for building time-resolved spatial models of actin regulation. These parameters are often lacking from both cell biological and biochemical studies preventing meaningful model construction. In cases where measurements are lacking, parameters must be estimated from knowledge of unrelated proteins or experimental systems (e.g. unrelated cell types) that may not provide realistic parameters for models. While we have measured most of the parameters necessary for 4D modeling, building reliable algorithms for automated T cell segmentation has proven difficult mostly due to unavoidable constraints of fluorescence microscopy. When using an overexpression system for imaging of fluorescently labeled signaling sensors, the level of expression must be kept to a minimum. Minimal overexpression is optimal as it reduces perturbation of the endogenous signaling systems, however, this results in cells that are close to fluorescent background levels. Unsupervised and robust segmentation of cells barely above background fluorescence levels across a range of intensities has proved difficult. Furthermore, molecules are not evenly distributed throughout the T cell resulting in local minima that make cell edge detection a difficult task. These issues must be largely resolved to build refined maps of local concentration of molecules in tens of thousands of

T cells. The latest iteration of the software has recently been optimized in the Murphy lab and our entire dataset will be analyzed to build whole T cell time-resolved maps of the distribution of each actin regulator under full stimulus and co-stimulation blockade conditions.

REFERENCES

1. Smith-Garvin JE, Koretzky GA, Jordan MS (2009) T cell activation. *Annu Rev Immunol* 27: 591-619.
2. Podack ER, Kupfer A (1991) T-cell effector functions: mechanisms for delivery of cytotoxicity and help. *Annu Rev Cell Biol* 7: 479-504.
3. Zhu J, Yamane H, Paul WE (2010) Differentiation of effector CD4 T cell populations (*). *Annu Rev Immunol* 28: 445-489.
4. Monks CR, Kupfer H, Tamir I, Barlow A, Kupfer A (1997) Selective modulation of protein kinase C- θ during T-cell activation. *Nature* 385: 83-86.
5. Grakoui A, Bromley SK, Sumen C, Davis MM, Shaw AS, et al. (1999) The immunological synapse: a molecular machine controlling T cell activation. *Science* 285: 221-227.
6. Bunnell SC, Hong DI, Kardon JR, Yamazaki T, McGlade CJ, et al. (2002) T cell receptor ligation induces the formation of dynamically regulated signaling assemblies. *J Cell Biol* 158: 1263-1275.
7. Singleton KL, Roybal KT, Sun Y, Fu G, Gascoigne NR, et al. (2009) Spatiotemporal patterning during T cell activation is highly diverse. *Sci Signal* 2: ra15.
8. Wulfig C, Davis MM (1998) A receptor/cytoskeletal movement triggered by costimulation during T cell activation. *Science* 282: 2266-2269.
9. Wulfig C, Sumen C, Sjaastad MD, Wu LC, Dustin ML, et al. (2002) Costimulation and endogenous MHC ligands contribute to T cell recognition. *Nat Immunol* 3: 42-47.
10. Tskvitaria-Fuller I, Rozelle AL, Yin HL, Wulfig C (2003) Regulation of sustained actin dynamics by the TCR and costimulation as a mechanism of receptor localization. *J Immunol* 171: 2287-2295.

11. Varma R, Campi G, Yokosuka T, Saito T, Dustin ML (2006) T cell receptor-proximal signals are sustained in peripheral microclusters and terminated in the central supramolecular activation cluster. *Immunity* 25: 117-127.
12. Campi G, Varma R, Dustin ML (2005) Actin and agonist MHC-peptide complex-dependent T cell receptor microclusters as scaffolds for signaling. *J Exp Med* 202: 1031-1036.
13. Yokosuka T, Sakata-Sogawa K, Kobayashi W, Hiroshima M, Hashimoto-Tane A, et al. (2005) Newly generated T cell receptor microclusters initiate and sustain T cell activation by recruitment of Zap70 and SLP-76. *Nat Immunol* 6: 1253-1262.
14. Vardhana S, Choudhuri K, Varma R, Dustin ML (2010) Essential role of ubiquitin and TSG101 protein in formation and function of the central supramolecular activation cluster. *Immunity* 32: 531-540.
15. Cemerski S, Das J, Giurisato E, Markiewicz MA, Allen PM, et al. (2008) The balance between T cell receptor signaling and degradation at the center of the immunological synapse is determined by antigen quality. *Immunity* 29: 414-422.
16. Douglass AD, Vale RD (2005) Single-molecule microscopy reveals plasma membrane microdomains created by protein-protein networks that exclude or trap signaling molecules in T cells. *Cell* 121: 937-950.
17. Pollard TD, Blanchoin L, Mullins RD (2000) Molecular mechanisms controlling actin filament dynamics in nonmuscle cells. *Annu Rev Biophys Biomol Struct* 29: 545-576.
18. Suarez C, Roland J, Boujemaa-Paterski R, Kang H, McCullough BR, et al. (2011) Cofilin tunes the nucleotide state of actin filaments and severs at bare and decorated segment boundaries. *Curr Biol* 21: 862-868.
19. Billadeau DD, Nolz JC, Gomez TS (2007) Regulation of T-cell activation by the cytoskeleton. *Nat Rev Immunol* 7: 131-143.
20. Burkhardt JK, Carrizosa E, Shaffer MH (2008) The actin cytoskeleton in T cell activation. *Annu Rev Immunol* 26: 233-259.

21. Gomez TS, Kumar K, Medeiros RB, Shimizu Y, Leibson PJ, et al. (2007) Formins regulate the actin-related protein 2/3 complex-independent polarization of the centrosome to the immunological synapse. *Immunity* 26: 177-190.
22. Tybulewicz VL (2005) Vav-family proteins in T-cell signalling. *Curr Opin Immunol* 17: 267-274.
23. Cantrell DA (2003) GTPases and T cell activation. *Immunol Rev* 192: 122-130.
24. Zeng R, Cannon JL, Abraham RT, Way M, Billadeau DD, et al. (2003) SLP-76 coordinates Nck-dependent Wiskott-Aldrich syndrome protein recruitment with Vav-1/Cdc42-dependent Wiskott-Aldrich syndrome protein activation at the T cell-APC contact site. *J Immunol* 171: 1360-1368.
25. Kim AS, Kakalis LT, Abdul-Manan N, Liu GA, Rosen MK (2000) Autoinhibition and activation mechanisms of the Wiskott-Aldrich syndrome protein. *Nature* 404: 151-158.
26. Chen Z, Borek D, Padrick SB, Gomez TS, Metlagel Z, et al. (2010) Structure and control of the actin regulatory WAVE complex. *Nature* 468: 533-538.
27. Goley ED, Welch MD (2006) The ARP2/3 complex: an actin nucleator comes of age. *Nat Rev Mol Cell Biol* 7: 713-726.
28. Gomez TS, McCarney SD, Carrizosa E, Labno CM, Comiskey EO, et al. (2006) HS1 functions as an essential actin-regulatory adaptor protein at the immune synapse. *Immunity* 24: 741-752.
29. Wear MA, Cooper JA (2004) Capping protein: new insights into mechanism and regulation. *Trends Biochem Sci* 29: 418-428.
30. Bernstein BW, Bamburg JR (2010) ADF/cofilin: a functional node in cell biology. *Trends Cell Biol* 20: 187-195.

31. Ghosh M, Song X, Mouneimne G, Sidani M, Lawrence DS, et al. (2004) Cofilin promotes actin polymerization and defines the direction of cell motility. *Science* 304: 743-746.
32. Sweeney HL, Houdusse A (2010) Structural and functional insights into the Myosin motor mechanism. *Annu Rev Biophys* 39: 539-557.
33. Wilson CA, Tsuchida MA, Allen GM, Barnhart EL, Applegate KT, et al. (2010) Myosin II contributes to cell-scale actin network treadmilling through network disassembly. *Nature* 465: 373-377.
34. Humphries CL, Balcer HI, D'Agostino JL, Winsor B, Drubin DG, et al. (2002) Direct regulation of Arp2/3 complex activity and function by the actin binding protein coronin. *J Cell Biol* 159: 993-1004.
35. Uetrecht AC, Bear JE (2006) Coronins: the return of the crown. *Trends Cell Biol* 16: 421-426.
36. Wulfig C, Bauch A, Crabtree GR, Davis MM (2000) The vav exchange factor is an essential regulator in actin-dependent receptor translocation to the lymphocyte-antigen-presenting cell interface. *Proc Natl Acad Sci U S A* 97: 10150-10155.
37. Ardouin L, Bracke M, Mathiot A, Pagakis SN, Norton T, et al. (2003) Vav1 transduces TCR signals required for LFA-1 function and cell polarization at the immunological synapse. *Eur J Immunol* 33: 790-797.
38. Villalba M, Bi K, Rodriguez F, Tanaka Y, Schoenberger S, et al. (2001) Vav1/Rac-dependent actin cytoskeleton reorganization is required for lipid raft clustering in T cells. *J Cell Biol* 155: 331-338.
39. Villalba M, Bi K, Hu J, Altman Y, Bushway P, et al. (2002) Translocation of PKC[theta] in T cells is mediated by a nonconventional, PI3-K- and Vav-dependent pathway, but does not absolutely require phospholipase C. *J Cell Biol* 157: 253-263.
40. Badour K, Zhang J, Siminovitch KA (2003) The Wiskott-Aldrich syndrome protein: forging the link between actin and cell activation. *Immunol Rev* 192: 98-112.

41. Labno CM, Lewis CM, You D, Leung DW, Takesono A, et al. (2003) Itk functions to control actin polymerization at the immune synapse through localized activation of Cdc42 and WASP. *Curr Biol* 13: 1619-1624.
42. Anton IM, de la Fuente MA, Sims TN, Freeman S, Ramesh N, et al. (2002) WIP deficiency reveals a differential role for WIP and the actin cytoskeleton in T and B cell activation. *Immunity* 16: 193-204.
43. Nolz JC, Gomez TS, Zhu P, Li S, Medeiros RB, et al. (2006) The WAVE2 complex regulates actin cytoskeletal reorganization and CRAC-mediated calcium entry during T cell activation. *Curr Biol* 16: 24-34.
44. Cannon JL, Burkhardt JK (2004) Differential roles for Wiskott-Aldrich syndrome protein in immune synapse formation and IL-2 production. *J Immunol* 173: 1658-1662.
45. Taylor MD, Sadhukhan S, Kottangada P, Ramgopal A, Sarkar K, et al. (2010) Nuclear role of WASp in the pathogenesis of dysregulated TH1 immunity in human Wiskott-Aldrich syndrome. *Sci Transl Med* 2: 37ra44.
46. Volkman BF, Prehoda KE, Scott JA, Peterson FC, Lim WA (2002) Structure of the N-WASP EVH1 domain-WIP complex: insight into the molecular basis of Wiskott-Aldrich Syndrome. *Cell* 111: 565-576.
47. de la Fuente MA, Sasahara Y, Calamito M, Anton IM, Elkhail A, et al. (2007) WIP is a chaperone for Wiskott-Aldrich syndrome protein (WASP). *Proc Natl Acad Sci U S A* 104: 926-931.
48. Gallego MD, de la Fuente MA, Anton IM, Snapper S, Fuhlbrigge R, et al. (2006) WIP and WASP play complementary roles in T cell homing and chemotaxis to SDF-1alpha. *Int Immunol* 18: 221-232.
49. Lebensohn AM, Kirschner MW (2009) Activation of the WAVE complex by coincident signals controls actin assembly. *Mol Cell* 36: 512-524.

50. Nolz JC, Nacusi LP, Segovis CM, Medeiros RB, Mitchell JS, et al. (2008) The WAVE2 complex regulates T cell receptor signaling to integrins via Abl- and CrkL-C3G-mediated activation of Rap1. *J Cell Biol* 182: 1231-1244.
51. Hao JJ, Zhu J, Zhou K, Smith N, Zhan X (2005) The coiled-coil domain is required for HS1 to bind to F-actin and activate Arp2/3 complex. *J Biol Chem* 280: 37988-37994.
52. Foger N, Rangell L, Danilenko DM, Chan AC (2006) Requirement for coronin 1 in T lymphocyte trafficking and cellular homeostasis. *Science* 313: 839-842.
53. Haraldsson MK, Louis-Dit-Sully CA, Lawson BR, Sternik G, Santiago-Raber ML, et al. (2008) The lupus-related Lmb3 locus contains a disease-suppressing Coronin-1A gene mutation. *Immunity* 28: 40-51.
54. Mueller P, Massner J, Jayachandran R, Combaluzier B, Albrecht I, et al. (2008) Regulation of T cell survival through coronin-1-mediated generation of inositol-1,4,5-trisphosphate and calcium mobilization after T cell receptor triggering. *Nat Immunol* 9: 424-431.
55. Shiow LR, Roadcap DW, Paris K, Watson SR, Grigorova IL, et al. (2008) The actin regulator coronin 1A is mutant in a thymic egress-deficient mouse strain and in a patient with severe combined immunodeficiency. *Nat Immunol* 9: 1307-1315.
56. Mugnier B, Nal B, Verthuy C, Boyer C, Lam D, et al. (2008) Coronin-1A links cytoskeleton dynamics to TCR alpha beta-induced cell signaling. *PLoS One* 3: e3467.
57. Eibert SM, Lee KH, Pipkorn R, Sester U, Wabnitz GH, et al. (2004) Cofilin peptide homologs interfere with immunological synapse formation and T cell activation. *Proc Natl Acad Sci U S A* 101: 1957-1962.
58. Klemke M, Wabnitz GH, Funke F, Funk B, Kirchgessner H, et al. (2008) Oxidation of cofilin mediates T cell hyporesponsiveness under oxidative stress conditions. *Immunity* 29: 404-413.

59. Akin O, Mullins RD (2008) Capping protein increases the rate of actin-based motility by promoting filament nucleation by the Arp2/3 complex. *Cell* 133: 841-851.
60. Jacobelli J, Chmura SA, Buxton DB, Davis MM, Krummel MF (2004) A single class II myosin modulates T cell motility and stopping, but not synapse formation. *Nat Immunol* 5: 531-538.
61. Ilani T, Vasiliver-Shamis G, Vardhana S, Bretscher A, Dustin ML (2009) T cell antigen receptor signaling and immunological synapse stability require myosin IIA. *Nat Immunol* 10: 531-539.
62. Shahinian A, Pfeffer K, Lee KP, Kundig TM, Kishihara K, et al. (1993) Differential T cell costimulatory requirements in CD28-deficient mice. *Science* 261: 609-612.
63. Sharpe AH, Freeman GJ (2002) The B7-CD28 superfamily. *Nat Rev Immunol* 2: 116-126.
64. Boomer JS, Green JM (2010) An enigmatic tail of CD28 signaling. *Cold Spring Harb Perspect Biol* 2: a002436.
65. Michel F, Attal-Bonnefoy G, Mangino G, Mise-Omata S, Acuto O (2001) CD28 as a molecular amplifier extending TCR ligation and signaling capabilities. *Immunity* 15: 935-945.
66. Manickasingham SP, Anderton SM, Burkhart C, Wraith DC (1998) Qualitative and quantitative effects of CD28/B7-mediated costimulation on naive T cells in vitro. *J Immunol* 161: 3827-3835.
67. Viola A, Lanzavecchia A (1996) T cell activation determined by T cell receptor number and tunable thresholds. *Science* 273: 104-106.
68. Kaye J, Hsu ML, Sauron ME, Jameson SC, Gascoigne NR, et al. (1989) Selective development of CD4⁺ T cells in transgenic mice expressing a class II MHC-restricted antigen receptor. *Nature* 341: 746-749.

69. Bolte S, Cordelieres FP (2006) A guided tour into subcellular colocalization analysis in light microscopy. *J Microsc* 224: 213-232.
70. Weisswange I, Newsome TP, Schleich S, Way M (2009) The rate of N-WASP exchange limits the extent of ARP2/3-complex-dependent actin-based motility. *Nature* 458: 87-91.
71. Rak GD, Mace EM, Banerjee PP, Svitkina T, Orange JS (2011) Natural killer cell lytic granule secretion occurs through a pervasive actin network at the immune synapse. *PLoS Biol* 9: e1001151.
72. Mandl JN, Monteiro JP, Vriskoop N, Germain RN (2012) T Cell-Positive Selection Uses Self-Ligand Binding Strength to Optimize Repertoire Recognition of Foreign Antigens. *Immunity*.
73. Chen WW, Schoeberl B, Jasper PJ, Niepel M, Nielsen UB, et al. (2009) Input-output behavior of ErbB signaling pathways as revealed by a mass action model trained against dynamic data. *Mol Syst Biol* 5: 239.
74. Carlsson AE (2010) Actin dynamics: from nanoscale to microscale. *Annu Rev Biophys* 39: 91-110.
75. Angermann BR, Klauschen F, Garcia AD, Prustel T, Zhang F, et al. (2012) Computational modeling of cellular signaling processes embedded into dynamic spatial contexts. *Nat Methods* 9: 283-289.
76. Sigal A, Milo R, Cohen A, Geva-Zatorsky N, Klein Y, et al. (2006) Variability and memory of protein levels in human cells. *Nature* 444: 643-646.
77. Sigal A, Milo R, Cohen A, Geva-Zatorsky N, Klein Y, et al. (2006) Dynamic proteomics in individual human cells uncovers widespread cell-cycle dependence of nuclear proteins. *Nat Methods* 3: 525-531.
78. Niepel M, Spencer SL, Sorger PK (2009) Non-genetic cell-to-cell variability and the consequences for pharmacology. *Curr Opin Chem Biol* 13: 556-561.

79. Fooksman DR, Vardhana S, Vasiliver-Shamis G, Liese J, Blair DA, et al. (2010) Functional anatomy of T cell activation and synapse formation. *Annu Rev Immunol* 28: 79-105.
80. Coward J, Germain RN, Altan-Bonnet G (2010) Perspectives for computer modeling in the study of T cell activation. *Cold Spring Harb Perspect Biol* 2: a005538.
81. Li P, Banjade S, Cheng HC, Kim S, Chen B, et al. (2012) Phase transitions in the assembly of multivalent signalling proteins. *Nature* 483: 336-340.
82. Harding CV, Unanue ER (1990) Quantitation of antigen-presenting cell MHC class II/peptide complexes necessary for T-cell stimulation. *Nature* 346: 574-576.
83. Demotz S, Grey HM, Sette A (1990) The minimal number of class II MHC-antigen complexes needed for T cell activation. *Science* 249: 1028-1030.
84. Irvine DJ, Purbhoo MA, Krogsgaard M, Davis MM (2002) Direct observation of ligand recognition by T cells. *Nature* 419: 845-849.
85. Davis MM, Boniface JJ, Reich Z, Lyons D, Hampl J, et al. (1998) Ligand recognition by alpha beta T cell receptors. *Annu Rev Immunol* 16: 523-544.
86. Rudolph MG, Stanfield RL, Wilson IA (2006) How TCRs bind MHCs, peptides, and coreceptors. *Annu Rev Immunol* 24: 419-466.
87. Valitutti S, Dessing M, Aktories K, Gallati H, Lanzavecchia A (1995) Sustained signaling leading to T cell activation results from prolonged T cell receptor occupancy. Role of T cell actin cytoskeleton. *J Exp Med* 181: 577-584.
88. Lyons DS, Lieberman SA, Hampl J, Boniface JJ, Chien Y, et al. (1996) A TCR binds to antagonist ligands with lower affinities and faster dissociation rates than to agonists. *Immunity* 5: 53-61.
89. Kersh GJ, Kersh EN, Fremont DH, Allen PM (1998) High- and low-potency ligands with similar affinities for the TCR: the importance of kinetics in TCR signaling. *Immunity* 9: 817-826.

90. Smoligovets AA, Smith AW, Wu HJ, Petit RS, Groves JT (2012) Characterization of dynamic actin associations with T-cell receptor microclusters in primary T cells. *J Cell Sci* 125: 735-742.
91. Tivol EA, Schweitzer AN, Sharpe AH (1996) Costimulation and autoimmunity. *Curr Opin Immunol* 8: 822-830.
92. Depoil D, Zaru R, Guiraud M, Chauveau A, Harriague J, et al. (2005) Immunological synapses are versatile structures enabling selective T cell polarization. *Immunity* 22: 185-194.
93. Henrickson SE, Mempel TR, Mazo IB, Liu B, Artyomov MN, et al. (2008) T cell sensing of antigen dose governs interactive behavior with dendritic cells and sets a threshold for T cell activation. *Nat Immunol* 9: 282-291.
94. Singleton K, Parvaze N, Dama KR, Chen KS, Jennings P, et al. (2006) A large T cell invagination with CD2 enrichment resets receptor engagement in the immunological synapse. *J Immunol* 177: 4402-4413.
95. DeFord-Watts LM, Dougall DS, Belkaya S, Johnson BA, Eitson JL, et al. (2011) The CD3 zeta subunit contains a phosphoinositide-binding motif that is required for the stable accumulation of TCR-CD3 complex at the immunological synapse. *J Immunol* 186: 6839-6847.
96. Tanaka KA, Suzuki KG, Shirai YM, Shibutani ST, Miyahara MS, et al. (2010) Membrane molecules mobile even after chemical fixation. *Nat Methods* 7: 865-866.
97. Bray D, Levin MD, Morton-Firth CJ (1998) Receptor clustering as a cellular mechanism to control sensitivity. *Nature* 393: 85-88.
98. Meyers J, Craig J, Odde DJ (2006) Potential for control of signaling pathways via cell size and shape. *Curr Biol* 16: 1685-1693.
99. Neves SR, Tsokas P, Sarkar A, Grace EA, Rangamani P, et al. (2008) Cell shape and negative links in regulatory motifs together control spatial information flow in signaling networks. *Cell* 133: 666-680.

100. Wang N, Tytell JD, Ingber DE (2009) Mechanotransduction at a distance: mechanically coupling the extracellular matrix with the nucleus. *Nat Rev Mol Cell Biol* 10: 75-82.
101. Antonny B (2011) Mechanisms of membrane curvature sensing. *Annu Rev Biochem* 80: 101-123.
102. Thiel M, Wolfs MJ, Bauer S, Wenning AS, Burckhart T, et al. (2010) Efficiency of T-cell costimulation by CD80 and CD86 cross-linking correlates with calcium entry. *Immunology* 129: 28-40.
103. Hogan PG, Lewis RS, Rao A (2010) Molecular basis of calcium signaling in lymphocytes: STIM and ORAI. *Annu Rev Immunol* 28: 491-533.
104. Ambach A, Saunus J, Konstandin M, Wesselborg S, Meuer SC, et al. (2000) The serine phosphatases PP1 and PP2A associate with and activate the actin-binding protein cofilin in human T lymphocytes. *Eur J Immunol* 30: 3422-3431.
105. Samstag Y, Henning SW, Bader A, Meuer SC (1992) Dephosphorylation of pp19: a common second signal for human T cell activation mediated through different accessory molecules. *Int Immunol* 4: 1255-1262.
106. Lindstein T, June CH, Ledbetter JA, Stella G, Thompson CB (1989) Regulation of lymphokine messenger RNA stability by a surface-mediated T cell activation pathway. *Science* 244: 339-343.
107. Iyengar R (2009) Why we need quantitative dynamic models. *Sci Signal* 2: eg3.